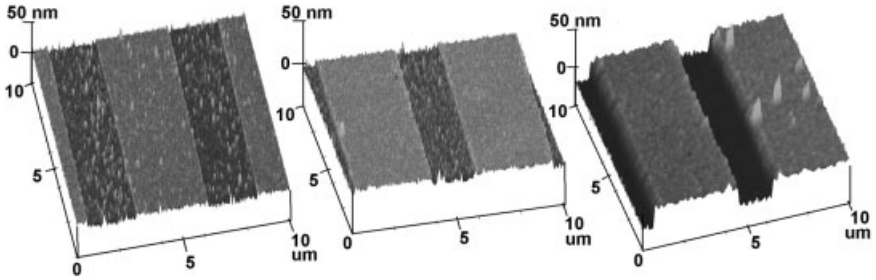

Fig. 10.2 Films formed from varying amounts of added electrolyte (NaCl): (a) 0.001 M NaCl, (b) 0.01 M NaCl and (c) 0.1 M NaCl solutions of SPS and PDAC.

added salt, as seen in Fig. 10.2c, at 0.1 M NaCl concentration. At these conditions, optimal selectivity is achieved for the SPS/PDAC system, with thicker films formed on the COOH surface, and very little, if any, deposition on the EG surface. The effects of shielding result in the adsorption of thicker SPS/PDAC multilayer films due to shielding of the polyion chains, which leads to a lowering of self-repulsive interactions between segments, and loopier, thicker adsorbed layers. This screening enhanced adsorption has been observed by a number of researchers in studies of continuous films of single polyelectrolytes and polyelectrolyte multilayers [17–21]. The interesting observation that the EG surface becomes a more effective resist at moderate salt concentrations is believed to be due to the fact that sodium ions intercalate into the matrix of the oligoethylene glycol monolayer, which can act as a ligand for small metal cations. This intercalation of ions increases the degree of hydration of the EG surface, bolstering the hydration shell; similar effects have been observed and reported by the Grunze group for protein adsorption on oligoethylene glycol surfaces [11, 12].

Large increases in the ionic strength serve to screen attractive ionic interactions between the solvated polyion and the surface until, ultimately, polyelectrolyte deposition is no longer observed on the COOH regions of the surface due to shielding of the COOH surface regions. In contrast, the EG surface changes from an area that resists polyion adsorption at low ionic strengths (Fig. 10.3a) to a region that promotes adsorption at high ionic strength in Fig. 10.3b). Above approximately 1 M NaCl concentrations, the salt ions, when coupled with the nitrogen drying step, dehydrate the EG monolayer and allow the macroscopic deposition of the polyelectrolytes [8]. These two simultaneous behaviors work in conjunction to reverse the templating of the ionic multilayers, resulting in negative selectivity on the surface, as illustrated in the electron micrographs in Fig. 10.33. If the ions used as electrolytes are changed, the ionic strength at which this transition is observed is shifted based on the relative affinity of the ions to each surface region [16].

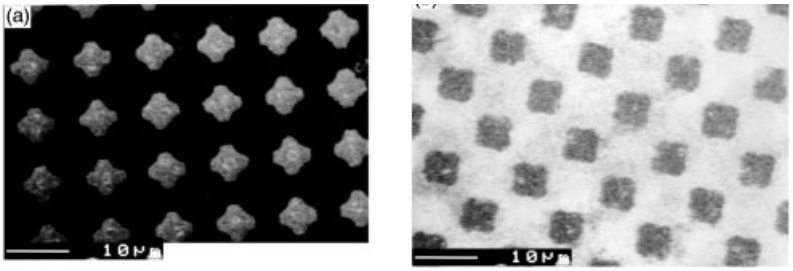

Fig. 10.3 SEM micrographs of SPS/PDAC polyion pairs deposited onto a patterned SAM for which the ionic content was (a) 0.1 M NaCl and (b) 1.0 M NaCl.

10.2.1.2 **Formation of Complex Multilayer Structures**

The ability to direct the deposition of polyions to specific regions of a surface is central to the concept of patterning polymer thin films. The reversal of the deposition behavior, such as that observed with SPS/PDAC multilayers at high ionic content, presents a useful new tool for fabricating complex microstructures from one or more sets of polyion pairs [22]. For example, an initial set of SPS/PDAC polyelectrolyte multilayers can be patterned onto a surface templated with COOH/EG surface groups at optimal adsorption conditions, resulting in selective deposition of a series of lines on the COOH surface A second set of polyion pairs can then be adsorbed onto the original patterned multilayer at a new set of adsorption conditions with high ionic strength. In this second case, deposition occurs on the EG surface, and on the top surfaces of the original SPS/PDAC film structures. The result is the formation of a blanket layer of polymer film over the original structures, as demonstrated in Fig. 10.4 (a–d). As the number of bilayers is increased from 2, 3 and 5 negative polyion pairs respectively, the ridges between the polymer begin to fill; ultimately, at 6 bilayers and greater, a continuous film surface is

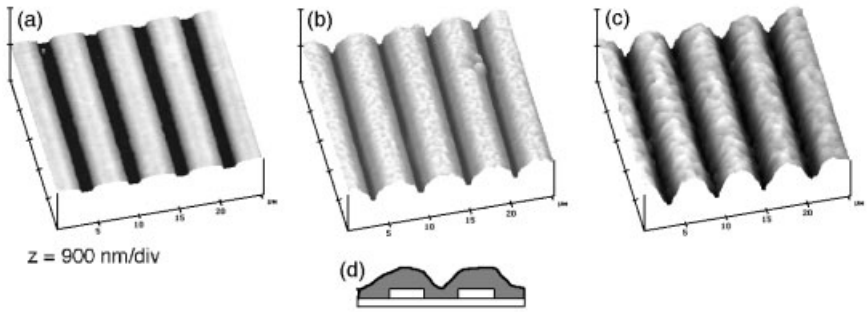

Fig. 10.4 Result of negative deposition at high salt concentrations onto a 10 polyion pair patterned film [22]. Film growth occurs over both the resist and the polyelectrolyte layer regions, resulting in a blanketing of the entire structure. (a) 2 negative polyion pairs; (b) 3 negative polyion pairs; (c) 5 negative polyion pairs; (d) schematic illustration of cross-section.

observed. This approach leads to the formation of a cladding layer, which can be applied to the formation of complex microstructures for a number of different applications from waveguide elements, to insulating layers, or as a means of advancing a third level in the formation of a 3D film structure.

10.2.2 Understanding and Utilizing Secondary Interactions in Selective Deposition

At low to moderate ionic strength, strong, highly charged polyelectrolytes such as sulfonated polystyrene or poly(diallyldimethyl ammonium chloride) deposit almost solely on the COOH regions, with very little deposition on the EG resist, creating well-defined, highly selective patterned polymer thin films [22]. For strong polyelectrolytes, it is essentially the electrostatic interactions that play the predominant role in determining the selectivity of deposition on the patterned surface [22], and, as discussed in the previous section, selectivity can be reversed at high ionic strengths. On the other hand, weak polyelectrolytes such as polyamines and polyacids are more likely to undergo additional secondary interactions such as hydrogen bonding and hydrophobic interactions, particularly as a function of the degree of ionization, or pH. By understanding the interfacial interactions between the polyelectrolyte and the chemical functional group at the surface, it is possible to manipulate the deposition of polyion pairs based on electrostatic, hydrogen bonding and hydrophobic interactions. These variations in the interactions between the polyion and the surface groups can lead to new and interesting means of manipulating selective deposition of multilayer films. Specifically, studies of weak polyion multilayer systems have led to a greater understanding of the importance of secondary interactions for these materials.

10.2.2.1 Establishing the Rules for Weak Polyelectrolyte Deposition

A systematic study of selective deposition of multilayers containing structurally different weak polyions, including polyamines and polyacids, was carried out to determine the role of molecular architecture and chemical structure on selectivity. It was found that for certain sets of synthetic polyelectrolytes, the oligoethylene oxide functional group appears to promote rather than discourage deposition over a certain pH range. Weak polyelectrolytes that are hydrophobic by nature, including polymethacrylic acid (PMAA), which has a pendant methyl group, and poly(allylamine hydrochloride) (PAH) which has a hydrophobic backbone, will preferentially adsorb to an oligoethylene oxide functionalized self-assembled monolayer (EG SAM) versus an acid functionalized monolayer (COOH SAM). More specifically, Fig. 10.5 contains the structures of three synthetic polyamines with similar atomic compositions, but different molecular architectures; the two surface functional groups, the COOH and EG SAMs, are also shown. These polyamines are an ideal choice for an examination of hydrophobic versus hydrophilic secondary interactions, electrostatic forces, and steric interactions, because their architectures are so different, with an all hydrocarbon backbone in one case

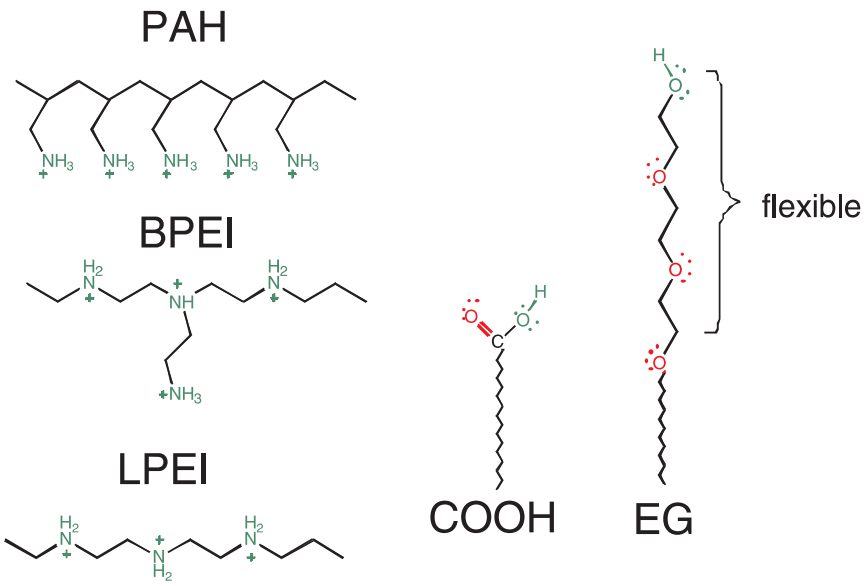

Fig. 10.5 Chemical structures of polyamines and surface functional groups used in selective adsorption studies.

(PAH), and a heteroatomic, hydrophilic backbone at the other extreme (linear polyethyleneimine or LPEI). These polyamines were co-adsorbed with polyacrylic acid to form polyelectrolyte multilayers on continuous and patterned films of the two surface groups [9]. Selectivity was measured on patterned films using atomic force microscopy; the amount of film adsorbed on both surfaces was determined and used to calculate the selectivity. We found that LPEI, a weak polyelectrolyte with hydrophilic backbone, will direct the multilayers to adsorb preferentially on the charged COOH surface at medium pH condition; while PAH, a weak polyelecyrolyte with hydrophobic backbone, has maximal selectivity towards the neutral EG surface at medium pH condition. Intermediate, pH dependent behavior was observed for branched polyethyleneimine (BPEI), which has both hydrophobic and hydrophilic groups in its branched backbone structure. It was hypothesized that strong secondary interactions between PAH and the EG surface lead to the negative selectivity of the PAH/PAA films. In particular, the hydrophobic nature of the PAH backbone can induce dispersion, or hydrophobic interactions with the ethylene groups in PEO. These interactions would not be possible with LPEI, which is highly hydrated in aqueous solution, thus introducing strong steric and hydration repulsions with the similarly hydrated EG oligomer. This hypothesis was supported by similar experiments in which the COOH and EG surfaces were replaced by sulfonated ionic surfaces and a methyl surface; under the same pH conditions, PAH adsorbs to the methyl surface preferentially.

10.2.2.2 Confirming the Rules of Selective Adsorption: SFM Investigations

To better elucidate the nature of the interactions that seemed to dominate adsorption at certain pH ranges, surface force microscopy (SFM) was used to examine the relationships between polyions and both charged acid surface groups (COOH) and neutral oligoethylene oxide (EG) functionalized surfaces. Polymer surface modified colloidal particles were used as force probes to examine the interactions of polyamines with hydrophilic backbones, such as LPEI, and those with hydrophobic backbones, such as PAH, on alkanethiol monolayers. The adsorption and force curves of these two model polyamines with COOH and EG surfaces at a range of pH values were determined with a sensitive molecular force probe [23]. Figure 10.6 contains force curves derived for PAH and LPEI on each surface at pH 4.8, when large differences in adsorption behavior are observed.

Polyamine modified polystyrene latex colloids were prepared successfully by surface grafting via electron beam irradiation and used as force probes. The surface force probe results indicate that the architecture of the polyion chain, as well as its charge density, can greatly influence the selectivity of deposition on charged versus neutral EG surfaces. The adhesion of the more hydrated LPEI on the COOH surface was dominated by ionic attractions at intermediate and high pH; whereas hydration forces led to steric repulsion of LPEI from the EG surface due to the hydrated nature of the LPEI backbone. In contrast, the adhesion of PAH to the COOH surface was reduced with respect to that of LPEI, but strong and very favorable adhesive interactions take place between the hydrophobic PAH polyamine and the EG surface at pH 4.8. This observation confirmed the adsorption studies described in the earlier section, in which LPEI based multilayers deposit preferentially on the COOH surface to yield positive selectivity, but PAH based multilayer films deposit preferentially on the EG surface, resulting in negative selectivities, at pH 4.8. Chemical force microscopy has proven to be a valuable tool in discerning the interactions which can drive self-assembly and selective deposition.

10.2.2.3 Using the Rules: Side-by-side Structures

We have taken advantage of the differences in adsorption behavior of these and other polymers, using directed adsorption as a tool to effectively control the region of film deposition and create two component, laterally patterned polyelectrolyte multilayer films on the surface [24]. A demonstration of side-by-side multilayer adsorption using LPEI and PAH was accomplished by first adsorbing multilayers of LPEI with polyacrylic acid (PAA) onto the COOH surface, followed by the adsorption of PAH/polyanion based multilayers onto the EG regions of the surface. The red sulfonated ruthenium dye, $Ru(phen')_3^{4-}$, was chosen as the multiply charged anionic species to be directed to the EG regions by PAH. The resulting composite structure, shown in the AFM micrograph in Fig. 10.7 a, consists of the PAH/$Ru(phen')_3^{4-}$ surrounded by a continuous region of LPEI/PAA multilayers. This technique can be extended to demonstrate the adsorption of two independent dye systems on one substrate, as shown by the images in Fig. 10.7 b. The permanently charged polycation, poly(diallyldimethylammonium chloride) (PDAC)

was used to assemble patterned films with a sulfonated poly-*p*-phenylene ($PPP^{(-)}$) blue dye on the COOH regions. PAH was then co-adsorbed with the ruthenium dye at pH 4.8, resulting in the adsorption of the red dye on the EG circular re-

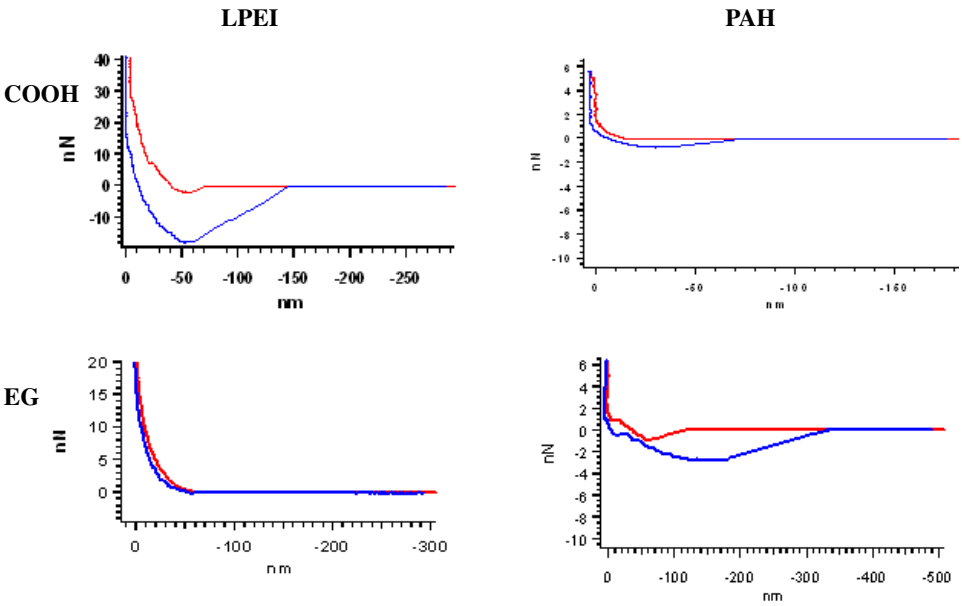

Fig. 10.6 Surface force curves obtained from chemical force microscopy utilizing a molecular force probe with a polyamine modified colloid functionalized tip and COOH and EG SAMs on gold. Force measurements shown were made at a pH of 4.8. Advancing curve is shown in red; retracting curve is in blue. Area under the curve indicates adhesion force.

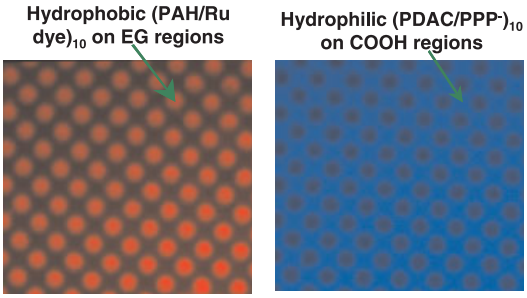

Fig. 10.7 (a) An AFM topographic image of patterned (LPEI/PAA) multilayers adsorbed on a patterned COOH SAM surface (outer regions) and (LPEI/PAA)10(LPEI/$Ru(phen^{4-}$) adsorbed on the EG surface respectively (circular dots). Schematic shows cross-sectional view. (b)Laterally patterned bicolor OLED model structure, containing 10($PDAC/PPP^{(-)}$) on COOH surface and 5(PAH/PAA)10(PAH/$Ru(phen)^{4-}$) on the EG surface. The image on the left is a fluorescence micrograph taken with the filter for red dye on the EG surface and the image on the right is the same sample taken with the fluorescence filter for the blue dye on the COOH surface.

gions. The result was an alternating surface pattern of red and blue luminescent dye multilayers on a single surface.

10.2.2.4 The Next Steps: Surface Sorting of Multilayers and Other Elements

In the previous studies described above, it was found that secondary interactions such as hydrophobicity can be used to selectively direct deposition of specific charged polymers, despite the presence of strong competing ionic attractions. These findings suggest that such interactions might be used, in conjunction with electrostatic interactions and steric forces, to guide the assembly of multi-element arrays of polymers on surfaces. This idea has been demonstrated with the use of the polyamines LPEI and PAH to direct the deposition of two different dyes to alternating regions of a surface. The ability to use different chemical functional groups as a guide to directing assembly leads to the simple concept that we have termed "surface sorting", a process by which elements with different chemical functionality are drawn to specific complementary surface sites. This idea has been used successfully in biological fields, in which specific binding sites are created with DNA segments or proteins such streptavidin and biotin, for the creation of sensors or arrays. The schematic in Fig. 10.8 illustrates a general approach which may be used to form a three component array; the "objects" indicated in the schematic can represent polyions, molecular dyes or chromophores, nanometer scale quantum dots, or micron sized particles. An adaptation of this approach can be used to create complex electro-optical devices, three color pixel displays, biological arrays for sensors, and even biomaterials surfaces for co-cell cultures.

In the example of this concept given above, with red and blue luminescent dye systems, surface groups are used which can promote adhesion of one polymer, but resist or repel deposition of other polyion types, leading to the formation of laterally patterned, or side-by-side, multilayer thin films. More complex multiple layer assemblies can be formed by using surfaces which are selective to one polyion multilayer system, but not another, allowing the creation of blanket layers such as those described in Section 10.2.1 with strong polyelectrolytes, as well as multiple component lateral films. *This approach can lead to novel approaches to device fabrication which would be difficult to emulate with traditional photolithography.* In particular, a single patterned surface can be prepared at low cost to guide deposition of materials in situ without further processing steps. Photolithography

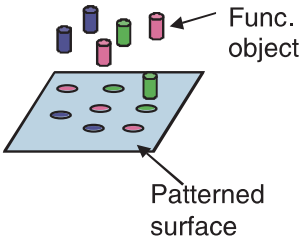

Fig. 10.8 Schematic representation of the concept of surface sorting with multiple surface components during the adsorption process. Cylinders represent charged functional "objects" present in solution ranging from macromolecules to micron sized particles with a specific binding group. Colored dots on the surface indicate surface regions with complementary functionality which act as regions for deposition.

traditionally involves masking and etching processes that are required subsequent steps following each materials deposition to form a lateral or vertically patterned film. This concept is universal, in that it can apply to polymers, low molar mass dyes and other small molecules, as well as mesoscale systems and objects, as will be discussed in the section on colloidal assembly.

10.3 Polymer-on-Polymer Stamping

It is clear from the use of surface chemistry described above, as well as a myriad of other studies from numerous groups which utilize surface monolayer chemistry [15, 25–27], that the ability to create chemically patterned surfaces can lead to the templating of one, two or more materials systems to a surface through adsorption, polymerization, and other materials deposition methods. The use of alkanethiols on gold [4, 6] or trichloro and triethoxy silanes on glass [4] has brought with it a broad range of potential systems for surface templating; however, the use of such systems can be limiting in the numbers of commercially viable applications that are accessible using traditional chemisorbed SAMs on metal or metal oxide surfaces as substrates. There is a strong interest in the use of polymers as lightweight substrates for displays, sensors, electronic media, and other applications; however, most such surfaces are not accessible to patterning using silane or thiol chemistry. The use of thiols or silanes also often requires targeted synthesis to gain new functional systems. Finally, the ability to pattern on top of an existing polyelectrolyte multilayer can lead to the development of complex patterned 2D or 3D multilayers and hybrid materials systems, allowing the possibility of taking full advantage of the range of functional groups that can be incorporated into multilayer films for device and other applications. We have developed a new approach to the creation of chemical surface patterns which does not rely on the use of traditional chemisorbed monolayers [28], and have since begun to explore the use of functionalized polymers, polyions and low molar mass substituents which can be stamped directly onto other surfaces, particularly plastic substrates and multilayer films, by careful selection of surface chemistry [29]. Our motivations for exploring these routes are two-fold: 1. The functionalization and subsequent patterning of ionic multilayers and other materials on a broad range of substrates, including polymeric surfaces, without elaborate pretreatment; 2. the creation of complex multiple level heterostructures via stamping atop continuous or patterned polymer thin films, followed by subsequent selective adsorption or deposition steps.

Fig. 10.9 illustrates the polymer-on-polymer stamping process schematically. A polymer is transferred directly to the top surface of a polyelectrolyte multilayer thin film based on covalent and/or non-covalent interactions. For example, a polyanion can be stamped directly onto a charged polycation top multilayer surface to create alternating regions of plus and minus charge. On the other hand, block and graft copolymers can present a reactive functional group for attachment to

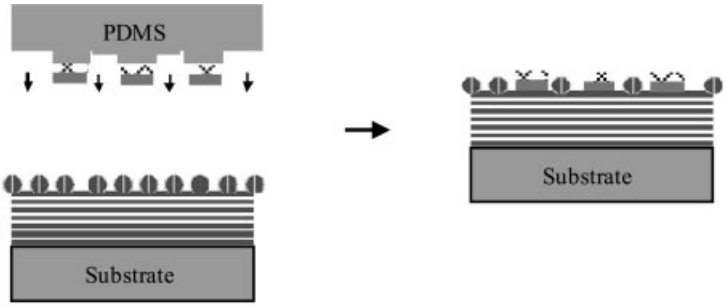

Fig. 10.9 Schematic illustrating the concept of polymer-on-polymer stamping (POPS). Utilizing a PDMS stamp and a polymer "ink" to microcontact print a polyelectrolyte or block copolymer to a multilayer surface.

the surface, and a second functional group to modify the surface, as will be discussed further. We have found that even a *single* adsorbed layer of polyelectrolyte can be used as a functional surface for stamping. By creating patterned functional chemistry atop a polyelectrolyte surface, we ultimately introduce a broad approach that enables modification of any surface which can be covered with at least one surface layer of polyion. Because a number of existing polymers may be used for this technique, many new functional surfaces can be achieved through the use of block copolymers or graft copolymers. This approach is much more commercially viable for the modification of flexible film using roll-by-roll processing than lithography or ink jet printing, and does not require a metallization or the creation of an oxide layer on the substrate, as with most SAMs.

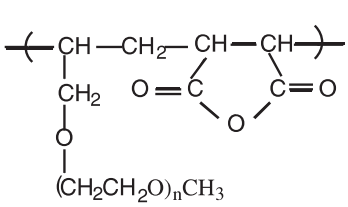

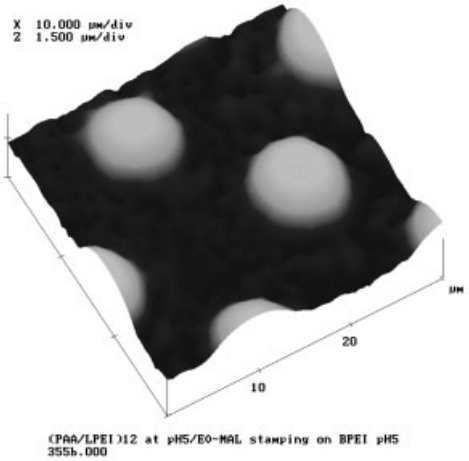

Fig. 10.10 An AFM image of a multilayer surface adsorbed onto a polystyrene substrate, which has been functionalized with the EO–MAL graft copolymer, followed by multilayer adsorption of SPS/PDAC bilayers, which deposit only on the regions which did not contact the stamp [28].

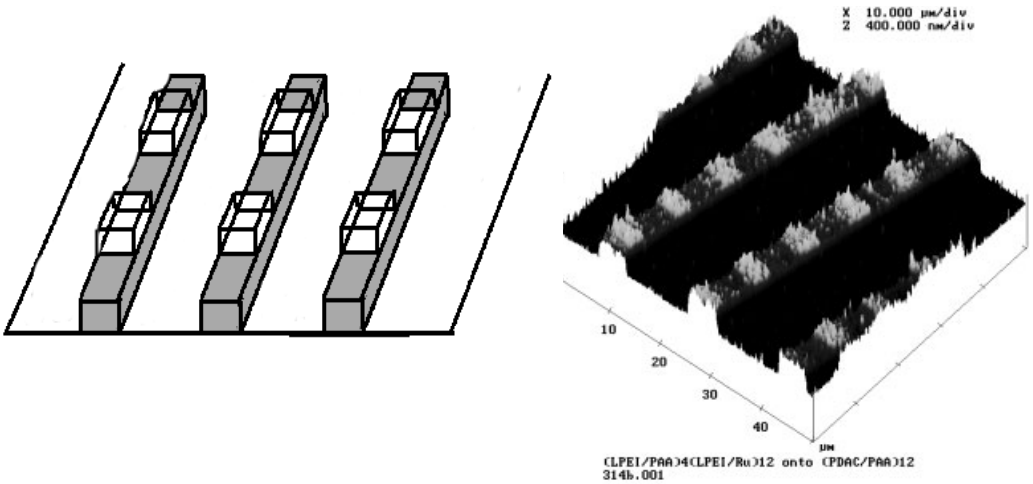

Fig. 10.11 An illustration of multiple level patterning, in which an existing patterned multilayer set of stripes is patterned with a second set of lateral stripes using EO–MAL [28].

The polymer stamping concept has been illustrated through the patterning of an oligoethylene glycol resist atop a polyelectrolyte multilayer surface. A resist layer was created by stamping an oligoethyleneoxide–maleic anhydride graft copolymer (EO–MAL) onto the top polyamine surface. Further deposition of polymer multilayers results in the formation of a patterned polymer film atop the original continuous multilayer thin film platforms as shown in Fig. 10.10. When a patterned polyelectrolyte film is used as the base layer or substrate in this process, a second pattern can be stamped atop the original patterned array. Subsequent selective adsorption of polymers yields a second level of microstructures, illustrating the concept of multiple level patterning for layer-by-layer thin films, as demonstrated in Fig. 10.11 [28].

Polymer-on-polymer stamping can be broadened to include selective deposition of numerous materials on top of multilayer polymer systems [28] and other functional surfaces. These films may then be used to template materials deposition, including other layer-by-layer thin films [28], polymers, metals [30], and colloidal particles [31].

10.3.1
Fundamental Studies of Polymer-on-Polymer Stamping

A number of issues exist for the application of polymer-on-polymer stamping. The transfer of polymers using a direct contact method requires that the polymer be applied to the PDMS stamp, and transferred in a dry or highly concentrated state after the removal of solvent. Due to the high molecular weight and lowered diffusion rate of polymers, the kinetic timescales of polymer transfer to the surface are expected to differ from those of typical alkanethiols on gold. It is also important

to consider differences in reactivity between the chemisorption of thiols or silanes, and the much less reactive groups on many polymer systems involved in ionic or hydrogen bonding interactions between the polymer and the surface. Perhaps more importantly, the nature of the transferred layer will be a function of the type of interaction used, the solvent used to create the polymer "ink", and the wetting properties of the polymer with the stamp and the multilayer surface.

10.3.1.1 **Stamping of Ionic Polymers**

Charged polymers can be transferred directly to a polymer surface of opposite charge using microcontact printing. This approach has been demonstrated for the transfer of strong polyelectrolytes to a polyelectrolyte multilayer platform. In the stamping process, a solution containing the polymer of interest is applied to a PDMS stamp. The excess solvent is then removed through air or nitrogen drying, and the stamp is placed on the substrate surface to be patterned. We have found that when a permanently charged polycation, PDAC is transferred to a negatively charged surface of an SPS/PDAC multilayer, a thin layer of positively charged polymer adheres to the surface even after thorough rinsing and sonication in water [32]. The thickness of the stamped layer is approximately 30 to 40 Å, close to the amount of film adsorbed from solution in the formation of multilayer thin films. A fundamental question that must be answered is whether the stamping process is analogous to the adsorption of polymers from solution. If the stamping process is comparable to adsorption from solution, then it should be possible to manipulate the thickness and the number of "free" ionic or functional groups present on the surface by varying the ionic strength or pH of the inking solution [32].

The rate at which the polymer is transferred in such processes is also of great interest; the kinetics of transfer of the polymer chains to the surface will influence the processing times for this technique. It is generally known that during the solution adsorption process used to form multilayers, more than 90–95% of the final amount adsorbed is achieved in the first few minutes of the adsorption process, making short contact times feasible for the formation of multilayers. To achieve good surface coverage during the stamping process, the kinetics of macromolecular rearrangements at the surface must be accommodated; for this reason, it is expected that stamping time will be a critical factor in polymer-on-polymer stamping. Furthermore, the solvent used, as well as temperature and other parameters, may greatly influence polymer dynamics and the required time required for contact of the stamp with the surface.

10.3.1.2 **Stamping of Block Copolymers**

Block and graft copolymers present an opportunity to introduce long polymer chains as a means of surface modification; thus these systems are expected to be particularly effective in creating chemical patterns or templates. A second benefit of using block copolymers is the wealth of copolymer systems already in existence and commercially accessible, many of which contain charged or ionizable polymer

segments such as polyvinylpyridine, polymethacrylic acid, polyacrylic acid, sulfonated polystyrene, and many others. Further, a number of straightforward techniques are available to synthesize graft and block copolymers containing a functional group of interest.

In general, a copolymer presents two different chemical groups, one block that acts as an anchor, and interacts with the underlying surface, and a second, functional block that acts to present a new functionality on the surface, as illustrated in the left and center images of the schematic in Fig. 10.12. The stability of chemi- or physisorbed block copolymers on the surface is of critical importance, as the anchoring block must remain bound to the surface, and the polymer chains in the graft segments or second block must provide dense coverage of the exterior of the surface. Rearrangements of copolymers at interfaces can occur when the polymer is introduced to different solvent media due to minimization of interfacial free energy. For this reason, it is important to understand and control the adhesion of the first block to the surface. The stamping of polystyrene–PAA block copolymers has been examined recently [32]. The stability of the monolayer can be tested by examining the contact angle with water following stamping after a series of treatments in aqueous and organic solvents. We have found that when the surface is pretreated to obtain neutral, basic $-NH_2$ groups, the monolayer is more stable than when stamped onto a protonated amine surface containing primarily $-NH_3^+$ groups. Similarly, more stable films are formed at high rather than room temperature. Both of these observations suggest that the formation of covalent, as well as ionic or dipolar interactions, may be critical to the formation of a stable block copolymer monolayer.

Polymer-on-polymer stamping of block copolymers allows patterned modification of the surface properties of a film, and can be used to vary reactivity, charge, or wetting characteristics selectively. For example, a PS–PAA block copolymer stamped onto a polyamine functional surface can yield alternating hydrophobic and hydrophilic regions, as seen in Fig. 10.13. Such surfaces can act as templates for materials deposition, as will be discussed in detail below. A real advantage of this process is that it can be done on virtually any substrate onto which a multilayer can be adsorbed: polystyrene, Mylar® film, ink jet transparencies, glass surfaces, and metals of all types.

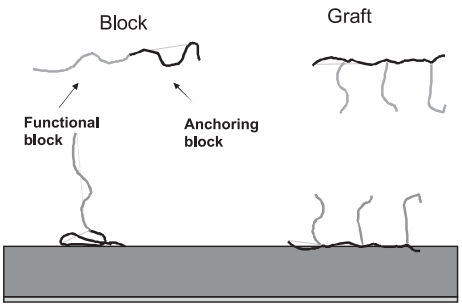

Fig. 10.12 Illustration of surface functionalization via polymer-on-polymer stamping of block and graft copolymers and polyelectrolytes.

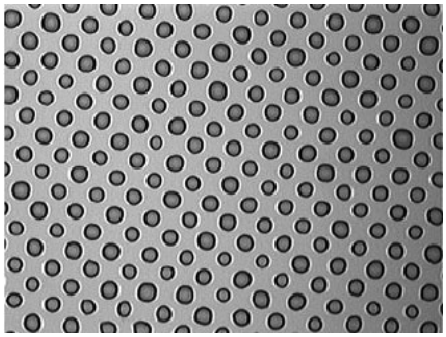

Fig. 10.13 Water condensation figures are formed on an amino functional surface stamped with a PS–PAA block copolymer. The stamped hydrophobic regions are the exterior areas of the pattern, and the underlying amine functionalized hydrophilic regions are circles onto which water droplets are pinned. These results can be achieved on glass and polymer surfaces [29].

In the printing of polymers on multilayer surfaces, the composition of the multilayer surface is a critical component of the stability of the film. In particular, weak polyelectrolyte multilayers can vary a great deal in their thickness, degree of interpenetration, and surface functional density [33, 34]. In collaboration with the Rubner research group at MIT, the role of the weak polyelectrolyte multilayer is currently being examined in polymer-on-polymer stamping. Weak polyelectrolyte systems such as PAH and PAA are also being stamped directly onto multilayer surfaces to create functional amino and acid functionalized surfaces for a variety of applications.

10.3.2 POPS as a Template for Other Materials Deposition

The chemically templated surfaces formed using polymer-on-polymer stamping can be used to direct materials deposition onto glass, metal, semiconductor, and plastic surfaces. By selecting a block or functional polymer with a given interaction or reactivity, various materials deposition processes will be examined. One example of materials deposition is metal plating. Early investigations have shown that polymer-on-polymer stamping can be used to template electroless plating on polymer surfaces. In this work, the electroless plating chemistry developed in the groups of Rubner and Cohen for plating of continuous multilayer films [35] was applied to stamped polyelectrolyte multilayer surfaces in a collaborative effort. An oligoethylene oxide allyl ether–maleic anhydride alternating copolymer (EO–MAL) was stamped atop the PAH surface of a PAA/PAH multilayer. When the substrate is immersed in the catalyst bath, followed by the Ni plating bath, only the regions that were stamped are plated, resulting in a patterned metal film with high edge resolution and fidelity to the original pattern, as seen in Fig. 10.14 [30]; templating may also be accomplished through the use of stamped polyelectrolyte patterns utilizing strong polyelectrolytes. We have found that the metal plated onto the surface exhibits excellent adhesion to the underlying multilayer thin film. This approach provides a simple means of creating micron scale patterned metal regions for electrodes and device applications atop an existing polyelectrolyte multilayer. What is particularly attractive about this approach is that the multilayer may

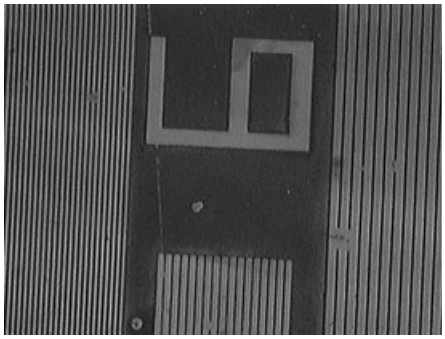

Fig. 10.14 Electroless metal deposition on a polymer template formed by stamping EO–MAL graft copolymer atop the surface of a PAA/PAH polyelectrolyte multilayer. Dark regions are Ni metal, smallest dimensions are 2–3 microns wide [30].

contain a functional system of interest, such as chromic or luminescent films for devices. Further, simple plastic surfaces may be treated with a single or a small number of polyion bilayers, and subsequently patterned without the use of elaborate surface treatments.

A second area in which the techniques described above can be applied to practical problems is the creation of conducting polymer electrodes such as polyaniline and the transparent conducting polymer, PEDOT with micron scale dimensions. Here the real challenges involve achieving unusually high adsorption selectivity on the surface, particularly with polymer systems which can undergo multiple secondary interactions such as hydrogen bonding. Conducting polymers are of particular interest for applications in which flexibility is an issue, such as Mylar substrates. Very recent preliminary results show that we can effectively pattern polyelectrolyte multilayers containing PEDOT (Baytron P® suspension with SPS from Bayer) utilizing alternating COOH/EG functional surfaces. Similar results have been found with polyaniline (PANI) multilayer thin films. At this time, we are continuing to investigate a number of conducting polymers using selective deposition onto patterned substrates, including plastic and silicon substrates. We can also use polymer-on-polymer stamped polyelectrolyte multilayer surfaces as templates for spin cast or solvent cast films of conducting polymers. MacDiarmid and coworkers have shown that alternating hydrophobic and hydrophilic regions of a surface created by laser printing [36, 37] can be used as a means of controlling the morphology of polyaniline deposited on the surface from solution, creating many orders of magnitude difference in the conductivity of films on the hydrophobic versus hydrophilic regions of the surface [36, 38]. In this work, the resolution of patterning was in the range of millimeters. Here we can examine similar effects with micron scale resolution utilizing alternating hydrophobic/hydrophilic surfaces created by stamping of block copolymers such as the PS–PAA system described above; the resulting surfaces can be exposed to a polymerizing bath of polyaniline to create patterned conducting films.

10.4
Directed Assembly of Colloidal Particles

Recently, there has been strong interest in the self-assembly of particles to create ordered structures in two and three dimensions. Such systems have a range of potential applications: functional templates and catalysts for chemical and biological processes, sensor arrays, masks for non-lithographic patterning of deposited species, and novel optical materials and photonic crystal devices. Fabrication of photonic crystals that operate at visible wavelengths, for example, benefits from the sub-micron size scale accessible using self-assembled systems. Self-assembly is thus a tool of great interest based on the need for an inexpensive approach to controlling the arrangement of small objects over large areas.

The stability and adhesion of colloids adsorbed to a molecular monolayer (SAM) can vary to a large extent, depending on the specific interactions of the particle with the surface, and the nature of the monolayer. Adhesion can be improved by manipulating the film thickness, or the density of functional groups on the uppermost surface layers. Further, a number of new applications for ordered colloidal arrays may be realized by incorporating functionality into the underlying layers. An ideal approach would therefore utilize patterned layer-by-layer thin films as functional templates for the assembly of particles on the polymer surface. We recently demonstrated for the first time an approach that utilizes patterned layer-by-layer thin films as functional templates for the assembly of particles on the polymer surface, as shown in schematically in Fig. 10.15 [39], and have extended it utilizing surface chemistry, secondary interactions and confinement effects [40–43]. In this process, multilayers patterned onto alternating COOH/EG surfaces act as regions for deposition of charged particles, and the bare EG regions act as neutral regions which resist particle deposition at standard adsorption conditions. The ability to incorporate functionality in the underlying film is a novel and promising approach that takes full advantage of the layer-by-layer assembly method. The inte-

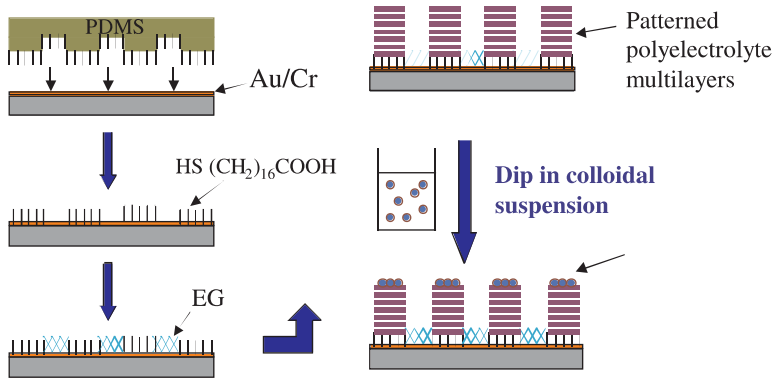

Fig. 10.15 Schematic of approach for templating of colloidal assembly on patterned polyelectrolyte multilayers.

gration of conducting or luminescent polyelectrolyte multilayer films, nonlinear optical dyes, or electrochemical mediators with patterned colloidal assemblies can lead to components in optical or photonics devices or sensors. Further, adhesion of the particle to the surface is greatly enhanced with the use of polymer templates over self-assembled monolayer films derived from low molar mass compounds.

10.4.1 Selective Deposition and Controlled Cluster Size on Multilayer Templates

We have demonstrated control over the density and selectivity of particle adsorption. Three mechanisms have been used to control adsorption of charged particles: 1) Adjustment of the pH of the colloid suspension, which determines the ionization of the uppermost surface of the polyelectrolyte multilayer; 2) adjustment of the ionic strength of the suspension, which determines the extent of charge screening about the colloid and polyelectrolyte; and 3) variation of the concentration of added surfactant, which introduces charge screening on the particle surface, and introduces hydrophobic interactions between the particles and the underlying surface. We have extended the concepts developed above for the selective deposition of polyelectrolyte multilayers onto micron-sized particles, demonstrating the appropriateness of the selective deposition approach for mesoscale as well as molecular scale systems. By varying these parameters, as well as the hydrophobic or hydrophilic nature of the particle surface, we can successfully template particles on the surface. These concepts were first explored in a series of studies utilizing silica particles and negatively charged latex spheres, and SPS/PDAC multilayers patterned as lines on surfaces as a template. When the area of the region of deposition is limited in width, we can direct single lines of particles onto a patterned polyelectroltye template, as shown in Fig. 10.16 (a) [39]. In more recent studies, we have extended this concept and examined the effect of confinement of the adsorbing particle by confining the size of a polyelectrolyte multilayer dot-

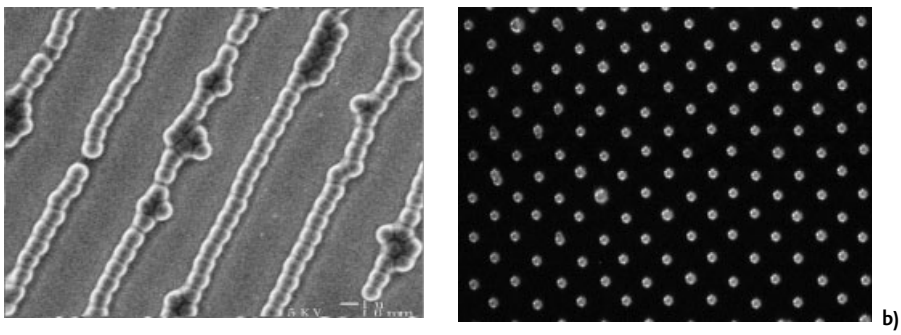

a) b)

Fig. 10.16 Colloids directed to confined regions of a surface arrange in ordered patterns. (a) one micron particles on a two micron wide stripe [39], and (b) a single particle array on a dot pattern multilayer surface [40].

shaped template to achieve a single particle array of particles, as shown in Fig. 10.16 (b) [40]. This concept allows us to direct the organization of colloidal particles and precisely control cluster size and organization on multilayer surfaces by a systematic variation in the size of the multilayer template onto which the particles can adsorb; the result of systematic changes in template size are illustrated in Fig. 10.17. The self-organization technique resulting from this work expands the possibility of fabricating complex micro- and nanostructures by the manipulation of submicron particles via an elegant, self-driven process.

Similar templating effects can also be achieved by using polymer-on-polymer stamping techniques to stamp a polyelectrolyte onto the oppositely charged top surface of a continuous, unpatterned polyelectrolyte multilayer [43]. The resulting patterning of alternating positive and negatively charged regions acts as a template for the deposition of particles, in which the oppositely charged regions attract and the like-charged regions repel the adsorbing particles. The advantages of this technique include the fact that a gold or silicon oxide is no longer needed to template the particle array; a multilayer on any surface will work effectively. It is also possible to stamp a positively charged polymer directly onto a Si oxide surface, and achieve a similar templating effect; however, the presence of the multilayer is important for enhanced adhesion to the original surface.

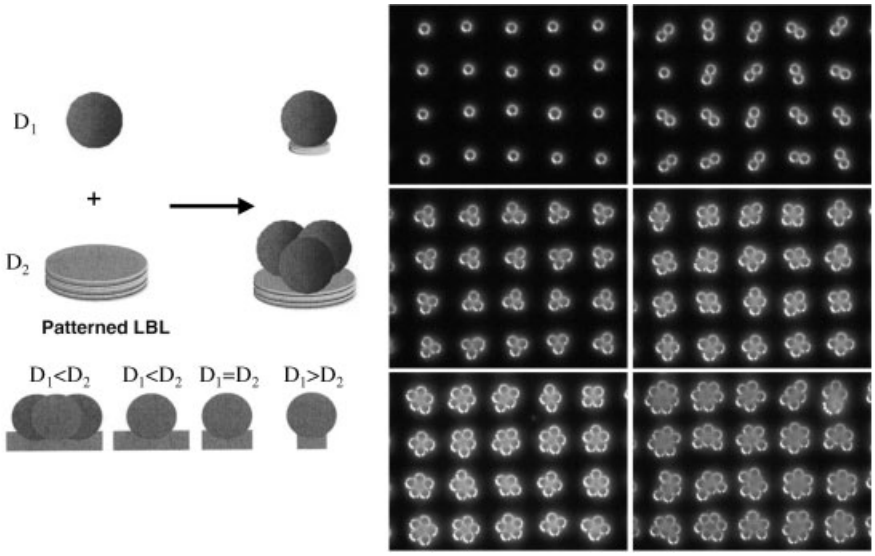

Fig. 10.17 Left: Schematic illustrating effect of confinement in a circular patterned layer-by-layer film in which the dot pattern is varied in size. Right: Controlled colloid cluster arrays adsorbed LBL templates of increasing size from top to bottom and left to right.

10.4.2 Surface Sorting with Particles on Multilayer Surfaces

Mesoscale objects may also be directed using the concept of surface sorting. A significant finding of the colloid adsorption studies was that by simply changing adsorption conditions such as pH and ionic strength, the preferred region of adsorption and degree of selectivity can be changed drastically [39]; these adsorption parameters can be used as tools in the construction of complex particle/polymer assemblies. A unique tool that we have found to be effective in controlling selectivity is the use of a positively charged surfactant, DTAB, added to shield the surface of a negatively charged particle. Without the addition of DTAB, the deposition of negatively charged polystyrene latex particles occurs selectively on the uppermost, positively charged PDAC surface of an SPS/PDAC multilayer via ionic interactions. Hydration and steric forces from the EG SAM resist region effectively prevent deposition of charged particles onto the EG surface. When low concentrations of DTAB are added to the colloidal suspension ($10^{-6} \sim 10^{-5}$ M), the particles deposit primarily on the multilayer surface, but with small increases in their packing density due to favorable inter-particle hydrophobic interactions and increased ionic shielding [39]. As more DTAB, ($10^{-4} \sim 10^{-3}$ M) is added, the surfaces of the particles become increasingly hydrophobic and the selectivity of the particles for the PDAC surface decreases sharply, resulting in little or no selectivity. Finally, at high degrees of shielding, the selectivity is reversed, and deposition occurs preferentially on the EG surface, with no deposition on the positively charged multilayer surface [39]. It was proposed that hydrophobicity is the main driving force in directing spheres to the EG surface when the degree of shielding with DTAB for 0.5 μm spheres reaches about greater than 100% shielding due to favorable interactions between the surfactant on the particle surface and the hydrophobic ethylene groups present in the EG SAM repeat units, in much the same manner that the polyion, PAH, is attracted to the EG surface in a specific pH range. Recent measurements indicate that the sharp transition from the EG SAM as a resist to a region for deposition occurs at about 190 and 95% charge shielding for the 1.0 and 1.9 μm PSS spheres, respectively. By taking advantage of the resulting differences in selectivity, we have successfully fabricated two component colloidal arrays on a single patterned PDAC/EG surfaces simply by varying the conditions for adsorption in each case, as shown in Fig. 10.18 (a) [42].

We can also use hydrogen bond interactions in place of hydrophobic interactions to achieve two component "surface-sorting" of colloidal particles on the multilayer/EG patterned surface. For example, the amidine functional group is known to undergo strong hydrogen bonding interactions. Adsorption of amidine functionalized polystyrene latex particles on an EG/polyelectrolyte multilayer surface at moderate to high pH levels leads to adsorption of the amidine functionalized particles on the EG regions of the surface. The image shown in Fig. 10.18 (b) illustrates the presence of two different sized particles on the surface. In this case, SPS/PDAC multilayers were adsorbed onto the COOH regions of a COOH/EG functionalized gold surface. Negatively charged sulfonated latex particles microns

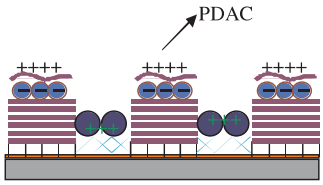

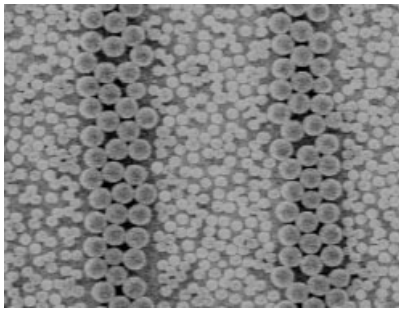

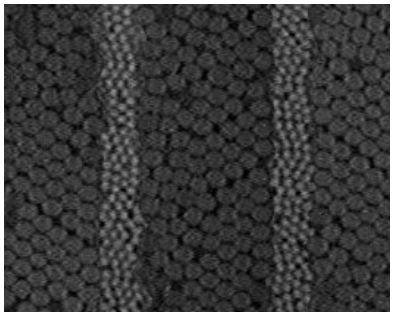

Fig. 10.18 Two different types of particles can be adsorbed to the charged multilayer surface or the alternating oligoethylene glycol monolayer based on ionic charge interactions combined with hydrophobic (left (a) large particles are DTAB shielded) and hydrogen bonding (right (b) large particles are amidine functionalized) interactions [42]. In both cases, small particles are on the multilayer surface, large particles are on the EG surface.

were then adsorbed onto the top layer of PDAC on the polyelectrolyte multilayer films. To prevent the desorption of sulfonated particles on exposure to aqueous basic solution, a single layer of polycation was adsorbed onto the sulfonated particles. Following this adsorption step, a second set of smaller amidine functionalized spheres was then adsorbed onto the EG regions of the surface at high pH [42]. The result for each of these two examples is a patterned two-dimensional array in which particles are confined to specific regions of the surface based on surface chemistry. On both surface regions, in this case, the particles form single monolayer arrays with good edge resolution.

10.4.3
Selective Electroless Plating of Colloidal Particle Arrays

It is possible to utilize the plating chemistry adapted for multilayer thin films [35], and apply it to the selective plating of colloidal arrays. Because catalysts containing a positively or a negatively charged palladium complex can be used to direct electroless nickel plating on charged surfaces, we can utilize this approach to plate the particle without plating the underlying multilayer, or both the multilayer and the particle. Fig. 10.19 shows the results of a two-step metal plating technique for the formation of particle arrays on the surface using the patterned polyelectrolyte multilayer technique, in which metal coated particle arrays on surfaces are prepared [41]. These controlled and stable metal coated particle arrays on surfaces

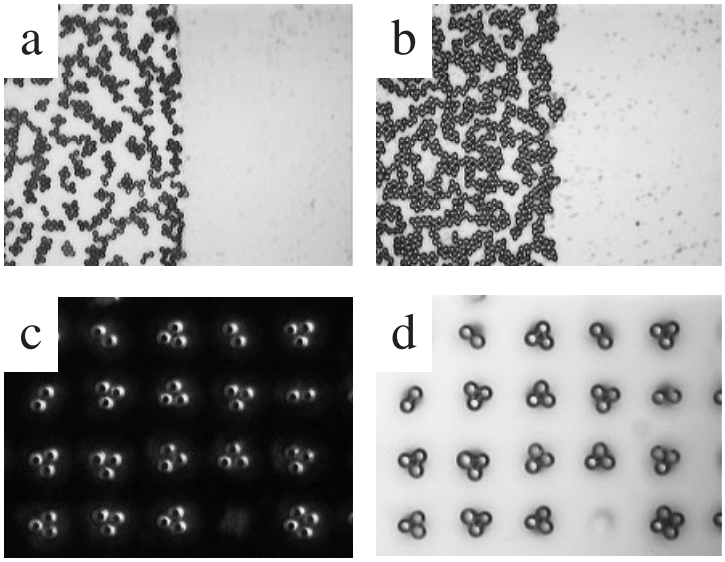

Fig. 10.19 Selective nickel deposition in controlled particle arrays. Catalyst 1 (Na_2PdCl_4) was used in b to plate the multilayer, EG region and particle, and catalyst 2 ($[NH_4]_4PdCl_2$) in a, c, and d, to plate the particle and surrounding EG regions, but not the underlying multilayer
.

have a great potential application in many areas, including opto-electronic and magnetic, sensor, photonic, and bio-chip applications. Samples of 2D colloidal arrays on patterned polyelectrolyte templates were pretreated with Na_2PdCl_4 (a negatively charged Pd complex, see Fig. 10.19b) and $[NH_4]_4PdCl_2$ (a positively charged Pd complex, see Fig. 10.19a, c, and d) at 5 mM concentration in DI water for 10 s; then the pretreated samples were dipped into a Ni bath containing nickel sulfate (Ni source). Negatively charged colloidal particles selectively adsorb on the positively charged multilayer region only, not on the EG SAM resist area, but nickel selectively plates to the positively or negatively charged surfaces depending on the charge of the catalyst. Positively charged Pd complexes also go readily to the EG SAM area.

10.5
Functional Polymer Thin Films for Electrochemical Device and Systems Applications

The motivation for creating patterned thin films is, in many cases, the development of devices and sensors on the sub-micron to millimeter length scale for a number of applications, including displays. Many of the interesting functional properties of polyelectrolyte multilayer films utilize electrochemistry in their application. In this section, preliminary work involving the formation of ionically con-

ducting polyion multilayers, and work focused on the assembly of electrochromic thin films is addressed. The goal of this project has been to construct an electrochromic device using layer-by-layer (LBL) assembly. The elements of such a device are an electrochemically reactive cathode and anode, along with a solid electrolyte that separates the two electrodes and provides sufficient ionic conductivity to support a fast electrochemical reaction within the electrodes. Candidate polymers for anodes and cathodes include the electrically conducting polymers, most of which are electrochromic in the UV–Vis range, and most of which are polycations in the doped state. This class of polymers was originally assembled using layer-by-layer techniques by Rubner et al. [44–48], with a focus on the investigation of electronic conducting properties of these films; our recent studies have examined the electrochemical behavior and electrochromic response of these films on applied potential. Electrochromism and redox behavior within polyelectrolyte multilayers has also been studied by the Schlenoff's research group using polyviologens to form redox-active polymer films [49, 50].

10.5.1
Electrochromic Polyelectrolyte Multilayer Device Construction

In our work, we have constructed solid state electrochromic films containing PANI and poly(3,4-ethylenedioxythiophene): sulfonated poly(styrene) colloid (PEDOT:SPS, Baytron P from Bayer), colayered with several counterpolyions [51]. The redox-active properties of the LBL films containing these two electrically conducting polymers have been demonstrated and characterized by cyclic voltammetry [51]. The films show redox activity typical of the conjugated polymer contained in the film. Co-layering with different polyanions can be shown to affect the number of redox states available in PANI. The spectral electrochemical properties of these films have been also been assessed [51]. Characteristic absorption can be observed at the different redox states for each polymer. For each of the polymers, the neutral, polaron, and (in some cases) bipolaron absorptions can be observed as the polymer is progressively doped to increasing degeneracy.

As PANI is an oxidatively coloring material (anodic electrochrome) and PEDOT is a reductively coloring material (cathodic electrochrome), the two materials were combined into a complementary coloring electrochromic device. This prototype device had an anode material consisting of PANI co-layered with poly(2-acrylamido-2-methyl-1-propane sulfonic acid) (PAMPS), LbL assembled for 20 bilayers – $(PANI/PAMPS)_{20}$. The PEDOT:SPS colloid was co-layered with linear poly(ethylene imine) (LPEI), also assembled for 20 bilayers – $(LPEI/PEDOT:SPS)_{20}$. The electrode materials were LBL assembled atop plasma treated ITO glass with a thickness of about 2000 Å for both. The electrolyte for this first device was a gel electrolyte consisting of a solvent-cast PAMPS film. An electrochromic cell with 40-bilayer elements was also constructed. These devices performed well for first-generation devices from commercially available materials, with a switching speed less than 2 s and maximum optical contrast of 30% (see Fig. 10.20).

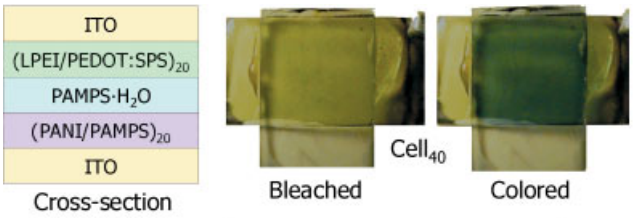

	$Cell_{20}$	$Cell_{40}$
max contrast at:	645 nm	673 nm
max contrast	24%	30%
bleach time	0.37 s	0.66 s
color time	1.22 s	1.77 s
charge/area	0.68 mC/cm²	1.01 mC/cm²
lifetime	>40,000 cycles	untested

Fig. 10.20 Demonstration of colored and bleached cell containing 40 bilayers of each chromic multilayer system. Table gives performance characteristics for 20 and 40 bilayer cell systems.

10.5.2 Ionically Conducting Multilayers for Electrochemical Device Applications

Candidate polymers for the ionically conducting solid polymer electrolyte vary widely, but include those employed as commercial gel-type polyelectrolytes, perfluorinated ionomers, and even weak polyelectrolytes with pH-dependent behavior. In all cases, the strategy in formulating solid electrolytes from LBL thin films has been to create a high dielectric constant, hydrophilic matrix in which small molecule ions (most often protons on polyacids) still contained in the LBL films can dissociate and migrate freely. The analysis of ionic conductivity in LBL thin films is currently underway, and should allow the replacement of the PAMPS gel as an ionic transport medium in the second-generation electrochromic cell with a layer-by-layer polymer system, so that the entire electrochromic cell can be assembled from the bottom up on a conductive substrate. The ionically conductive LBL films offer promise in a number of applications aside from eletrochromic devices, including membranes in lithium polymer batteries and proton exchange membranes in fuel cells. Thus far, (LPEI/PAMPS), (LPEI/PAA), and (LPEI/NAFION) films have been assembled at several pH conditions and tested by impedance analysis [52, 53]. Films constructed using hydrogen bonding interactions, (PEO/PAA), (PEO/PMAA), and (PEO/NAFION), have also been tested [52, 53]. The ionic conductivity of these systems at an intermediate humidity of ~50% varies by four orders of magnitude. The peak conductivity at this humidity is approximately 10^{-8} S cm^{-1}. However, we have shown that the conductivity of a single film can vary by almost 5 orders of magnitude, depending on the level of hydration as determined by relative humidity. At very high humidity conditions, the conductivity of (LPEI/PAMPS) approaches 10^{-5} S cm^{-1}, conductivity appropriate for electro-

chromic devices, but still too small for power delivery applications. Efforts continue to fully explore the response of these films to changes in humidity.

10.6 Summary

Surface chemistry can be used to effectively direct the deposition of layer-by-layer thin films formed from solution. By establishing a set of rules that define the conditions required for selective deposition on specific surface regions for both strong and weak polyelectrolyte adsorption, it is possible to use this understanding for the assembly of complex, multicomponent 2D lateral and 3D film microstructures. Surface patterns can be used to assemble two or more elements of different type onto a surface in a desired arrangement. This concept of adsorption directed by chemistry is universal, in that the same sets of rules derived for polymeric systems can also be applied to meso-scale systems as, including particles, colloids, and biologicial elements. We have successfully expanded this understanding of polyion–surface interactions to mesoscale systems, including functionalized micron sized colloidal particles. Arrays of particles of different surface functionality can be directed to different regions of a substrate, and single particle arrays on a lattice can be assembled on surfaces using patterned polyelectrolyte multilayers as a template. This deposition is driven by the spatially-varied electrostatic and secondary interactions between the colloid and the substrate. New developments include the investigation of hydrogen bonding, and other more specific interactions, as a means of directing the deposition of polymers and other materials.

A second important area of development is the ability to pattern polymer multilayer and other functional surfaces without the use of thiol or silane coupling chemistry, which is appropriate only for metal or metal oxide surfaces. This technique of polymer-on-polymer stamping opens up a broad range of possibilities with respect to the functionalization and manipulation of polymer thin films to make multi-level three-dimensional structures using cheap and easy processing techniques. Plastic substrates may now be used in place of the silicon, metal or metal oxide surfaces needed to functionalize surfaces with alkanethiols or triethoxysilanes. Further, the use of polymer-on-polymer stamping can be used to create multiple level patterns on surfaces and build up three-dimensional microstructures on the surface, in which more than one polymer system can be selectively placed on a surface. Ongoing collaborative efforts have led to new applications using this technique, including its use to direct colloid assembly, electroless metal plating, and even the growth of cells on engineered polyelectrolyte multilayer surfaces. Finally, new approaches to the assembly of polyelectrolyte functional multilayer systems which exhibit ionic as well as electronic conductivity and/or are electrochromic will prove useful for a number of new applications. New patterning techniques, combined with functional polyelectrolyte multilayer systems, lead the way to a wide range of applications in plastic electronics, thin film power devices, electro-optic systems, and biomaterials.

10.7 References

1 B.L. Booth, In *Polymers for electronic and photonic applications*; C.P. Wong, Ed., Academic Press: Boston, **1993**; pp. 549–597.

2 E. Reichmanis, In *Polymers for electronic and photonic applications*; C.P. Wong, Ed., Academic Press: Boston, **1993**; pp. 67–111.

3 P.T. Hammond, G.M. Whitesides, *Macromolecules* **1995**, *28*, 7569–7571.

4 Y. Xia, M. Mrksich, E. Kim, G.M. Whitesides, *J. Am. Chem. Soc.* **1995**, *117*, 9576–9577.

5 A. Kumar, G.M. Whitesides, *Science* **1994**, *263*, 60–62.

6 A. Kumar, H.A. Biebuyck, G.M. Whitesides, *Langmuir* **1994**, *10*, 1498–1511.

7 S.L. Clark, M. Montague, P.T. Hammond, *Supramol. Sci.* **1997**, *4*, 141–146.

8 S.L. Clark, M.F. Montague, P.T. Hammond, *Macromolecules* **1997**, *30*, 7237–7244.

9 S.L. Clark, P.T. Hammond, *Langmuir* **2000**, *16*, 10206–10214.

10 S.L. Clark, E.S. Handy, M.F. Rubner, P.T. Hammond, *ACS Polym. Prepr.* **1998**, *39*, 1079–1080.

11 P. Harder, M. Grunze, R. Dahint, G.M. Whitesides, P.E. Laibinis, *J. Phys. Chem. B* **1998**, *102*, 426–436.

12 R.L.C. Wang, H.J. Kreutzer, M. Grunze, *J. Phys. Chem. B.* **1997**, *101*, 9767–9773.

13 S.I. Jeon, J.H. Lee, J.D. Andrade, *J. Colloid Interface Sci.* **1991**, *142*, 149–158.

14 M. Mrksich, G.M. Whitesides in *Poly(ethylene glycol)*, **1997**; Vol. 680, pp. 361–373.

15 Y.N. Xia, G.M. Whitesides, *Angew. Chem.* **1998**, *37*, 551–575.

16 S.L. Clark, M.F. Montague, P.T. Hammond, *ACS Symp. Ser.* **1998**, *695*, 206–219.

17 M.R. Böhmer, O.A. Evers, J.M.H.M. Scheutjens, *Macromolecules* **1990**, *23*, 2288–2301.

18 G. Decher, J.-D. Hong, *Ber. Bunsen-Ges. Phys. Chem.* **1991**, *95*, 1430–1434.

19 N.G. Hoogeveen, M.A. Cohen Stuart, G.J. Fleer, *J. Colloid Interface Sci.* **1996**, *182*, 133–145.

20 Y. Lvov, G. Decher, H. Mohwald, *Langmuir* **1993**, *9*, 481–486.

21 H.G.M. van de Steeg, M.A. Cohen Stuart, A. de Keizer, B.H. Bijsterbosch, *Langmuir* **1992**, *8*, 2538.

22 S.L. Clark, P.T. Hammond, *Adv. Mater.* **1998**, *10*, 1515–1519.

23 X.-P. Jiang, C. Ortiz, P.T. Hammond, *Langmuir* **2001**, *18*, 2607–2615.

24 X.-P. Jiang, S.L. Clark, P.T. Hammond, *Adv. Mater.* **2001**, *13*, 1669–1673.

25 P. Ghosh, R.M. Crooks, *J. Am. Chem. Soc.* **1999**, *121*, 8395–8396.

26 M. Mrksich, L.E. Dike, J. Tien, D.E. Ingber, G.M. Whitesides, *Exp. Cell Res.* **1997**, *235*, 305–313.

27 T.K. Whidden, D.K. Ferry, M.N. Kozicki, E. Kim, A. Kkumar, J.L. Wilbur, G.M. Whitesides, *Nanotechnology* **1996**, *7*, 447–451.

28 X.-P. Jiang, P.T. Hammond, *Langmuir* **2000**, *16*, 8501–8509.

29 X.-P. Jiang, H. Zheng, S. Gourdin, P.T. Hammond, *Langmuir* **2002**, *18*, 2607–2615.

30 X.-P. Jiang, H. Zheng, J. Choi, M.F. Rubner, P.T. Hammond, *in preparation* **2002**.

31 X.P. Jiang, K.M. Chen, L.C. Kimerling, P.T. Hammond, *Abs. Papers ACS* **2000**, *220*, 301–COLL.

32 X.P. Jiang, P.T. Hammond, *Abs. Papers ACS* **2001**, *221*, 93–PMSE.

33 S. Shiratori, M.F. Rubner, *Macromolecules* **2000**, *33*, 4213–4219.

34 D. Yoo, S.S. Shiratori, M.F. Rubner, *Macromolecules* **1998**, *31*, 4309–4318.

35 T. Wang, B. Chen, M.F. Rubner, R. Cohen, *Langmuir* **2001**, *17*, 6610.

36 D. Hohnholz, A.G. MacDiarmid, *Synth. Met.* **2001**, *121*, 1327–1328.

37 P.C. Wang, Z. Huang, A.G. MacDiarmid, *Synth. Met.* **1999**, *101*, 852–853.

38 Z. Huang, P.C. Wang, A.G. MacDiarmid, Y. Xia, G.M. Whitesides, *Langmuir* **1997**, *13*, 6480.

39 K. Chen, X.-P. Jiang, L.C. Kimerling, P.T. Hammond, *Langmuir* **2000**, *16*, 7825–7834.

40 I. Lee, H. Zheng, M.F. Rubner, P.T. Hammond, *Adv. Mater.* **2002**, *14*, 573–577.

41 I. Lee, M.F. Rubner, P.T. Hammond, *in preparation* **2002**.

42 H. Zheng, I. Lee, M.F. Rubner, P.T. Hammond, *Adv. Mater.* **2002**, *14*, 569–572.

43 H. Zheng, M.F. Rubner, P.T. Hammond, *Langmuir* **2002**, *18*, 4505–4510.

44 J.H. Cheung, A.F. Fou, M.F. Rubner, *Thin Solid Films* **1994**, *244*, 985–989.

45 J.H. Cheung, W.B. Stockton, M.F. Rubner, *Macromolecules* **1997**, *30*, 2712–2716.

46 M. Ferreira, J.H. Cheung, M.F. Rubner, *Thin Solid Films* **1994**, *244*, 806–809.

47 M. Ferreira, M.F. Rubner, *Macromolecules* **1995**, *28*, 7107–7114.

48 A.C. Fou, M.F. Rubner, *Macromolecules* **1995**, *28*, 7115.

49 J. Stepp, J.B. Schlenoff, *J. Electrochem. Soc.* **1997**, *1444*, L155.

50 M. Li, H. Ly, J.B. Schlenoff, *J. Am. Chem. Soc.* **1998**, *120*, 7626.

51 D.M. DeLongchamp, P.T. Hammond, *Adv. Mater.* **2001**, *13*, 1455–1459.

52 D.M. DeLongchamp, P.T. Hammond, *Abs. Papers ACS* **2000**, *220*, 75–POLY.

53 D.M. DeLongchamp, P.T. Hammond, *Abs. Papers ACS* **2001**, *221*, 136–PMSE.

Multilayer Thin Films. Edited by Gero Decher, Joseph B. Schlenoff

Copyright © 2002 Wiley-VCH Verlag GmbH & Co. KGaA
ISBNs: 3-527-30440-1 (Hardback); 3-527-60057-4 (Electronic)

11
Layered Nanoarchitectures Based on Electro- and Photo-active Building Blocks

Xi Zhang, Junqi Sun and Jiacong Shen

Abstract

Layered multilayer assemblies based on electro- and photo-active building blocks were fabricated by the ionic self-assembly technique. It is demonstrated that this technique is a powerful way to fabricate multilayer film-based chemically modified electrodes. By incorporating electroactive materials into multilayers, chemically modified electrodes based on both single and binary active species were fabricated. This technique allows tailoring of the properties of the chemically modified electrodes by incorporating multi-component species in a designed way. By combining the ionic self-assembly technique with post photoreaction between the film, an easy way to fabricate covalently attached multilayer assemblies has been developed. This concept is applicable to building blocks containing diazonium groups and their counterparts containing sulfonate, acrylic acid and even phenol groups. The stability of the covalently attached assemblies increases dramatically when compared with those held together by electrostatic interaction or ionic bonds. It is anticipated that active components could be engineered into stable assemblies that take synergic interaction to produce new functions.

11.1
Introduction

Supramolecular chemistry at interfaces has made continuous progress [1]. When molecular assembly occurs at the liquid/solid or gas/liquid interface, the molecules are in a confined state, in contrast with molecular self-assembly in solution. This may allow fabrication of molecular assemblies with controlled composition and orientation. Many types of state-of-the-art surface and interface instruments can be used to characterize the assembling process in situ. Moreover, this may facilitate the integration of molecular architecture and functional assembly, leading to various thin-film-based devices and sensors.

There are many kinds of interfacial assembly techniques, such as the Langmuir–Blodgett (LB) technique [2], self-assembly based on interfacial chemical reaction [3], the layer-by-layer (LbL) assembly technique [4], etc. Among them, the io-

nic self-assembly technique, introduced by Decher in 1991 [5], provides an elegant way of controlling the composition of the resulting assemblies and the thickness of an individual layer on the nanometer scale. Large varieties of charged materials, including almost all kinds of polyions, dyes, organic/inorganic particles, proteins, viruses, and other biosystems have been incorporated into multilayer assemblies using this technique [6, 7]. These thin film assemblies have potential applications in nonlinear optical materials [8], conductive films [9], permselective gas membranes [10], light emitting devices [11, 12], sensors [13], etc.

Furthermore, the driving force for the layer-by-layer assembly need not be electrostatic interaction. Other forces, such as hydrogen bonding [14, 15], coordination bonding [16, 17], charge transfer [18], molecular recognition [19], etc. can also be used as the driving force for the assembly process. For example, the alternating deposition between polyelectrolyte and bolaform amphiphile bearing mesogenic groups led to the formation of multilayer assemblies with an improved interfacial structure, as shown in Fig. 11.1A [20]. The driving force for the layer buildup is electrostatic interaction as well as π–π stacking. Xiong et al. fabricated a multilayer film on the basis of coordination bonds by alternate adsorption of poly(copper 4-styrene sulfonate) (PSS-Cu) with poly(4-vinylpyridine) [16]. Through in situ chemical reaction, an organic–inorganic hybrid nanocomposite can be obtained, as shown in Fig. 11.1 B. Moreover, Wang et al. fabricated alternate multilayer assemblies of poly(4-vinylpyridine) and poly(acylic acid) based on hydrogen bonding between pyridine and acrylic acid (Fig. 11.1 C) [14]. Even though FTIR data have clearly revealed that hydrogen bonding is the dominant driving force for the layer-by-layer assembly, recent data of single molecular force spectroscopy have demonstrated that the force value was much larger than that of hydrogen bonding, indicating that combined interaction of different forces must be responsible for the multilayer formation. Actually, in most cases, multilayer assemblies are not based

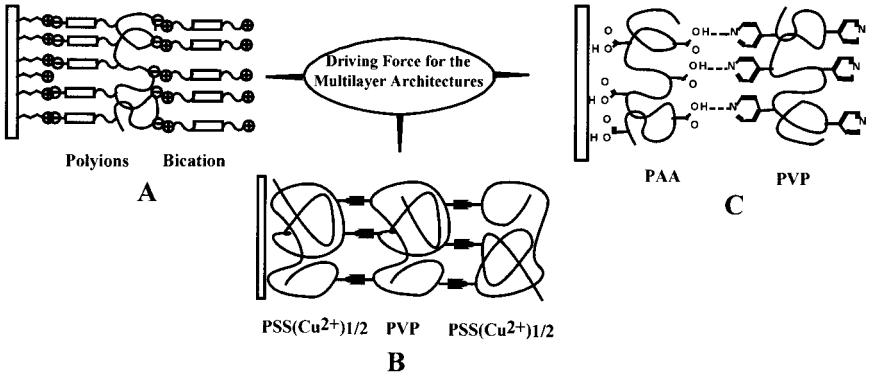

Fig. 11.1 Attempts to fabricate layered nanoarchitectures: (A) Electrostatic multilayer assemblies of polyelectrolyte and bication bearing a mesogenic group; (B) multilayer assemblies of PSS$(Cu^{2+})_{1/2}$ and PVP based on coordination bonding; (C) multilayer assemblies of PAA and PVP based on hydrogen bonding.

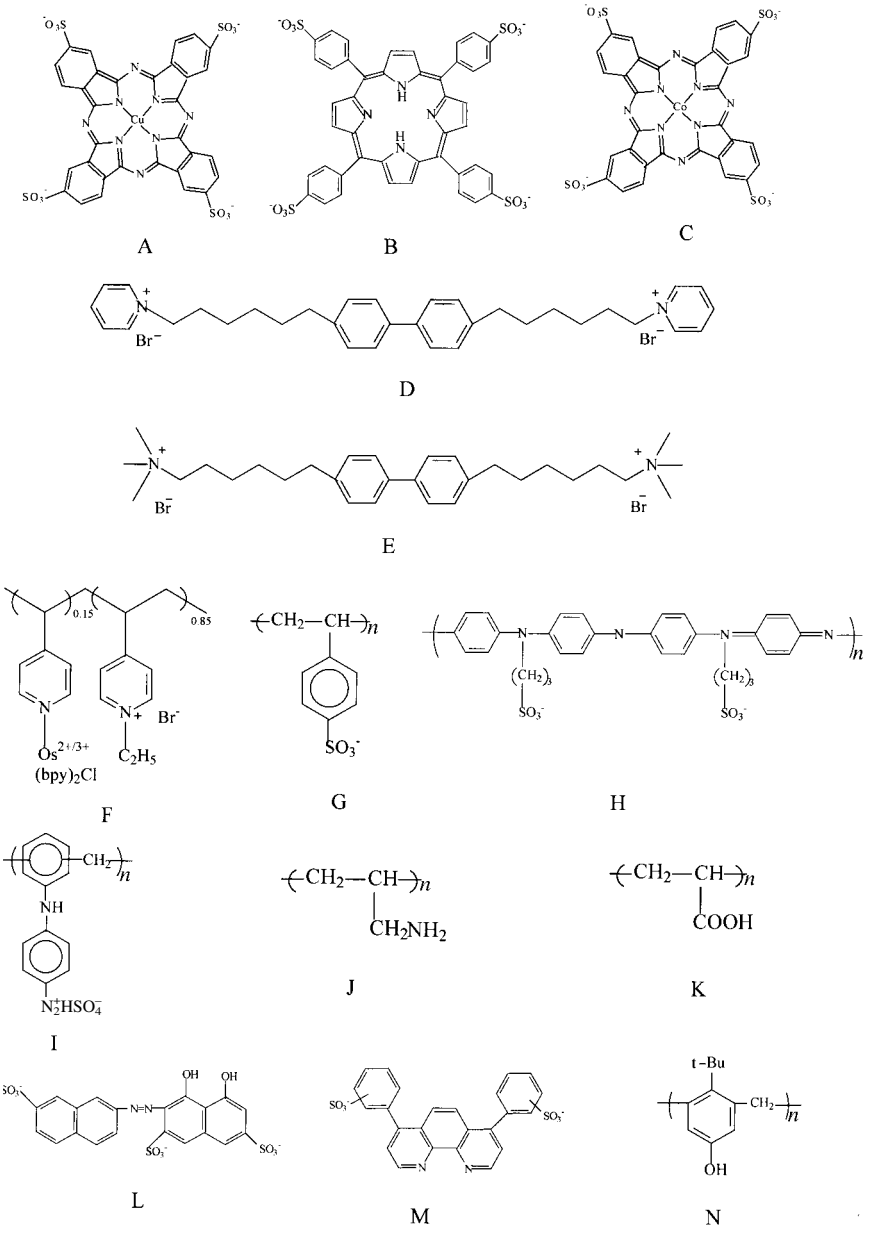

Fig. 11.2 Building blocks for layer-by-layer assembly. (A) CuTsPc, (B) $tpps_4$, (C) CoTsPc, (D) PyC_6BPC_6Py, (E) NC_6BPC_6N, (F) PVP-Os, (G) PSS, (H) PAPSAH, (I) DAR, (J) PAH, (K) PAA, (L) SNAN, (M) BST and (N) PR.

on a single type of driving force, but on a synergetic interaction of several kinds of forces.

Among other charged species, assemblies of electro- and photo-active materials have attracted considerable attention. On the one hand, these materials will endow the resulting assemblies with novel properties and finally realize functional assemblies due to the boundless materials with different functions that can be incorporated. On the other hand, assemblies with photo- and electro-active groups will provide models for the investigation of the relationship between nanostructures and their functions. The integration of nanoarchitecture and function in one self-assembly system is one of the ultimate goals of scientists and the best way to fabricate nanosized devices and sensors [21]. However, there is still a long way to go to bridge the gap between structural architecture and functional assemblies.

In this chapter, the assemblies of electro- and photo-active polyelectrolytes produced by the ionic self-assembly technique, based mainly on our work, will be presented and discussed in detail. All the building blocks used are shown in Fig. 11.2.

11.2 Multilayer Assemblies of Electroactive Species for Chemically Modified Electrodes

The interest in chemically modified electrodes (CMEs) has increased tremendously during the last decade. To develop a general method for production of CMEs in which electroactive materials can be controlled at the molecular level and deposited in a three-dimensional manner is of importance not only in basic research but also in technical applications. It is known that there exist several strategies for fabricating high quality CMEs [22]. Covalent immobilization and self-assembly of alkanethiol-containing electroactive compounds have proved to be particularly attractive. Polymers have been coated onto electrodes by dipping, spin coating, organosilane bonding, electrochemical precipitation and polymerization, adsorption from solution, and plasma discharge polymerization, etc. However, there are also requirements to produce multilayer-based CMEs, which guarantee that both the type and quantity of electroactive materials will be loaded onto the electrode surface in a controlled way. Ionic self-assembly of charged electroactive materials may be an alternative approach to the fabrication of CMEs.

Since Sun et al. reported the first example of a chemically modified electrode fabricated by the ionic self-assembly technique in 1995 [13], the research and fabrication of CMEs or sensors based on this technique has received extensive interest. A large variety of chemically modified electrodes and sensors have been fabricated and their properties have been well studied [13, 23–30]. The ionic self-assembly technique has three main advantages over other techniques when used to fabricate CMEs: (1) It is applicable to electrodes of any material, size and topology. This is due to the self-adjusting ability of the technique, which makes the influence of the substrates on which the layers are built up decrease after several cycles of deposition. (2) It is particularly suitable for the production of chemically

modified electrodes with multi-components in a designed way. This is determined by the ability of this technique to produce three-dimensional composite multilayer assemblies. Usually, the detection of the substrates in these types of electrodes is based on a series of reactions between the substrate and the electroactive materials bound to the electrode surface. The sequence of the materials assembled on the electrode surface will play an important role in the detection of the substrate. (3) Electrodes fabricated by this technique are satisfactory with respect to their reproducibility. This originates from the ability to control the assemblies at the molecular level.

11.2.1
Controlled Fabrication of Multilayers with a Single Active Component

The ionic self-assembly technique can be used to fabricate layered nanoarchitectures not only for polyelectrolytes, but also for oligo-charged species, e.g., disk-shaped porphyrins and phthalocyanines containing sulfonic groups. These porphyrins and phthalocyanines are planar conjugating molecules that have unique physiochemical properties. Assembly of these molecules into multilayer assemblies can find applications in catalysis, voltaics, electrochromics and nonlinear optics, etc. Zhang et al. incorporated meso-tetra(4-suofonyl)porphyrin ($tpps_4$) or copper phthalocyanine tetrasulfonic acid, tetrasodium salt (CuTsPc) into multilayer assemblies by a method based on the ionic self-assembly technique, alternately depositing with bipolar pyridine salt (PyC_6BPC_6Py) [31]. Furthermore, this technique has been utilized to fabricate functional supramolecular assemblies of pure rigid porphyrin and phthalocyanine [32]. Combining the ionic self-assembly and electroanalytical chemistry, we have demonstrated a series of chemically modified electrodes of porphyrins and phthalocyanines which have the ability to detect Cu^{2+}, I^-, carbohydrates, glucose, hydrazine, etc. in solution [13, 23–25]. At the beginning of this work, single component electrodes were fabricated on which only one type of electroactive material was alternately deposited on the electrode surfaces. This method of constructing electrodes is simple, but has provided a new way to fabricate complex sensing surfaces, as summarized in Tab. 11.1.

Copper(II)-selective electrodes based on mixed copper(II) sulfide and silver(I) sulfide membranes have been reported in the past. The nature of the potential response of these kinds of electrodes is complex and their sensitivity towards copper (II) ions is lost in highly oxidizing systems or in the presence of chloride ions. Therefore the development of potentiometric copper (II) sensors with good performance remains a fascinating challenge for scientists. Herein, we discuss a new kind of copper(II)-selective electrode fabricated by alternately depositing negatively charged copper phthalocyanine tetrasulfonic acid (CuTsPc) with a bipolar pyridine salt (PyC_6BPC_6Py) on a gold electrode [13]. The original motivation was to characterize the multilayer assemblies of $CuTsPc/PyC_6BPC_6Py$ with an electroanalytical method. We failed in this regard because of the very small redox currents. However, it shows, interestingly, a potential dependence on the copper(II) ions. Compared with conventional copper(II)-selective electrodes, it has advantages such as

Tab. 11.1 Examples of chemically modified electrodes fabricated by ionic self-assembly

Assemblies	*Electrode*	*Detection*	*Comments*	*Ref.*
CuTsPc/PyC_6BPC_6Py	Gold	Cu^{2+}	1×10^{-5}–0.1 mol L^{-1}, potentiometry	[13]
CoTsPc/PyC_6BPC_6Py	Gold	Carbohydrates	Detection limit: 150 pmol for glucose, 6 pmol for maltose	[23]
CoTsPC/PyC_6BPC_6Py	Gold	Hydrazime	1×10^{-5}–1×10^{3} mol L	[24]
$tpps_4$/polypyrrole	Silver	I^-	1×10^{-6}–0.1 mol L	[25]
PVP-Os/PSS PVP-Os/PAPSAH	Gold	NO_2^-	PAPSAH can improve the response of the electrode	[26]
Bis-bipyridinium/Au nanoparticles	ITO	*p*-Hydroquinone	Receptor-colloid superlattice acts as a rough interface for the preconcentration and electrochemical interface	[27]
Glucose oxidase/ferrocene derivative	Gold	Glucose	An electrical "wire" is introduced between glucose oxidase and electrode surface	[28]
Polyoxometalate/PVP-Os	Gold		Cyclic potential sweeps was used for the multilayer deposition	[29]
Glucose oxidase/glucoamylase	Gold	Maltose/glucose	Take the co-functions of bienzyme for catalyzing	[30]

low resistance, short conditioning time, fast response and perfect operation in the presence of chloride ions.

The fabrication of CuTsPc/PyC_6BPC_6Py multilayer assemblies on a gold electrode is shown schematically in Fig. 11.3. A freshly cleaned gold electrode was immersed in an ethanolic solution containing 0.01 M 3-mercaptopropionic acid to get a self-assembled monolayer. Afterwards, the gold electrode with negatively charged surface was alternately immersed in aqueous solutions of PyC_6BPC_6Py (0.5 mg ml^{-1}) and CuTsPc (0.1 mg ml^{-1}), and washed with water and dried in N_2. By repeating the two immersion steps in a cyclic fashion, an electrode modified with a multilayer of PyC_6BPC_6Py/CuTsPc can be obtained. The progressive deposition was confirmed by means of UV–Vis spectroscopy. In the experiments, a gold electrode with 6 layers of CuTsPc deposited on it was used throughout. Between measurements, the sensor was stored in a dry state at room temperature.

Fig. 11.4 shows cyclic voltammograms of a gold electrode modified with 6 layers of CuTsPc in 0.2 M acetate buffer solution (pH 4.5). It can be seen that a pair of redox peaks of CuTsPc appear in the potential range +0.8 to –0.5 V (vs. SCE) in each cyclic voltammogram. The peak current of the electrode modified with 6 bilayers of PyC_6BPC_6Py/CuTsPc is proportional to the square root of the scan rate. This indicates that CuTsPc has been modified on the gold electrode and the elec-

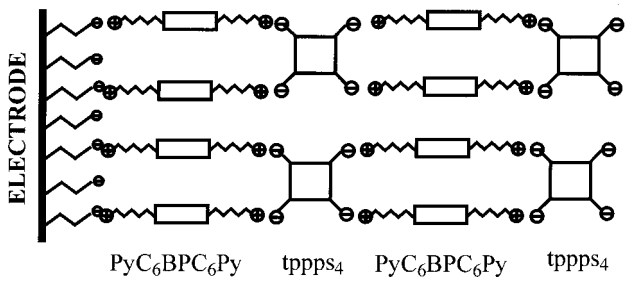

Fig. 11.3 Schematic illustration of the structure of a CuTsPc/PyC_6BPC_6Py modified electrode.

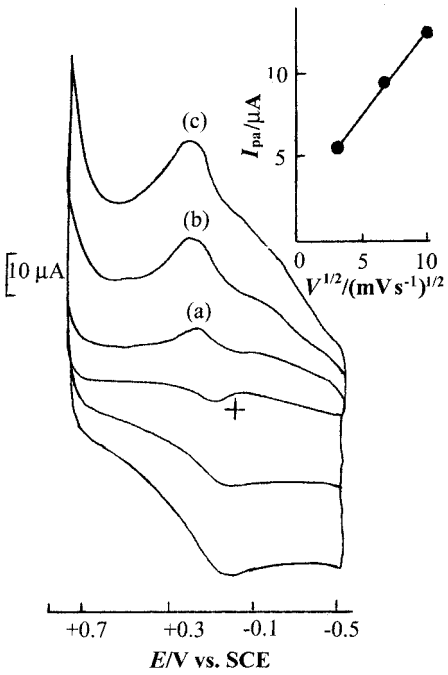

Fig. 11.4 Cyclic voltammograms of the Au electrode modified with 6 layers of CuTsPc in 0.2 M acetate buffer (pH 4.5). Scan rate: (a) 10, (b) 50, (c) 100 mV s^{-1}. The inset shows anodic peak current as a function of the square root of the scan rate.

trochemical reaction in the multilayer assemblies is a diffusion-controlled redox process.

It was found that the properties of the PyC_6BPC_6Py/CuTsPc modified electrode were dependent on the pH of the solution. A stable response potential was obtained in a pH range of 1–5 in 0.2 M potassium nitrate in the presence of 1×10^{-3} M copper (II). Meanwhile, we also found that there existed a dependence of the response of the electrode on the types of buffer at the same pH value and concentration. As indicated in Fig. 11.5, the electrode has its best performance in the acetate buffer and potassium nitrate solutions, with its response slopes being 29 and 31 mV $decade^{-1}$, respectively. In sodium dihydrogenphosphate medium, the response of the elec-

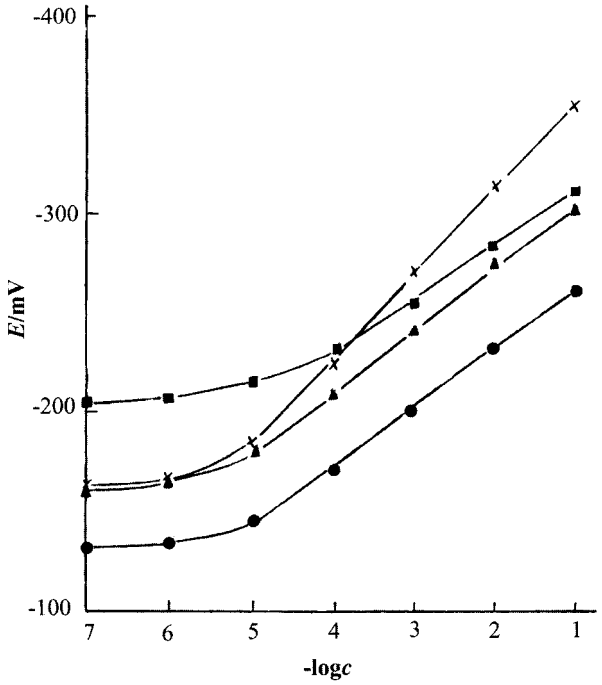

Fig. 11.5 Effects of different buffer media on the responses of the electrode to copper (II). Buffer: 0.2 M, pH 4.5, sodium dihydrogenphosphate (■); acetate (●); potassium nitrate (▲); potassiumchloride (×).

trode was worst, with a response slope of 25 mV decade^{-1} and linear range between 10^{-4} and 10^{-1} M. In a potassium chloride medium, the response of the electrode was good, but its response slope of 41 mV decade^{-1} was higher than Nernstian.

From the typical calibration graph for the gold electrode modified with 6 layers of CuTsPc in an optimized condition of 0.2 M acetate buffer (pH 4.5), it can be seen that the electrode has a linear response over the range 1×10^{-5} to 0.1 M with a Nernstian response slope of 29 mV decade^{-1} and a detection limit (extrapolation of linear graph) of 7×10^{-6} M. The typical dynamic response time of the electrode (t_{95}) was 15–30 s with stirring. The steady state potential response after the addition of copper (II) remained constant for 60–120 s, then slowly increased in the negative direction and reached a final steady potential value.

The potential response of the electrode towards copper (II) ions has a good reproducibility. The relative standard deviation (RSD) is 1.7% for ten determinations of 1×10^{-5} M Cu^{2+} at pH 4.5 in 0.2 M acetate buffer. The selectivity of the electrode toward copper(II) is very satisfactory, as shown in Tab. 11.2. Except for Fe^{3+}, Fe^{2+} and Co^{2+}, other common inorganic cations do not interfere in the determination of copper (II). The interference of Fe^{2+} ions can be eliminated by oxidizing

Tab. 11.2 Selectivity coefficients of CuTsPc/PyC_6BPC_6Py modified copper(II) selective electrode

Cation	$\log K_{ij}^{pot}$	*Cation*	$\log K_{ij}^{pot}$
Ca^{2+}	–3.0	Al^{3+}	–3.0
Mg^{2+}	–3.0	Co^{2+}	–1.0
Zn^{2+}	–3.1	Mn^{2+}	–3.0
Cd^{2+}	–3.0	Fe^{3+}	0
Ni^{2+}	–3.1	Fe^{2+}	0
Pb^{2+}	–3.2		

them to Fe^{3+}, which can be masked with F^- ions. Anions such as NO_3^-, Cl^-, acetate and SO_4^{2-} do not interfere with copper (II) during the detection.

As metallophthalocyanines and porphyrins represent a family of compounds well known for their catalytic activity for a wide range of redox processes, a similar concept can be applied to fabricate chemically modified electrodes with designed sensing properties. When CuTsPc is replaced by cobalt phthalocyanine tetrasulfonate (CoTsPc), PyC_6BPC_6Py/CoTsPc alternating assemblies can be fabricated similarly on gold electrodes. It was found that the gold electrode modified with 6 bilayers of PyC_6BPC_6Py/CoTsPc exhibited an excellent electrocatalytic response for the oxidation of hydrazine, therefore it could act as an amperometric sensor of hydrazine [24]. In combination with flow-injection analysis, hydrazine can be detected with high sensitivity using the above electrode. The linear response of the electrode towards hydrazine ranges from 1×10^{-3} to 1×10^{-6} M, with a detection limit of 6×10^{-7} M. Meanwhile, this electrode also shows an electrocatalytic response for the oxidation of carbohydrates, such as glucose, fructose, sucrose and maltose, as shown in Tab. 11.1 [23]. Furthermore, tetraphenylporphine tetrasulfonic acid ($tpps_4$) can alternately assemble with polycationic polypyrrole on a silver electrode, which can act as a potentiometric sensor for iodide ions [25]. The electrode has good selectivity compared with a poly[tetrakis(*p*-aminophenyl)porphyrin] film-modified electrode.

As mentioned, the above electrodes fabricated by the ionic self-assembly technique have many advantages. Among them, the incorporation of more than one kind of correlative electroactive species in a designed way, which may endow the electrode with novel functions by a synergetic effect of these electroactive species giving better results than any one of them alone.

11.2.2
Controlled "Cascade" Modification with Binary Active Components

The assembly of ultrathin films containing biological macromolecules such as proteins and DNA has attracted considerable interest, e.g. for the construction of bioreactors and biosensors containing enzymes and other biological catalysts. Protein can be adjusted to be anionically or cationically charged by simply changing the pH value of the solution to be higher or lower than its isoelectric point (IEP). In this sense, proteins can be treated as anionic or cationic polyelectrolytes and al-

ternately assemble with oppositely charged species. Kong et al. extended the concept of Decher and immobilized glucose isomerase in a layer-by-layer fashion by alternating deposition with a bipolar amphiphile [33]. Moreover, the same concept was applied to enzyme immobilization in porous trimethylamine polystyrene [34]. To our knowledge, this is the first demonstration of ionic self-assembly on a non-flat substrate. At almost the same time, Lvov et al. constructed multilayer films containing DNA [35], biological colloids such as charged virus particles [36], and many other enzymes such as myoglobin (Mb), lysozyme (Lys), hemoglobin (Hb) and glucose oxidase (GOD), etc. [37]. The possibility of creating ordered protein layers on a solid substrate opens the way for microreactors and biosensors.

11.2.2.1 **Bienzyme Assemblies of Glucose Oxidase and Glucoamylase**

Glucose oxidase (GOD) and glucoamylase (GA) are widely used enzymes in the fields of enzyme engineering and biosensors. Sun et al. selected GOD and GA as a model system to demonstrate the possibility of incorporating these two enzymes in one-multilayer assembly. GOD and GA have IEPs of pH 4.3 and 4.2, respectively. Under a deposition condition of pH 7.0, both enzymes can become negatively charged. So a positively charged bipolar quaternary ammonium salt NC_6BPC_6N was used to alternately assemble with these two enzymes. An enzyme multilayer film was fabricated in which GOD and GA are alternately sandwiched between the bi-cationic compound NC_6BPC_6N [30]. Quartz crystal microbalance (QCM) measurements show that both GOD and GA are loosely, rather than densely packed in the film. The relatively loose packing of enzymes is favorable for the easy diffusion of the substrate in the film, which will guarantee that the reaction of the substrate with the immobilized enzyme proceeds smoothly.

Fig. 11.6 shows the change in overall activity of the bienzyme in multilayers with the number of layers. The total activity increases with the number of layers, which means the higher the number of layers deposited, the more enzyme is immobilized. On the other hand, since the diffusion of the substrate plays an important role in the determination of enzyme activity, the average activity per enzyme layer decreases with the increase in the number of layers. These results are consistent with those reported previously.

In the electrochemical experiment, two layers of GOD followed by two layers of GA were alternately deposited with NC_6BPC_6N on the surface of a 3-mercaptopropionic acid modified gold electrode. The conceptual construction of bienzyme multilayer assemblies is shown schematically in Fig. 11.7. The enzymes were arranged in this way in the multilayer film because of the coupled reaction between GOD and GA, as shown below:

$$\text{Maltose} + H_2O \xrightarrow{\text{Glucoamylase}} \text{2D-Glucose}$$

$$\beta\text{-D-Glucose} + O_2 \xrightarrow{\text{Glucose Oxidase}} \text{Gluconic} + H_2O_2$$

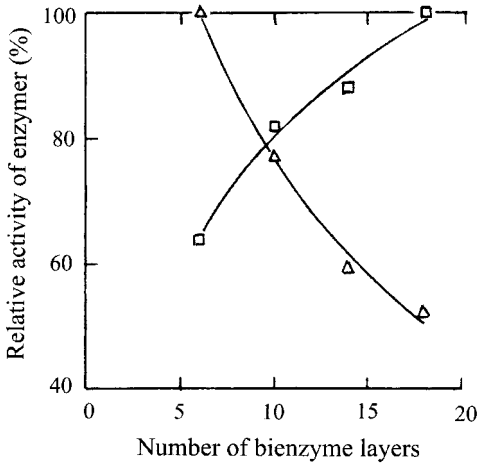

Fig. 11.6 Relationship between relative activity and the number of bienzyme layers. Total activity of bienzyme on the slide (□); average activity per bienzyme layer (△). (Total activity of 18 layers of bienzyme is defined as 100% in curve (□); average activity of 6 layers of bienzyme is defined as 100% for curve (△)).

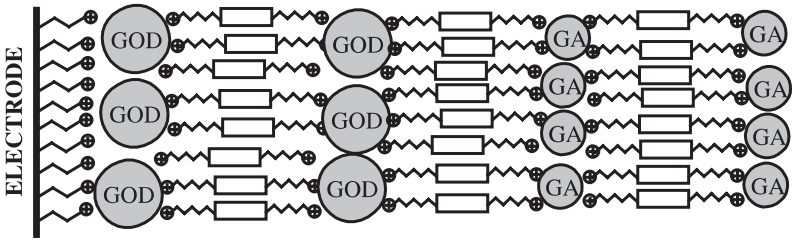

Fig. 11.7 The schematical construction of a bienzyme multilayer of GOD and GA on a gold electrode surface.

$$H_2O_2 \longrightarrow O_2 + 2e^- + 2H^+$$

The resulting multilayer can act as a maltose sensor in which maltose can first react with outside GA layers to produce glucose. β-D-glucose then diffuses and reacts with the inside GOD layers to produce H_2O_2, which is oxidized on the electrode surface and detected. Fig. 11.8 shows a typical maltose response curve, from which it can be seen that the time required to reach 95% of the steady-state current is less than 60 s after the addition of maltose. The calibration curve for the determination of maltose is given in Fig. 11.9. A linear relationship up to 6 mmol L^{-1} was obtained between the response current and the maltose concentration. In comparison with a similar electrochemical sensor, the uppermost detection concentration of the present sensor is higher. The reason being that the multilayer limits the diffusion of the substrate and reduces the effective substrate concentration within the enzyme layer to well below the saturation threshold.

It was confirmed that only when GA and GOD are fabricated rationally on the surface of gold electrode could the sensor be used to detect maltose. The GA as-

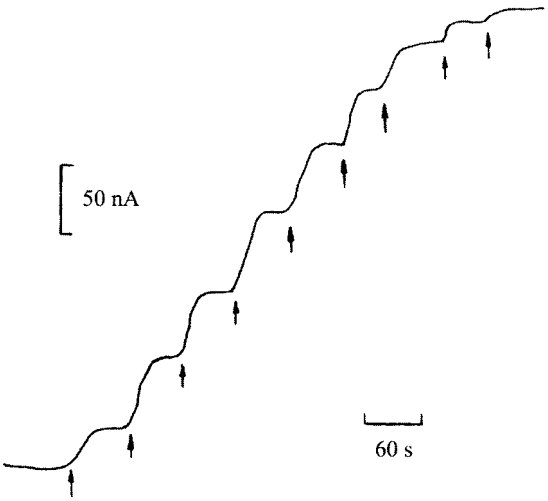

Fig. 11.8 Typical response of the sensor to addition of maltose. Arrows indicate the addition of 0.1 mL of 0.1 M maltose to the test solution (initial solution volume 10 mL). Operating potential controlled at +0.7 V vs. SCE. 0.1 M phosphate buffer of pH 7.0 was used as the supporting electrolyte.

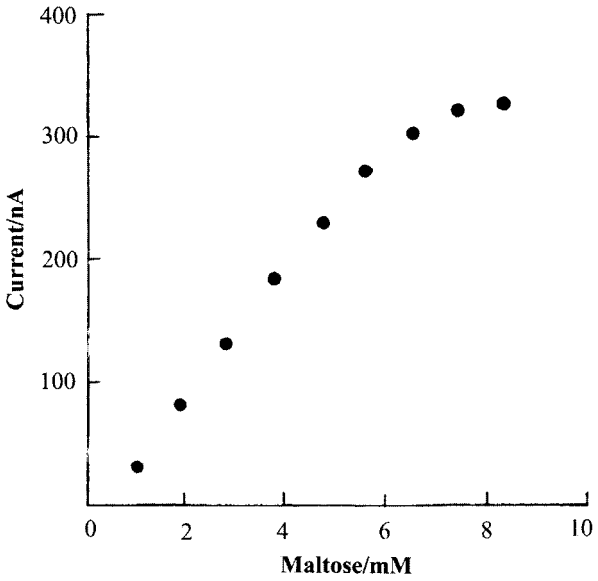

Fig. 11.9 Relationship between steady-state current and concentration of maltose.

sembled alone on the gold electrode does not have the ability to detect maltose. This supports the idea that new functions could come from assemblies. Meanwhile, it was discovered that the gold electrode fabricated with GOD and GA can catalyze the oxidation of glucose due to the existence of the inner GOD layers. For the determination of either maltose or glucose, the current response examined was all the oxidizing current of H_2O_2 that was produced in the enzymatic reactions.

11.2.2.2 Alternating Assemblies of Glucose Oxidase and Polycationic Electron Transfer

The redox active centers of GOD, i.e., flavin adenine dinucleotide (FAD)/hydrogenated flavin adenine dinucleotide ($FADH_2$) are situated at the inner core of the glycoprotein, and covered by a non-conducting oligosaccharide shell. This makes direct electron transfer between GOD and the electrode surface on which it was immobilized difficult. An efficient method to solve this problem is to establish an easy electrical communication between GOD and the electrode surface by using an electron mediator. Its role can be described as follows:

$$\text{Glucose} + \text{GOD(FAD)} \rightarrow \text{Gluconic acid} + \text{GOD}(FADH_2)$$

$$\text{GOD}(FADH_2) + 2M_{ox} \rightarrow \text{GOD(FAD)} + 2M_{red} + 2H^+$$

$$2M_{red} \rightarrow 2M_{ox} + 2e^-$$

Here GOD(FAD) and GOD($FADH_2$) represent oxidized and reduced forms of GOD, M_{ox} and M_{red} the oxidized and reduced forms of the mediators. The intimate contact between the GOD redox centers and the electroactive species facilitates the flow of electrons from the enzyme to the electrode surface.

Combining the enzyme assembly with the concept of electron transfer, we have realized alternating assemblies of GOD and quarternized poly(4-vinylpyridine) partially complexed with $[Os(bpy)Cl]^{+/2+}$ (PVP-Os) on the surface of a gold electrode [38, 39]. The ideal structure of PVP-Os/GOD multilayer assemblies on the surface of a gold electrode is shown in Fig. 11.10. As indicated in this figure, the adsorbed PVP-Os on the underlayer GOD could fold along the enzymes and penetrate into them, thus mediating electron transfer from the $FADH_2$ center of the enzyme to the electrodes. Fig. 11.11 shows the response of a 3-bilayer PVP-Os/GOD modified gold electrode in the presence of 40 mM glucose. In the absence

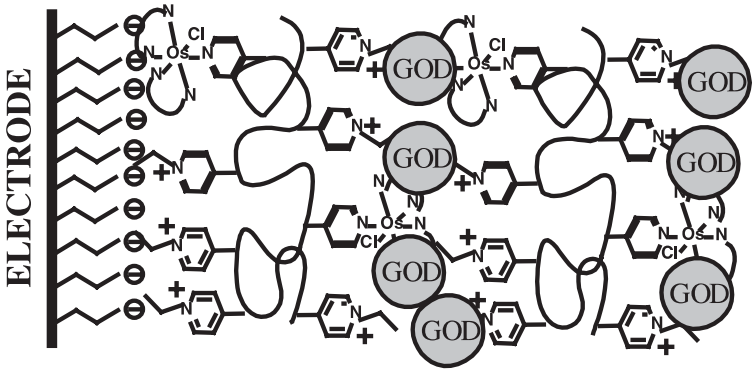

Fig. 11.10 The ideal structure of PVP-Os/GOD multilayer assemblies on the surface of a gold electrode.

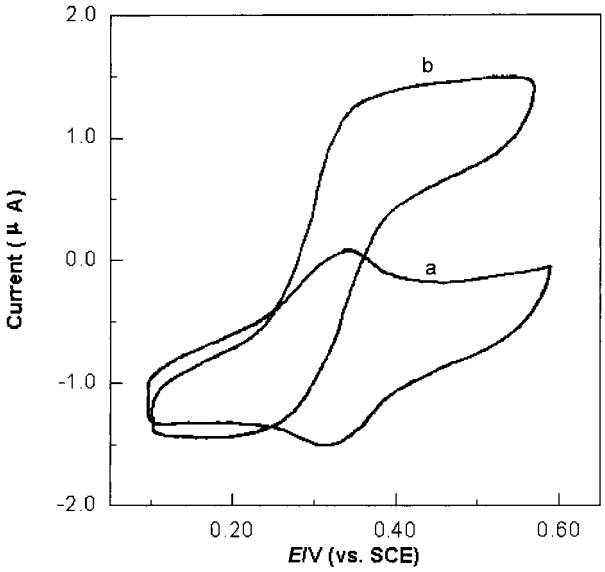

Fig. 11.11 Cyclic voltammograms of the three bilayers of a PVP-Os/GOD modified electrode (a) without glucose and (b) in the presence of 40 mmol l^{-1} of glucose. Conditions: 0.1 mol l^{-1} phosphate buffer, pH 6.4: scan rate 5 mV s^{-1}.

of glucose, a pair of cathodic/anodic peaks of almost equal magnitude could be observed over the range 0.1 to 0.6 V (*vs.* Ag/AgCl), which corresponds to the reversible redox reaction of PVP-Os. Upon addition of glucose, an obvious increase in the oxidative current and concomitant decrease in the reductive current were found, indicating that GOD was reduced by glucose diffusing into the assembled films, then electrons were transferred through the polymer bearing osmium complex films to the electrode surface. From the dependence of the glucose catalytic oxidation current on the electrode potential, the optimized potential for the detection of glucose could be selected as 0.35 V (vs. SCE), which is much lower than without electron transfer. At this low potential, the influence of some interfering materials, such as ascorbic acid and uric acid can be largely eliminated.

11.2.3
The Incorporation of Conductive Species to Improve the Performance of the Modified Electrodes

It thus has been proven that the ionic self-assembly technique is a very easy and efficient way to fabricate a composite film modified electrode, in which more than one kind of electroactive material can be incorporated in the normal direction of the electrode surface. The properties of the electroactive material in the multilayer-modified electrode will depend much on the way it is assembled. It is meaningful to investigate the structure-related function in multilayer-modified electro-

des in order to find a general way to improve their performance. We have studied comparatively the molecular assemblies of PVP-Os with the conductive polyanion of poly(aniline-*co*-*N*-propanesulfonic acid aniline) (PAPSAH) [40] and the non-conductive polyanion of poly(sodium 4-styrene sulfonate) (PSS) in an attempt to find a way to improve the performance of the chemically modified electrodes fabricated by the ionic self-assembly technique [26].

Two kinds of electrodes were fabricated. The electrode modified with PVP-Os/PSS was denoted electrode I, and that modified with PVP-Os/PAPSAH was denoted electrode II. Cyclic voltammetry was employed to characterize the electrochemical properties of the modified electrodes. The resulting cyclic voltammograms (CVs) of electrode I (PVP-Os + $(PSS/PVP\text{-}Os)_5$) and electrode II (PVP-Os + $(PAPSAH/PVP\text{-}Os)_5$) in 0.2 M Na_2SO_4 (pH 1.0, adjusted by H_2SO_4) at different scan rates are shown in Fig. 11.12(A) and (B), respectively. For electrode I, only one pair of anodic/cathodic peaks appears with formal potential ($E_{1/2}$), taken as the average value of the anodic and cathodic peak potentials, of 340 mV, which is related to the Os^{2+}/Os^{3+} redox couple in PVP-Os. While, for electrode II, two pairs of anodic/cathodic peaks appear with $E_{1/2}$ peaks at 150 mV and 295 mV, which correspond to those of PAPSAH and PVP-Os, respectively. As can be seen, with increasing scan rate, the anodic/cathodic peak currents of PVP-Os in both electrodes increase linearly in the range from 10 to 200 mV s^{-1}, which indicates a surface redox process. Comparing the CVs of electrodes I and II, it is obvious that electrode II yields more symmetrical voltammograms, e.g., at a scan rate of 200 mV s^{-1}, the peak-to-peak separation was 30 mV for electrode II and 80 mV for electrode I (with respect to the redox peak of PVP-Os on both electrodes). This shows that the electron transfer on electrode II is much easier than that on electrode I.

We further examined the dependence of the electrode response on the number of deposition layers for electrodes I and II. There exists a critical number of deposition layers (CNDL) for both electrodes, beyond which the electrode response begins to decrease. The existence of a CNDL in a multilayer-modified electrode is related to the vertical electron transfer within the film. Fig. 11.13 shows the dependence of the cathodic peak currents of both electrodes on the number of PVP-Os layers deposited, from which it can be seen that the CNDLs for electrodes I and II are 8 and 12, respectively. This confirms again that by replacing PSS with PAPSAH, electron transfer becomes much easier.

It is found that both electrodes consisting of PVP-Os have the ability to catalyze the reduction of nitrite in 0.2 M Na_2SO_4 (pH 1.0). Catalytic currents obtained on both electrodes with an operating potential controlled at 200 mV (vs. SCE) are proportional to the concentration of nitrite as shown in Fig. 11.14(A) and (B). It is worth noting that the reduction currents of electrode II are much larger than those at electrode I.

Based on the difference in peak-to-peak separation, CNDL and the response to nitrite reduction, it has been proven that by replacing PSS with PAPSAH, the performance of the resulting PVP-Os modified electrode can be improved to some extent. The only difference between these two electrodes is the polyanions used. For electrode I, PSS is nonconductive and should act as a barrier to electron transfer

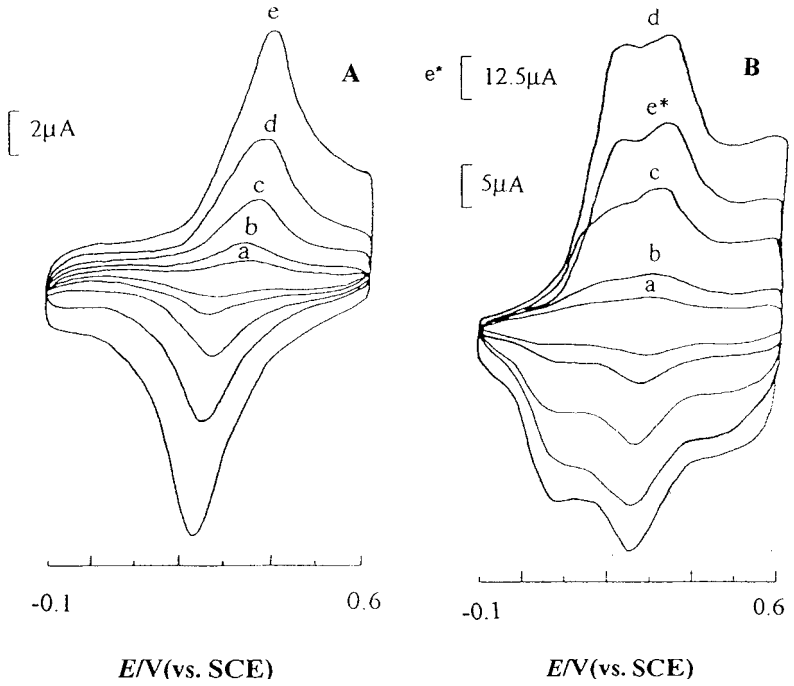

Fig. 11.12 Cyclic voltammogram of (A) electrode I and (B) electrode II in 0.2 M Na_2SO_4 at pH 1.0. Electrode I consists of 1 layer of PVP-Os and 5 bilayers of PSS/PVP-Os, while electrode II consists of 1 layer of PVP-Os and 5 bilayers of PAPSAH/PVP-Os. Scan rates ($mV\,s^{-1}$): (a) 10, (b), 20, (c) 50, (d) 100 and (e) 200.

within the film, whereas, for electrode II, PAPSAH is conductive and should thus facilitate the electron transfer. In our experiment, the supporting solution used was 0.2 M Na_2SO_4 with pH 1.0. It is believed that the acidic condition of the solution may help to keep the PAPSAH layers more conductive. Thus, PAPSAH incorporated between PVP-Os layers may act as a conductive "wire" and decrease the ohmic film resistance, which provides a way for easy transfer of electrons.

From the view of increasing the electrical conductivity of the multilayer film to improve the performance of the electrode, it is believed that the incorporation of Au nanoparticles should have a similar effect to that of the conductive polymer PAPSAH. Au nanoparticles have good conductivity and their surface is easily modified negatively or positively making it suitable for assembling with any charged electroactive materials. Another advantage of Au particles as linker between electroactive PVP-Os or other electroactive materials is that, in general, the roughness of the particle-covered surface is greater than that of the polymers which can increase largely the area of the electrode, and thus the amount of electroactive materials immobilized. To increase the load of the electroactive materials on the electrode surface by a simple and general method is very important in practical applications because it can improve the sensitivity and detection limit of

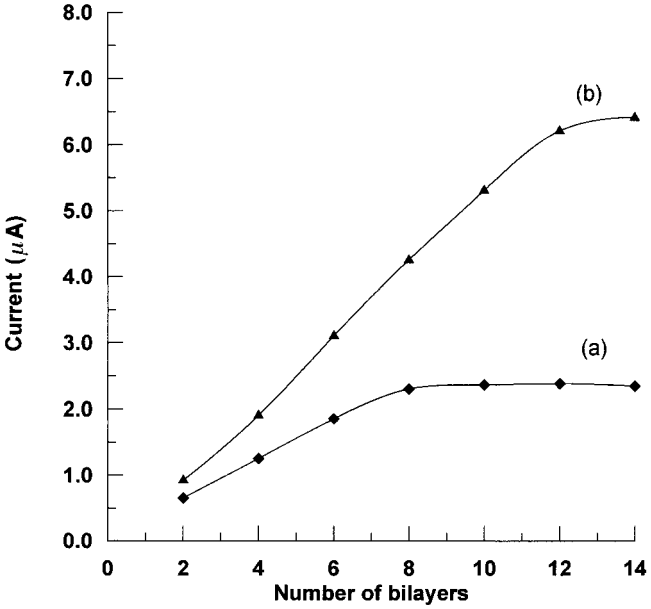

Fig. 11.13 Dependence of cathodic peak current on the number of PVP-Os layers deposited. (a) electrode I and (b) electrode II. Scan rate: 70 mV s^{-1}.

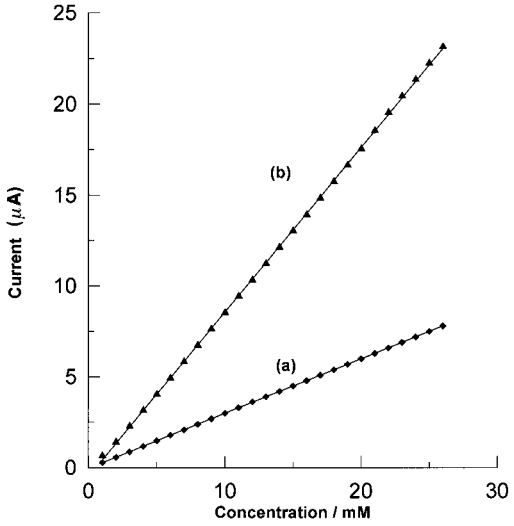

Fig. 11.14 The calibration curves of current vs. nitrate concentration (a) on electrode I and (b) on electrode II.

the resulting chemically modified electrode. Briefly, by carefully choosing the conductive species as counterpart for the construction of a multilayer-modified electrode, the performance of the resulting chemically modified electrode can be optimized to some extent.

11.3
Ionic Self-assembly of Photoactive Materials and the Fabrication of "Robust" Multilayer

The neighboring layers of an ionically self-assembled multilayer are held together by electrostatic interaction or ionic bonds. The stability of this kind of multilayer assembly can be affected by the environmental conditions, e.g., the type of solvent, ionic strength, pH of the solvent, etc. In some cases, the stability of the films is particularly important. Films having the ability to resist the etching of some special solvents and to work under more severe conditions are required. Since the covalent bond is, in general, stronger than the electrostatic interaction, it is reasonable to use covalent bonds instead of electrostatic interaction to form stable multilayer assemblies. The traditional method using stepwise chemical reaction to fabricate covalently attached multilayer films is one of the choices, but suitable chemical reactions are limited and tiresome work is involved. We have considered whether or not we can make use of the simplicity of the ionic self-assembly technique in operation and the subsequently induced reaction within multilayers to get covalently attached multilayer assemblies. The possibility of achieving this hinges on the discovery of charged pair groups which can undergo reaction to form covalent bonds. It is well known that diazonium groups can undergo photoreaction with a variety of polyions containing sulfonate or acrylic acid groups under UV irradiation or by heating. By deliberately choosing a photoreactive diazo-resin (DAR) as the polycation and combining its post photoreaction with sulfonate groups induced by UV irradiation, we successfully achieved this, as shown in Fig. 11.15 [41]. The stability of the thus-fabricated multilayer assemblies improved remarkably, as expected. Till now, we have fabricated stable multilayer assemblies from polyanions containing sulfonate and carboxylic acid groups, e.g. (PSS), PAPSAH, oligo-charged organic molecules, inorganic colloids and poly(acrylic acid) (PAA) [42–46]. Along the same line of research, Bruening et al. used poly(allylamine hydrochloride) (PAH) and PAA to construct multilayer films, and the following heat treatment induced the formation of amide bonds, through which the films were crosslinked thus improving their stability greatly [47]. A variety of other crosslinked multilayer films which employed the photo-induced addi-

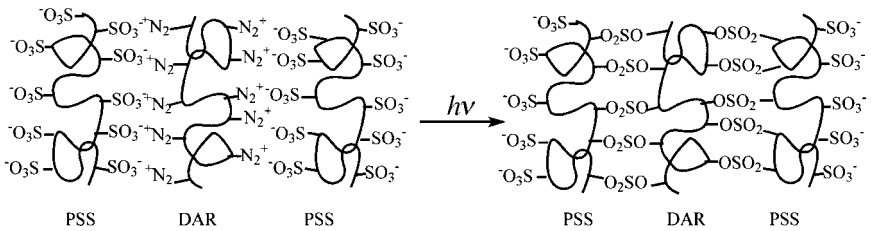

Fig. 11.15 Schematic representation for structure changes of multilayer assemblies from ionically to covalently attached upon UV irradiation.

tive reaction of oligo-molecules containing double carbon–carbon bonds within the layers have also been constructed.

11.3.1
Ways to Fabricate Covalently Attached Multilayer Assemblies

In general, the above way to fabricate covalently attached multilayer assemblies involves two steps: ionic self-assembly followed by UV irradiation. Take the fabrication of covalently attached DAR/PSS multilayer on a positively charged substrate for example [41, 42]. First, an electrostatic interaction based multilayer of DAR/PSS is obtained by alternately dipping the substrate in aqueous solutions of PSS and DAR. Next, the films are exposed to UV irradiation for a given time to ensure complete photoreaction. In this way, the covalently attached multilayer films can be obtained. It is worth noting that the ionic self-assembly step must be conducted in the dark to avoid decomposition of the DAR.

UV–Vis spectroscopy was used to follow the ionic self-assembled multilayer fabrication process. Fig. 11.16 shows the UV–Vis absorption spectra of 2, 4, 6 and 8 bilayers of DAR/PSS assembled on a quartz slide. The absorbance at 380 nm was attributed to the π–π^* transition of the diazonium group. The linear increase in absorbance at 380 nm with the number of layers indicates a progressive deposi-

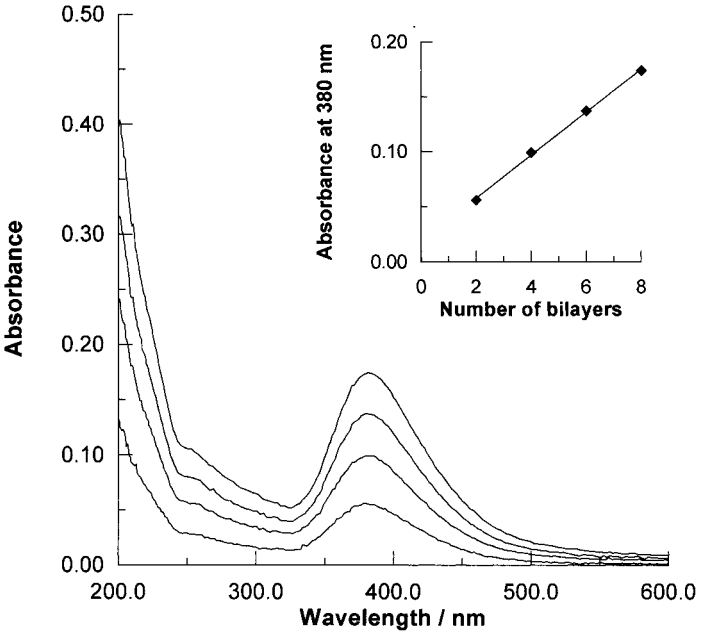

Fig. 11.16 UV–Vis absorption spectra of multilayer films of DAR/PSS. From the lower to upper, the number of bilayers is 2, 4, 6 and 8. Inset shows the absorption at 380 nm vs. the number of bilayers.

tion with almost equal amount of deposition of the polyions in each cycle. Owing to the well known high reactivity of diazonium and sulfonate groups, the above assembled films containing 8 bilayers of DAR/PSS were irradiated with a 30 W mercury lamp at a distance of 10 cm. Fig. 11.17 shows the changes in the UV–Vis spectra of the films with irradiation time, from which we can clearly see that with UV irradiation, the diazonium groups decomposed with a dramatic decrease in the absorbance at 380 nm and a concomitant increase in the absorbance in the vicinity of 290 nm. At the same time, an isosbestic point at 332 nm appears. Throughout the experiment, it was found that the decomposition proceeded completely within 5 min. The presence of photo-induced sulfonic ester within the layers was confirmed by FTIR. The photoreaction between diazonium connected phenyl and sulfonate groups takes place, as shown in Fig. 11.18. First, DAR was converted into its phenyl cationic form after releasing N_2 upon UV irradiation, then an S_N1 type of nucleophilic reaction by sulfonate occurred.

The photoreaction in between the film can also be confirmed by the improved stability of the film after UV irradiation. The ionically assembled film of DAR/PSS was etched by immersing in a ternary mixture of H_2O–DMF–$ZnCl_2$ (3 : 5 : 2, w/w/w) to test its stability. The ternary system was chosen because of the high solubility of the DAR/PSS polyelectrolyte complex in this solvent. Nearly 30% of the assembled film was dissolved after 5 min immersion, according to the decrease in absorbance at 250 and 380 nm. This result shows that this type of ionically self-assembled film is not adequately stable in the ternary solvent. As a comparison, we etched the irradiated film by sonicating it in the same ternary solvent

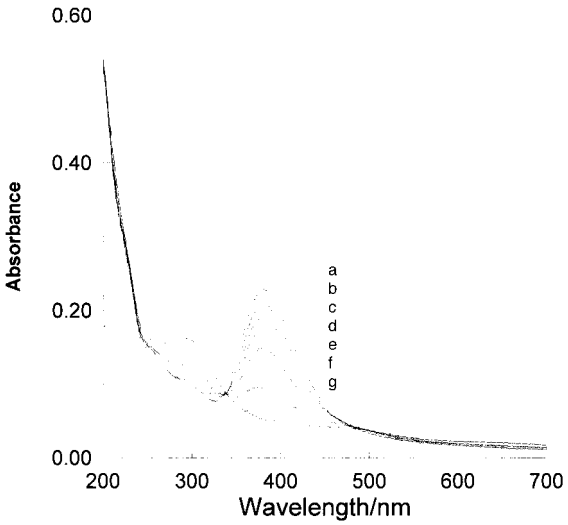

Fig. 11.17 UV–Vis absorption spectra of eight bilayers of DAR/PSS upon UV irradiation for (a) 0 s, (b) 20 s, (c) 40 s, (d) 1 min, (e) 1.5 min, (f) 3 min and (g) 5 min.

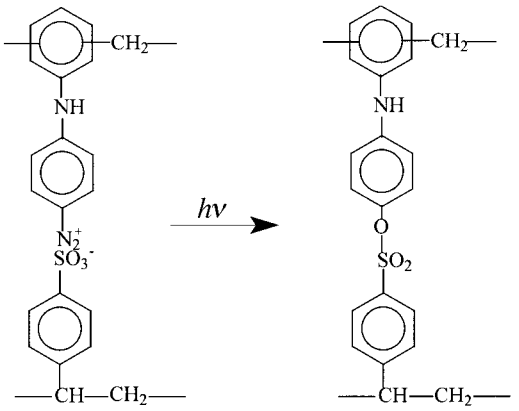

Fig. 11.18 Photoreaction between diazonium connected phenyl and sulfonated groups in DAR/PSS multilayer assemblies.

for 0.5 h. No detectable damage of the film was found, according to the absorbance at 250 nm, indicating a much greater stability of the UV irradiated film. Photoreaction changes the crosslinking structure of multilayer films from ionic to covalent bonds so that a three-dimensional network is formed which covers the whole substrate including the four side faces. This can explain why, although the interaction between the substrate and the first layer of multilayer films was not covalent, the films were stable in many solvents, like MeOH, DMSO, DMF, $CHCl_3$, and even the ternary solvent as described previously.

It has been observed that the thickness of an individual adsorbed polyion layer can be influenced by the ionic strength of the solution, changed by adding inorganic salt or adjusting its concentration. In our experiment, we kept the concentration of PSS at 1.0 mg ml^{-1} while changing the concentration of DAR or adding NaCl to DAR solution to realize thickness tuning of the films. Three cases were investigated, (1) DAR 1.5 mg ml^{-1} dissolved in 0.5 M NaCl; (2) DAR 1.5 mg ml^{-1}; (3) DAR 0.3 mg ml^{-1}. Thickness measurements by X-ray diffraction were performed on the above samples after UV irradiation. As shown in Fig. 11.19, a series of well resolved Kiessig fringes is found in all cases, which proves the homogeneousness of the films. The existence of only Kiessig fringes but no Bragg peaks was similar to typical polycation/polyanion systems based on electrostatic interaction, indicating an interpenetrating structure between the layers. For a quartz slide covered with 10 bilayers of DAR/PSS deposited from solutions of different concentration or ionic strength of DAR after UV irradiation, the total thickness of films in the cases (1), (2) and (3) was calculated to be about 23.4 nm, 16.8 nm and 15.2 nm, respectively. So the thickness of one bilayer can be tuned in the range 15 Å to 23 Å by simply changing the ionic strength or the concentration of DAR solution. The control of the individual layer thickness of polyion deposited is simply due to the well-known changes in the coil structure of the polyions in solutions of different ionic strength. Most importantly, all films after UV irradiation were very stable in the ternary solvent, examined in the same way as described before. This means that this method of fabricating covalently attached multilayer

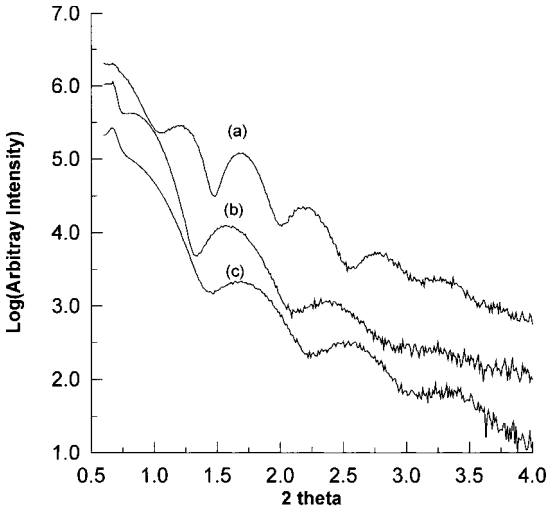

Fig. 11.19 X-ray diffraction of 10-bilayer DAR/PSS film deposited on quartz slides. (a) DAR 1.5 mg ml^{-1} dissolved in 0.5 M NaCl; (b) DAR 1.5 mg ml^{-1}; (c) DAR 0.3 mg ml^{-1}.

film is applicable for multilayers whose individual layer thickness can be tuned in a wide range.

By using a heat treatment after ionic self-assembly, Bruening et al. developed a way of fabricating a kind of passivating, nylon-like coating through crosslinking ultrathin polyelectrolyte film [47]. First, multilayer assemblies of poly(allylamine hydrochloride) (PAH) and poly(acrylic acid) (PAA) were fabricated by the ionic self-assembly technique, then the film was heated at 130 °C or 215 °C for some time under N_2 atmosphere. In this way, crosslinking between the ammonium groups of PAH and the carboxylate groups of PAA occurs through formation of an amide bond, as confirmed by FTIR spectroscopy. The change in the structure of the PAH/PAA film after heat treatment is shown in Fig. 11.20. Both cyclic voltammetry and impedance spectroscopy show that the film permeability decreases dramatically upon cross-linking and depends on the heating conditions. Crosslinking of a PAH/PAA multilayer film stabilizes the film over a wide pH range. These nylon-like, crosslinked films could find potential applications as ultrathin membranes or corrosion-resistant coatings.

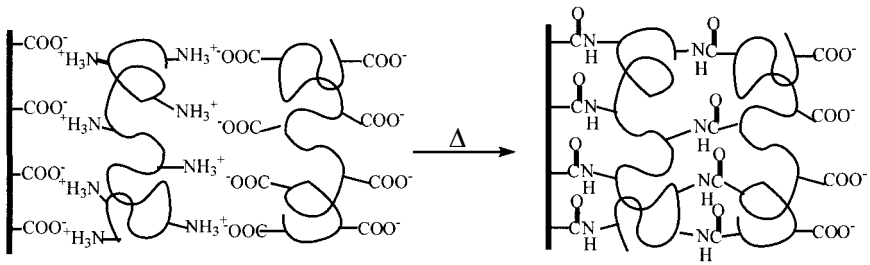

Fig. 11.20 The chemical reaction in PAH/PAA multilayer assemblies after heat treatment.

11.3.2 Stable Entrapment of Oligo-charged Molecules Bearing Sulfonate Groups in Multilayer Assemblies

As mentioned before, the ionic self-assembly technique has provided an effective way to realize the three-dimensionally layered assembly of oligo-charged organic molecules. Compared with the polycation/polyanion assemblies, a multilayer containing small organic molecules is even less stable because the bonding sites on small organic molecules are relatively fewer. As a continuous program of work, we have further developed this method in an attempt to realize the stable entrapment of organic dyes bearing sulfonate groups [44, 46]. Covalently attached multilayer assemblies were fabricated by exposing the assemblies of DAR and a variety of organic dyes bearing sulfonate groups, ranging from 2 to 4 per molecule, such as $tpps_4$, CuTsPc, SNAN and BST. As indicated in Tab. 11.3, the stability of the films after UV irradiation improved greatly compared with those before UV irradiation. However, it failed to stabilize each small molecule in the film because the reaction between diazonium and sulfonate in the film cannot reach 100%. By covering the DAR/dye assemblies with additional layers of photoreactive DAR/PSS or fabricating DAR/dye/DAR/PSS alternate film, the stability of dyes in the assemblies will be further improved.

The electrochemical response of $Fe(CN)_6^{3-/4-}$ on DAR/$tpps_4$ film was largely suppressed after UV irradiation. This means that the UV irradiation made the film more impermeable. As for a 6 bilayers $tpps_4$/DAR covered ITO electrode, after UV irradiation, the electron communication between the ITO electrode and $Fe(CN)_6^{3-/4-}$ could be blocked almost completely. The impermeability of the film makes it a good candidate for corrosion prevention but not for multilayer-film-based sensors. A sensor requires the film to be both stable and permeable. How to make the film stable and permeable at the same time becomes crucially important for its applications in mulilayer-film-based sensor. It was found that solvent etching the covalently attached film could make it more permeable. As shown in Fig. 11.21(a), an ITO electrode covered with 3 bilayers of DAR/$tpps_4$ film was scanned in 0.1 M KCl solution containing 1 mM $Fe(CN)_6^{3-}$, the peak currents are very small. After sonicating this electrode

Tab. 11.3 Stability test of small molecules bearing sulfonate groups in the multilayer assemblies of DAR/dyes

Multilayer assemblies	*Fraction desorbed*[a)]				
	a	*b*	*c*	*d*	*Absorbance/nm*
(DAR+tpps4)*8+DAR	84	91	5.6	11	426
(DAR+CuTsPc)*8+DAR	71	83	6.8	12	232
(DAR+SBT)*8+DAR	47	72	9	12	284
(DAR-SNAN)*8+DAR	70	80	7	23	535

a) a: Immersion for 5 min (before UV irradiation); b: Sonicated for 5 min (before UV irradiation); c: Immersion for 5 min (after UV irradiation); d: Sonicated for 5 min (after UV irradiation).

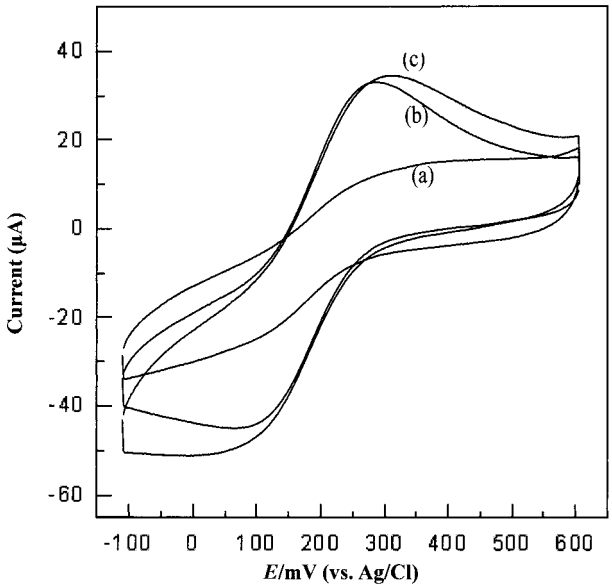

Fig. 11.21 CVs of a (DAR+tpps$_4$)*3 + DAR modified ITO electrode (a) after UV irradiation, (b) after sonication for 5 min in ternary solvent and (c) after another 5 min sonication in ternary solvent. Conditions: 0.5 M KCl solution containing 1 mM $Fe(CN)_6^{3-}$, scan rate: 100 mV s^{-1}.

in ternary solvent for 5 min, the peak currents increase obviously (Fig. 11.21 (b)). Another 5 min sonication increased the peak currents lightly again but not as much as the first sonication did (Fig. 11.21 (c)). We would speculate that the solvent etching of the unreacted absorbates would be responsible for the increasing permeability, and the reacted tpps$_4$ in the film is stable enough to resist further solvent etching. It is believed that the permeability of the resulting film could be controlled easily by many factors, e.g., by the reaction ratio, by trapping some larger template molecules or by replacing DAR with diazonium-containing copolymers. The possibility to covalently entrap electro-active species in the multilayer assemblies, combined with the high permeability caused by solvent etching should make this technique a preferred candidate for the fabrication of stable chemically modified electrodes.

11.3.3
Covalently Attached Multilayer Assemblies of Polycationic Diazo-resins and Polyanionic Poly(Acrylic Acid)

Acrylic acid-containing materials are another kind of everyday used negatively charged species. Now it is important to know whether this new method of fabricating covalently attached multilayer film is applicable for acrylic acid-containing species. Herein, we choose poly(acrylic acid) (PAA) as a model material to investi-

gate the possibility of using this method to fabricate DAR/PAA covalently attached multilayers [45]. It was well demonstrated that DAR could alternately assemble with PAA in aqueous solution to form multilayer assemblies. Within the PAA chain, there are two kinds of groups, acrylic acid and acrylate. The ratio of these two groups is dependent on the pH of the solution. Therefore the driving force for the assembly is based on a combination of electrostatic interaction between diazonium and acrylate groups and hydrogen bonds between secondary amine and acylic acid groups. Upon UV irradiation, a partially covalently attached multilayer of DAR/PAA can be formed, which improves the stability of the resulting film greatly compared with that without UV irradiation. The reaction in the DAR/PAA film is shown in Fig. 11.22 (A). Since PAA is a weak polyelectrolyte, the

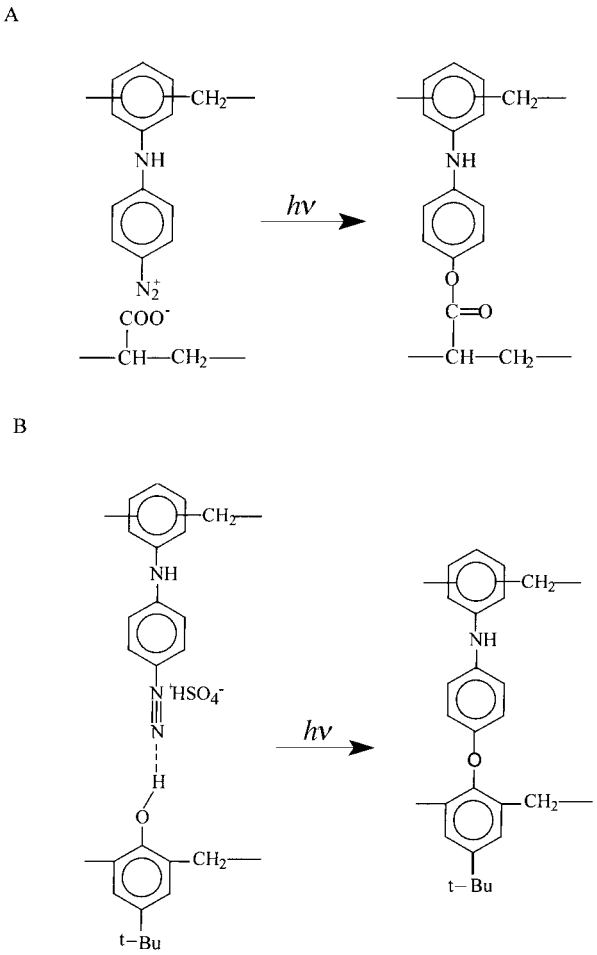

Fig. 11.22 Photoreaction of (A) DAR and PAA, (B) DAR and PR in the multialyer assemblies.

conformation of PAA chains is very sensitive to the change in pH of the solution. By changing the pH of the PAA solution, the thickness of an individual layer can be finely tuned on the nanometer scale. One more interesting example is concerned with hydrogen bonding directed self-assembly and post-chemical reaction to fabricate covalently attached films. Cao et al., reported the fabrication of alternately assembled multilayer film of DAR and phenol-formaldehyde resin (PR) based on hydrogen bonding as the driving force [48]. UV irradiation converted the hydrogen bonds into a covalently attached multilayer, as shown in Fig. 11.22(B). Its stability towards polar solvents was proved to increase dramatically. We would anticipate that the same concept might be applied to other building blocks bearing carboxylic and phenol groups.

11.3.4
Robust Nanoassemblies with Complex and Hybrid Structures

The improved stability leads to these kinds of covalently attached multilayer assemblies finding applications in a wider range. When functional species were incorporated, functional assemblies with high stability could be obtained. For example, when an electroactive material was used, this technique could produce a chemically modified electrode with high stability. PAPSAH is a kind of water-soluble self-acid-doped conducting polyaniline in which the sulfonic acid groups are located in the polyaniline chain [40]. The sulfonate groups along its chain makes PAPSAH suitable for fabricating a covalently attached film with DAR [43]. Fig. 11.23 shows the cyclic voltammagrams of (a) a self-assembled monolayer (SAM) of 3-mercapto-1-propane-sulfonate (MPS) on a gold electrode, (b) a 3-bilayer-(DAR/PAPSAH) modified gold electrode and (c) a 6-bilayer-(DAR/PAPSAH) modified gold electrode (both after UV irradiation) in 0.2 M Na_2SO_4 (pH 1.0) at a scan rate of 10 mV s^{-1}. Within the potential range studied, –0.1 to 0.7 V, no redox peaks are observed in curve (a) for electroinactive MPS. In contrast, both the PAPSAH-containing multilayer films exhibit one minor (I–I′) and one major (II–II′) redox peak at ca. 0.15 and 0.44 V, respectively. These two redox peaks should be assigned to the two-step PAPSAH-based redox processes. The first redox peak corresponds to oxidation from the fully-reduced insulating leucoemeraldine salt form to the partially-oxidized conducting emeraldine salt form; the second redox peak corresponds to oxidation from emeraldine to fully-oxidized insulating permigraniline. Like the other types of polyaniline, the redox properties of PAPSAH incorporated in a covalently attached film is also pH dependent. When the pH of the solution decreases, the redox peak potentials of PAPSAH shift positively and the peak currents increase obviously. The increase in peak currents with the decrease in pH value should arise from the fact that the acidic condition of the solution is helpful in keeping the PAPSAH multilayers conductive because of the protonic doping effect. All these results show that the properties of PAPSAH still remain in the covalently attached mulilayer. It is anticipated that this robust PAPSAH-containing film could find applications in chemically modified electrodes and electrochromics.

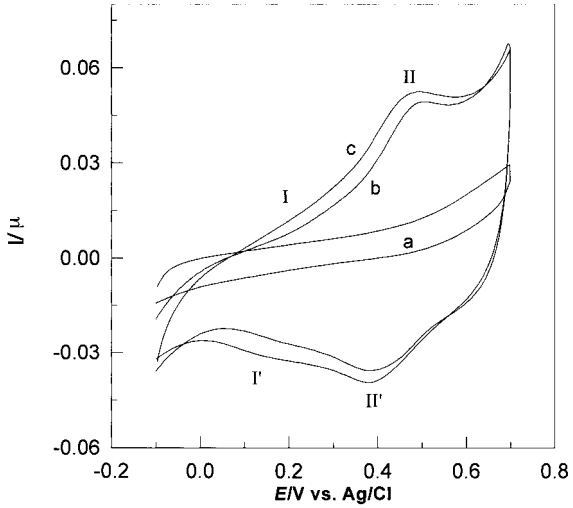

Fig. 11.23 CVs of (a) a monolayer of MPS modified gold electrode, (b) 3 bilayers of DAR/PAPSAH modified gold electrode in 0.5 M KCl solution containing 1 mM $Fe(CN)_6^{3-}$ and (c) 6 bilayers of DAR/PAPSAH modified gold electrode in 0.5 M KCl solution. Scan rates: 50 mV s^{-1}.

Organic–inorganic hybrid materials, with fascinating properties stemming from their synergic effect, have been paid increasing attention [49–52]. More recently, a robust gold nanoparticles/polymer hybrid multilayer was fabricated by alternately assembling DAR and MPS covered gold nanoparticles followed by UV irradiation [53]. The ideal structure of this covalently attached gold nanoparticles/polymer hybrid multilayer is shown schematically in Fig. 11.24. The properties of gold nanoparticles were kept in the covalently attached multilayer assemblies, meanwhile, the stability of the resulted film increased greatly. It is believed that the same concept may be applied to other particles containing sulfonate or carboxylic acid

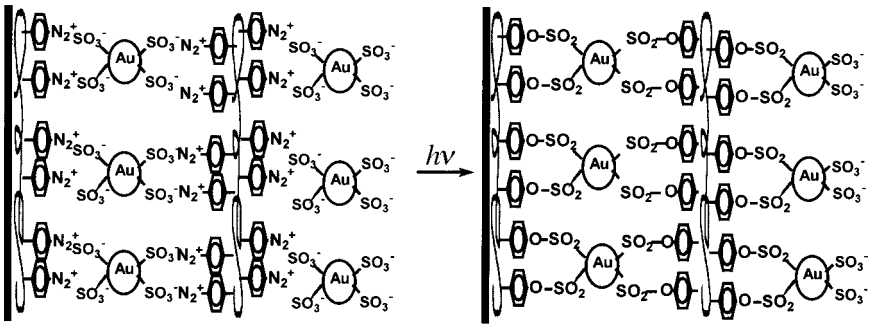

Fig. 11.24 The ideal structure of a gold nanoparticles/DAR hybrid multilayer and its change upon UV irradiation.

groups to fabricate a variety of robust hybrid multilayer assemblies with tailored properties.

11.4 Summary and Outlook

We have demonstrated a variety of multilayer assemblies of electro- and photoactive species by means of the ionic self-assembly technique. By combining the ionic self-assembly technique with in situ chemical reaction in between the film, robust multilayer assemblies in which the neighboring layers are held together by covalent bonds can be easily fabricated. This technique is particularly suitable for charged building blocks containing diazonium groups and their counterparts containing sulfonate, acrylic acid and even phenol groups, but it can also be extended to other systems when pairs of appropriate reactive materials are selected. This technique to fabricate covalently attached multilayer films could be used to produce chemically modified electrodes with high stability, which guarantees the application of these electrodes under severe conditions. Because DAR or diazonium-containing polycations are photosensitive, this will also provide a new kind of surface patterning material. For example, due to the different solubility of the multilayer assemblies before and after UV irradiation, when a proper solvent is chosen which can dissolve the multilayer formed without UV irradiation but not that formed after UV irradiation, robust multilayer patterning surfaces can be produced. By incorporating electroactive materials into multilayers, chemically modified electrodes based on both single and binary active species have been fabricated. In the binary active species modified electrodes, two components can be incorporated in such a way that the function is based on their organization. In other words, multi-component active species could use their synergy to produce new functions which are unavailable for any individual species.

11.5 References

1 H. Ringsdorf, B. Schlarb, J. Venzmer, *Angew. Chem. Int. Ed. Engl.*, **1991**, *27*, 113–158.
2 K. B. Blodgett, *J. Am. Chem. Soc.*, **1935**, *57*, 1007–1010.
3 A. Ulman, *Chem. Rev.*, **1996**, *96*, 1533–1554.
4 G. Decher, *Science*, **1997**, *277*, 1232–1237.
5 G. Decher and J.-D. Hong, *Makromol. Chem. Macromol. Symp.*, **1991**, *46*, 321–327.
6 P. Bertrand, A. Jonas, A. Laschewsky, R. Legras, *Macromol. Rapid Commun.*, **2000**, *21*, 319–348.
7 P. T. Hammond, *Curr. Opin. Colloid Interface Sci.*, **2000**, *4*, 430–442.
8 A. Laschewsky, E. Wischerhiff, M. Kauranen, A. Persoons, *Macromolecules*, **1997**, *30*, 8304–8309.
9 J. H. Cheung, A. F. Fou, M. F. Rubner, *Thin Solid Films*, **1994**, *244*, 985–989.
10 F. Ackern, L. Krasemann, B. Tieke, *Thin Solid Films*, **1998**, *327–329*, 762–766.

11 H. Hong, D. Davidov, Y. Avny, H. Chayet, E. Z. Faraggi, R. Neumann, *Adv. Mater.* **1995**, *7*, 846–849.

12 A. C. Fou, O. Onitsuka, M. Ferreira, M. F. Rubner, B. R. Hsieh, *J. Appl. Phys.*, **1995**, *79*, 7501–7509.

13 C. Q. Sun, Y. P. Sun, X. Zhang, H. D. Xu, J. C. Shen, *Anal. Chim. Acta*, **1995**, *312*, 207–212.

14 L. Y. Wang, Z. Q. Wang, X. Zhang, J. C. Shen. *Macromol. Rapid Commun.*, **1997**, *18*, 509–514.

15 W. B. Stockton, M. Rubner, *Macromolecules*, **1997**, *30*, 2717–2725.

16 H. M. Xoing, M. H. Chen, Z. Zhou, X. Zhang, J. C. Shen, *Adv. Mater.*, **1998**, *10*, 529 –532.

17 M. Schütte, D. G. Kurth, M. R. Linford, H. Cölfen, H. Möhwald, *Angew. Chem. Int. Ed. Engl.*, **1998**, *37*, 2891–2893.

18 Y. Shimazaki, M. Mitsuishi, S. Ito, M. Yamamoto, *Langmuir*, **1997**, *13*, 1385–1387.

19 J. Anzai, Y. Kobayashi, N. Nakamura, M. Nishimura, T. Hoshi, *Langmuir*, **1999**, *15*, 221–226.

20 X. Zhang, Y. P. Sun, M. L. Gao, X. X. Kong, J. C. Shen, *Macromol. Chem. Phys.*, **1996**, *197*, 509–515.

21 X. Zhang, J. C. Shen, *Adv. Mater.*, **1999**, *11*, 1139–1143.

22 S. J. Dong, G. L. Che, Y. W. Xie, *Chemically Modified Electrodes*, Science Publishing House, Beijing, **1995**, p. 16–43.

23 C. Q. Sun, X. Y. Zhang, D. Jiang, Q. Gao, H. D. Xu, Y. P. Sun, X. Zhang, J. C. Shen, *J. Electroanal. Chem.*, **1996**, *411*, 73–78.

24 C. Q. Sun, Y. P. Sun, X. Zhang, X. Y. Zhang, D. Jiang, Q. Gao, H. D. Xu, J. C. Shen, *Thin Solid Films*, **1996**, *288*, 291–295.

25 C. Q. Sun, J. H. Zhao, H. D. Xu, Y. P. Sun, X. Zhang, J. C. Shen, *Talanta*, **1998**, *46*, 15–21.

26 J. Q. Sun, Y. P. Sun, S. Zou, X. Zhang, C. Q. Sun, Y. Wang, J. C. Shen, *Macromol. Chem. Phys.*, **1999**, *200*, 840–844.

27 A. N. Shipway, M. Lahav, R. Blonder, I. Willner, *Chem. Mater.*, **1999**, *11*, 13–15.

28 J. Hodak, R. Etchenique, E. J. Calvo, K. Singhal, P. N. Bartlett, *Langmuir*, **1997**, *13*, 2708–2712.

29 L. Cheng, L. Niu, J. Gong, S. J. Dong, *Chem. Mater.*,**1999**, *11*, 1465–1475.

30 Y. P. Sun, X. Zhang, C. Q. Sun, B. Wang, J. C. Shen, *Macromol. Chem. Phys.*, **1996**, *197*, 147–153.

31 X. Zhang, M. L. Gao, X. Q. Kong, Y. P. Sun, J. C. Shen, *J. Chem. Soc., Chem. Commun.*, **1994**, 1055–1056.

32 Y. P. Sun, X. Zhang, C. Q. Sun, Z. Q. Wang, J. C. Shen, D. J. Wang, T. J. Li, *Chem. Commun.*, **1996**, 2379–2380.

33 W. Kong, X. Zhang, M. L. Gao, H. Zhou, W. Li, J. C. Shen, *Macromol. Rapid Commun.*, **1994**, *15*, 405–409.

34 W. Kong, LP. Wang, M. L. Gao, H. Zhou, X. Zhang, W. Li, J. C. Shen, *Chem. Commun.*, **1994**, 1297–1298.

35 Y. Lvov, G. Decher, G. Sukgorukov, *Macromolecules*, **1993**, *26*, 5396–5399.

36 Y. Lvov, H. Hass, G. Decher, H. Möhwald, A Michailov, B. Mtchedlishvily, E. Morgunova, B. Varnshtain, *Langmuir*, **1994**, *10*, 4232–4236.

37 Y. Lvov, K. Ariga, I. Ichinose, T. Kunitake, *J. Am. Chem. Soc.*, **1995**, *117*, 6117–6123.

38 Y. P. Sun, J. Q. Sun, X. Zhang, C. Q. Sun, Y. Wang, J. C. Shen, *Thin Solid Films*, **1998**, *327–329*, 730–733.

39 J. Q. Sun, Y. P. Sun, Z. Q. Wang, C. Q. Sun, Y. Wang, X. Zhang, J. C. Shen, *Macromol. Chem. Phys.*, **2001**, *202*, 111–116.

40 S. A. Chen, G. W. Hwang, *J. Am. Chem. Soc.*, **1994**, *116*, 7939–7940.

41 J. Q. Sun, T. Wu, Y. P. Sun, Z. Q. Wang, X. Zhang, J. C. Shen, W. X. Cao, *Chem. Commun.*, **1998**, 1853–1854.

42 J. Q. Sun, Z. Q. Wang, L. X. Wu, X. Zhang, J. C. Shen, S. Gao, L. F. Chi, H. Fuchs, *Macromol. Chem. Phys.*, **2001**, *202*, 961–966.

43 J. Q. Sun, L. Cheng, F. Liu, S. J. Dong, Z. Q., Wang, X. Zhang, J. C. Shen, *Colloids Surf. A*, **2000**, *169*, 209–217.

44 J. Q. Sun, Z. Q. Wang, Y. P. Sun, X. Zhang, J. C. Shen, *Chem. Commun.*, **1999**, 693–694.

45 J. Q. Sun, T. Wu, F. Liu, Z. Q. Wang, X. Zhang, J. C. Shen, *Langmuir*, **2000**, *16*, 4620–4624.

46 J. Q. Sun, T. Wu, B. Zou, X. Zhang, J. C. Shen, *Langmuir*, **2001**, *17*, 4035–4041.

47 J. J. Harris, P. M. DeRose, M. L. Bruening, *J. Am. Chem. Soc.* **1999**, *121*, 1978–1979.
48 J. Y. Chen, W. X. Cao, *Chem. Commun.*, **1999**, 1711–1712.
49 P. Gomez-Romero, *Adv. Mater.*, **2001**, *13*, 163–174.
50 M. Y. Gao, X. Zhang, B. Yang, J. C. Shen, *Chem. Commun.*, **1994**, 2229–2230.
51 M. Y. Gao, M. L. Gao, X. Zhang, Y. Yang, B. Yang, J. C. Shen, *Chem. Commun.*, **1994**, 2777–2778.
52 Y. P. Sun, E. C. Hao, X. Zhang, B. Yang, J. C. Shen, L. F. Chi, H. Fuchs, *Langmuir*, **1997**, *13*, 5168–5174.
53 Y. Fu, H. Xu, J. Q. Sun, Z. Q. Wang, X. Zhang, *Macromol. Rapid Commun.*, **2002**, *23*, 256–259.

Multilayer Thin Films. Edited by Gero Decher, Joseph B. Schlenoff

Copyright © 2002 Wiley-VCH Verlag GmbH & Co. KGaA
ISBNs: 3-527-30440-1 (Hardback); 3-527-60057-4 (Electronic)

12
Coated Colloids: Preparation, Characterization, Assembly and Utilization

Frank Caruso and Gleb Sukhorukov

Abstract

The preparation of nanocomposite colloids with tailored properties, and the subsequent assembly of nanostructured materials from these particles provide new opportunities for the technological application of colloids in areas such as coatings, catalysis, sensing, separations, drug delivery, electronics and photonics. This chapter highlights a recently developed self-assembly layer-by-layer (LbL) process for the surface engineering of colloid particles at the nanoscale level. Through polymer-mediated adsorption of charged species from solution onto colloids, new classes of functional core–shell colloids are produced. The versatility of the LbL strategy is demonstrated by a number of examples of nanoengineered colloidal entities, including magnetic, fluorescent, and biocolloids. Extension of the LbL process to encapsulate a variety of biomacromolecules and low molecular weight compounds is also detailed. Additionally, the creation and potential applications of multilayered functional thin films and ordered colloidal assemblies from the core–shell colloids are described.

12.1
Introduction

Colloids are ubiquitous, present all around us. Technologically, they have been of importance for centuries, being exploited in diverse areas ranging from additives and pigments (e.g. in foods, cosmetics, inks and paints), to catalysis, as well as in the photography, agriculture and mining industries [1–5]. A prerequisite for the successful utilization of colloids for many applications is that they remain colloidally stable. The two main components of the intermolecular interactions that influence colloidal stability, namely the electrostatic repulsion and van der Waals attraction, have been intensively studied [1, 2]. These interactions can be tuned by, for example, the addition of salt and polymers to the colloidal dispersion, providing the basis for the use of optimized colloidal systems for various fundamental investigations or for the manufacture of hierarchically ordered structures. The size and type of colloids available nowadays is quite broad, varying from organic

(e.g., latexes) to inorganic (e.g., silica, gold, semiconductors). These types of colloids are routinely employed for scientific investigations and technology-driven applications [3–5]. The emerging nanotechnology and biotechnology fields, however, will require tailor-made building blocks for the construction of advanced materials and devices. Since colloid particles are useful components of such systems, the availability of colloids with unique and tailored functional properties (e.g., optical, mechanical, thermal, electrical, magnetic, catalytic, biological) is highly desired, and routes that allow their preparation have attracted considerable interest [6].

One strategy to prepare colloids with novel physical and chemical properties involves their surface modification and/or coating with a range of compounds, either organic or inorganic [6, 7]. Several techniques have been used for forming polymer coatings [7], although polymerization-based methods are the most commonly employed. These include direct polymerization of monomers adsorbed onto the particle surface [8, 9], heterocoagulation-polymerization [10], and emulsion polymerization [7, 11]. Inorganic coatings are often formed by precipitation and/or surface reactions of inorganic precursors with the particle surface [12–14] or by the sonochemical generation of nanoparticles in the presence of larger colloids [15, 16]. Such coated colloids often display improved properties over the single-component particles, thus making them attractive for use in a broader range as well as new applications. For example, coated (or core–shell) colloids have been applied in encapsulation technologies, as immobilized catalysts, in drug delivery, electronics, separations, and diagnostics, as well as in the synthesis of combinatorial libraries [7, 17–23]. Despite the widespread use of coated colloids in these areas, many of the existing coating methods do not allow nanoscale control of the coating composition and thickness, and often the particles are non-uniformly coated, thus promoting aggregation. Therefore, there is much interest in the development and implementation of new particle coating technologies, especially ones that are both flexible and facile, and that are independent of the particle surface morphology and composition to deposit multicomposite coatings.

This chapter presents an overview of a recent, new, versatile layer-by-layer self-assembly process (when applied to colloids) that permits the preparation of coated (and encapsulated) colloids of different shapes and sizes, with uniform layers of diverse composition as well as controllable thickness. Herein, the method is denoted layer-by-layer colloid templating, LbL-CT. Following some practical issues that are important for the successful coating of colloids using the LbL-CT technique, emphasis will be placed on the wide variety of layer constituents as well as core colloids that can be used in the process. This will be exemplified by presenting a number of systems, ranging from coatings comprised solely of polymers, to nanoparticle-, protein-, and phospholipid-based coatings on colloids. It will be demonstrated that the colloid cores can be varied from enzyme crystals to crystallized low molecular weight dyes to biological cells. In these cases, the LbL-CT approach is exploited for encapsulation of the cores. The nanoscale control that can be afforded over the wall thickness will also be highlighted. An alternative procedure for colloid coating, termed controlled precipitation, will also be described. This is of particular interest when thick coatings are desired. Examples

demonstrating the mesoscopic arrangement of the coated colloids will be presented, followed by the properties of various functional (e.g. catalytically, optically, etc.) core–shell colloids, along with their utilization in various areas, such as photonics and immunodiagnostics.

12.2 Preparation and Characterization of Coated Colloids

Application of the LbL self-assembly to colloid templates represents a new and promising approach for the construction of coated particles. The LbL technology for "coating" *macroscopically flat* surfaces is now well established. Its origins can be traced back to the mid-1960s, when Iler showed that it was possible to deposit particles onto solid substrates in a LbL manner [24]. However, it was only after the pioneering work of Decher in the early 1990s, involving the LbL assembly of a combination of linear polycations and polyanions [25, 26], that an explosive growth occurred in the use of the LbL technology [27]. In ensuing years, the LbL technique was expanded to include, among other species, a host of inorganic nanoparticles, biomolecules, clays, and dyes in polyelectrolyte multilayer assemblies [27]. The LbL method was also applied to various *particles*, thus permitting the formation of nanocomposite core–shell particles [28, 29] and the encapsulation of various species [30–33]. For example, in the mid-1990s, Keller et al. reported the construction of alternating composite multilayers of exfoliated zirconium phosphate sheets and charged redox polymers on silane-modified silica particles [28]. Several years later, Chen and Somasunduran deposited nanosized alumina particles in alternation with poly(acrylic acid), which acts as the bridging polymer, on submicrometer-sized alumina core particles [29]. In other related studies, it was shown that the use of sequentially deposited polycation/polyanion multilayer coatings on preformed alginate-based microcapsules are effective in controlling their permeability. Vogt et al. showed that enzymes could be retained within alginate microcapsules upon coating with polycation/polyanion multilayers [30, 31]. A later study showed that one bilayer of alginate and chitosan deposited on preformed alginate–chitosan capsules only had a minor influence on the permeability of immunoglobulin G (IgG), whereas four double layers yielded a large effect in limiting the diffusion of IgG [32]. In most of these aforementioned studies [28–33], experimental evidence was provided for the formation of the coatings, however, the coatings were not characterized in detail after deposition of each layer, step-by-step. This section will deal specifically with our recent work on the LbL coating of colloids [34–39], outlining the practical considerations for coating colloids, as well as illustrating the layer-by-layer growth of various species on a host of different colloids, as assessed by a range of experimental techniques.

12.2.1
Layer-by-Layer Adsorption

The LbL-CT method allows the deposition of multiple layers on colloids in a controlled fashion [34–39]. In this strategy, depicted in Fig. 12.1, the first added species usually has an opposite charge to that on the colloids, thereby adsorbing through electrostatic interactions. An overcompensation of charge often results with adsorption of each layer, and at this stage the charge on the surface of the particles is reversed. This facilitates the alternate deposition of subsequent layers of a wide range of charged components. As is the case on planar supports [27], generally a polyelectrolyte is used to separate layers of the same or different materials. These polyelectrolyte interlayers not only act as molecular "glue", but they can also impart enhanced colloidal stability to the coated particles via electrostatic as well as steric contributions.

Although there are various experimental parameters that need to be optimized in order to LbL coat particles uniformly (e.g., particle concentration and size, polymer type, length, and concentration, and total salt concentration in the adsorbing solution; see later), the chief issue in transferring the LbL technology from macroscopic (planar) supports to colloid particles is the effective separation of the remaining free (unadsorbed) charged species from the colloidal dispersion prior to the next deposition cycle. Here we consider the case of polyelectrolyte adsorption, although many charged species can be treated in the same way as described in the following. The LbL assembly of polyelectrolytes onto colloid particles can be performed in two main ways. Either the concentration of polyelectrolyte added at

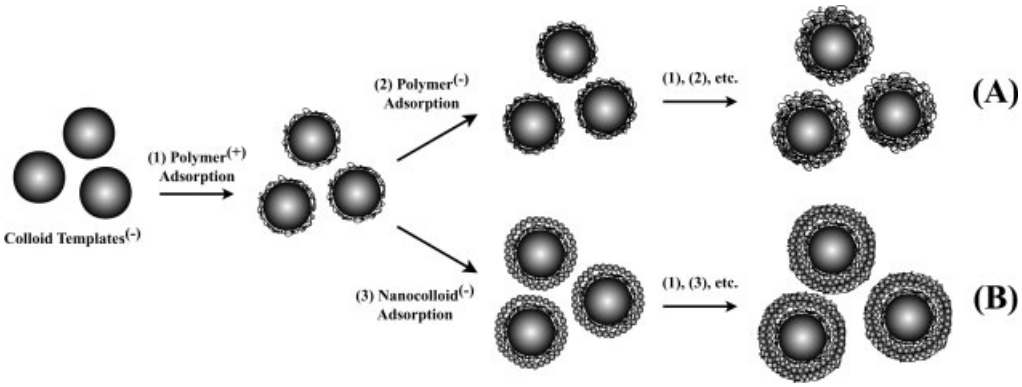

Fig. 12.1 Schematic illustration of LbL-CT constructed colloids. The coatings can be polyelectrolytes (A), or nanocolloids such as inorganic nanoparticles or proteins (B). Dyes or lipids can also be used as layer components (see text for details). The templates can be of synthetic (latexes, metal, crystallized low molecular weight compounds etc.) or biological origin (proteins, cells), with diameters in the nanometer to micrometer regime. The process typically involves the consecutive deposition of oppositely charged species onto the colloid particles, with repeated centrifugation or filtration and intermittent water washings between deposition of each layer.

each step is just sufficient to form a saturated layer [38], or adsorption is carried out at an excess concentration of polyelectrolyte [34–37]. Fig. 12.2 illustrates the ζ-potential behavior of PS particles, as well as the fluorescence of the non-adsorbed oppositely charged polyelectrolyte, as a function of total concentration of added polyelectrolyte [38]. The amount of "free" fluorescently labeled polyelectrolyte was measured in the supernatant after the particles were separated by centrifugation. The ζ-potential data show that with increasing bulk concentration of the adsorbing polyelectrolyte, recharging of the particle surface takes place. At a certain concentration, the ζ-potential levels off and, below this concentration, the polyelectrolyte is mostly adsorbed on the particles, depleting the bulk solution from the majority of polyelectrolyte. Further increasing the bulk polyelectrolyte concentration beyond this value does not influence the ζ-potential or the amount of polyelectrolyte on the particles. Repeating this process with optimized polyelectrolyte to particle concentrations can lead to the formation of polyelectrolyte multilayers on particles when oppositely charged polymers are employed.

In the second method, the excess, non-adsorbed polyelectrolyte is removed prior to the addition of the next polyelectrolyte (of opposite charge) in order to avoid the formation of polyelectrolyte complexes in bulk solution. The removal of excess polyelectrolyte can be achieved efficiently by performing several repeated centrifugation/washing cycles in pure water, followed by re-suspension of the particles [34–37], or by using a filtration set-up where the colloid particles are retained on the filter, but the polyelectrolytes are small enough to pass through the pores of the filter [40].

The above different approaches allow the formation of multiple layers of charged species on colloid particles, however some differences exist in the adsorbed amount of material, the number of particle aggregates, the ease of varia-

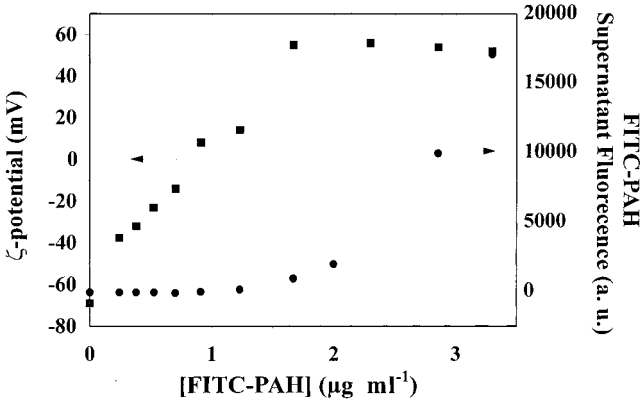

Fig. 12.2 ζ-potential of negatively charged 640 nm diameter PS particles and fluorescence intensity of non-adsorbed FITC-labeled PAH as a function of total concentration of added FITC-PAH. The adsorption of FITC-PAH was performed from aqueous solutions containing 0.5 M NaCl. The particle concentration was 2.2×10^8 particles mL^{-1} [38].

tion of the deposited substances, the degree of material loss during preparation, and the possibility to scale-up production of the coated particles [36, 38]. Regardless of the method used, typically, particle concentrations of a few (up to 10) wt.% are used in order to avoid particle aggregation upon addition of the coating species (e.g., polyelectrolyte, inorganic nanoparticles, proteins, lipids etc.).

In the following we address the main advantages and drawbacks of the aforementioned coating approaches. The main general challenge in the coating process is to suppress particle aggregation at different stages of the preparation, as it is often rather difficult (or even impossible) to resuspend strongly aggregated particles without significant modification or damage to the particle surface (e.g., due to sonochemical treatment when attempting to separate aggregated particles). The centrifugation/dispersion process can make the subsequent resuspension of the particles difficult if high centrifugal forces are applied. Other drawbacks of this strategy are the associated difficulties in centrifuging smaller particles (e.g. <50 nm) and the significant loss of particles during preparation. For instance, assembling 20 layers of polyelectrolytes on 640 nm diameter particles under typical coating conditions [36] can result in an accumulated total loss of 80% of the particles originally introduced. Washing and redispersing the particle suspension by means of centrifugation can also be rather time consuming, particularly if relatively small (<100 nm) particles are used. Nonetheless, the centrifugation approach continues to be widely used for the LbL coating of colloids, as the experimental conditions can be readily adapted for a variety of systems.

In the case of the sequential addition of polyelectrolyte at a suitable concentration to just coat the total available particle surface area, it is possible to prevent the direct formation of aggregates. In contrast to the centrifugation and filtration protocols, there is no loss of the polyelectrolytes used as layer constituents or the core particles. Further, once the conditions for the multilayer coating are determined (which may not always be straightforward), the coating process can be performed on a relatively short time scale because the adsorption of a polyelectrolyte layer (in the concentration range employed) usually takes only a few minutes. The major and highly limiting drawback of this procedure is that the probability of forming polyelectrolyte complexes and particle aggregates, as revealed by single particle light scattering (SPLS), is rather high [36]. This can, to some extent, be overcome by employing a dilute particle suspension. Notwithstanding, the concentrations of all components of the suspensions need to be accurately determined and controlled during the entire coating process; this can turn out to be laborious and highly involved. For these reasons, this method remains attractive only in a select few cases.

The filtration method is essentially the most practicable approach to scaling-up the LbL process for coating a large variety of colloid particles [40]. The particles are not subjected to intense centrifugal forces but are permanently and gently stirred. The liquid level above the filter can be exactly controlled by the interplay between the inflow and outflow of the components, including the suspension medium, and pressure applied for filtration. Since the filtrate can be recovered easily, this preparation procedure can, in principle, be readily automated. The membrane filtration unit has

adaptation capacity to meet the requirements of a variety of chemical and colloid chemical systems. Some limitations exist when dealing with smaller particles in this system, as this makes the use of filters with small pore size necessary, hence slowing down the process. This can lead to frequent replacement of filters due to clogging of the pores by the polyelectrolytes. Despite such issues, this method is the most attractive for preparing large quantities of coated particles.

The next subsections will deal with the fabrication and characterization of a range of novel core–shell materials using the LbL-CT approach. The first part will focus on the coating of colloids with multilayers of different composition and the second part on the use of different core materials. It will be shown that parameters such as shell thickness, composition and coating uniformity can be readily controlled. An alternative technique to obtain coatings on colloids via precipitation from solution onto particles will then be described.

12.2.1.1 **Multilayered Coatings**

As depicted in Fig. 12.1, colloid particles can be coated with a range of different species. These include, among other charged species, polyelectrolytes, inorganic nanoparticles, proteins, dyes and lipids. The following provides examples of such systems and data to verify their layer-by-layer preparation.

Polymers

Several experimental techniques can be employed to monitor the formation of each polyelectrolyte layer deposited sequentially on colloids. Microelectrophoresis provides a qualitative indication as to whether or not multilayers are deposited [34–38]. Fig. 12.3 shows the ζ-potential as a function of polyelectrolyte layer number for negatively charged polystyrene (PS) particles coated with poly(allylamine hydrochloride) (PAH) and poly(styrenesulfonate) (PSS), or with poly(diallydimethylammonium chloride) (PDADMAC)/PSS. As expected, the negatively charged (uncoated) PS particles show a negative ζ-potential, ca. 65 mV. The presence of a single layer of adsorbed positively charged polyelectrolyte on the PS particles causes a reversal in ζ-potential to positive values, and subsequent deposition of a negatively charged polyelectrolyte reverts the ζ-potential back to negative values. Further polyelectrolyte depositions cause the ζ-potential to alternate in sign, depending on whether the outermost layer is positively or negatively charged. This alternation in ζ-potential qualitatively demonstrates a successful recharging of the particle surface with deposition of each polyelectrolyte layer, suggesting that stepwise layer growth occurs on the particles. Similar data have been observed for a broad range of LbL assembled polyelectrolyte coatings [35, 36, 38, 40–43].

Quantitative evidence for the sequential deposition of polyelectrolyte multilayers on particles is provided by the technique of single particle light scattering (SPLS) [41]. SPLS involves recording the light scattered from a single particle at a given moment in time, and is therefore sensitive to the amount of adsorbed material on the colloid particles. This method is capable of unambiguously identifying coated

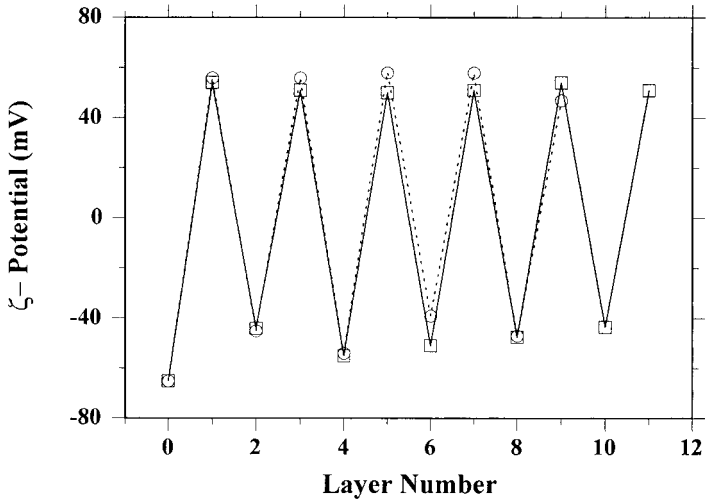

Fig. 12.3 ζ-potential of negatively charged 640 nm diameter PS particles as a function of polyelectrolyte layer number for (circles) PAH/PSS- and (squares) PDADMAC/PSS coatings. The odd layer numbers correspond to PAH or PDADMAC deposition and the even layer numbers to PSS adsorption. (Reproduced by permission of the American Chemical Society [41])
.

particles and discriminating between singlets, doublets, and triplets (as well as higher order aggregates) of particles. The layer thickness resolution of SPLS is about 1–2 nm. Currently, monodisperse particles as small as 200 nm up to about 950 nm in diameter can be investigated by SPLS. In Fig. 12.4, the intensity distribution of the control bare particles is compared with particles coated with 11 and 21 layers assembled by the filtration technique [40]. From the shift of the peak of the intensity distribution, the adsorbed mass can be derived. Given the refractive index of the polyelectrolyte layers (1.47), these data can be converted into layer thicknesses for the adsorbed polyelectrolyte multilayers. The polyelectrolyte film thickness increases proportionally with the number of layers deposited (Tab. 12.1) [41]. The mean polyelectrolyte layer thickness is approximately 1.5 nm (equivalent to approximately 1.0 mg m^{-2}) for PAH/PSS and PDADMAC/PSS coatings assembled from 0.5 M NaCl. Similar thickness values are obtained, regardless of whether the layers are prepared by centrifugation or filtration methods [40, 41]. It should be noted that the average layer thickness of polyelectrolyte multilayers can depend strongly on the type of polyelectrolytes and especially the salt concentrations used to process the layers [44]. Typically, increasing the salt concentration in the solution from which the polyelectrolytes are adsorbed leads to thicker layers. The above SPLS data show that the coating thickness can be controlled at the nanometer level for the polyelectrolyte layers, and that step-wise growth of the layers on colloids is achieved by using the LbL strategy. The thickness values obtained are also in agreement with those from X-ray reflectivity measurements for similar polymer multilayer films formed on planar silicon substrates under the

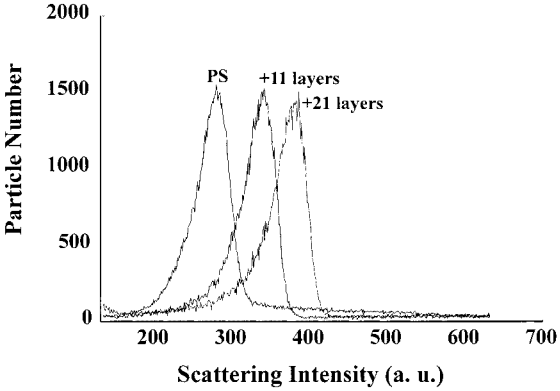

Fig. 12.4 Normalized SPLS intensity distributions (from left to right) of bare 640 nm diameter PS particles, and the same particles coated with a total of 11 and 21 PAH/PSS layers. (Reproduced by permission of the American Chemical Society [40].)

same ionic strength conditions [44]. The deposition of polyelectrolytes that contain strongly absorbing or fluorescing chromophores can be verified by UV–vis spectrophotometry and/or fluorescence spectroscopy, respectively [36, 42, 43].

Further confirmation for the successful nanoscale coating of colloids with polyelectrolyte multilayers is provided by transmission electron microscopy (TEM). Electron microscopy analysis of coated particles allows visualization of the increase in particle diameter with increasing layer number. Fig. 12.5 shows a TEM image of 640 nm diameter PS particles coated with 21 layers of PAH and PSS. The average diameter of the coated particles is increased to approximately 720 nm. The calculated coating thickness from TEM is in good agreement with the SPLS data (see Tab. 12.1). Uniformly coated and individual particles are seen.

Tab. 12.1 Thickness of polyelectrolyte multilayers assembled on 640 nm diameter PS particles as a function of layer number.

	Film thickness, d (nm) [a]	
Layers	***PAH/PSS***	***PDADMAC/PSS***
1	1.2	1.4
3	3.4	3.3
5	5.6	6.6
7	8.4	8.5
9	11.5	11.7
11	15.0	–
15 [b]	24.8	–
21 [b]	33.9	–

a) Thicknesses were determined from SPLS data and using a refractive index of 1.47.

b) The layers for these samples were prepared by using filtration (instead of centrifugation) to separate excess, unadsorbed polyelectrolyte. Adapted from [41].

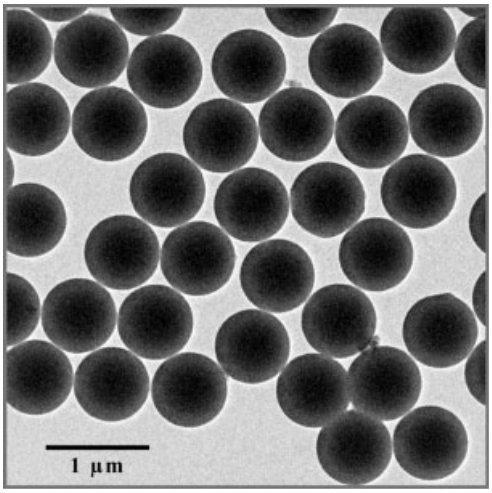

Fig. 12.5 TEM image of 640 nm diameter PS particles coated with a total of 21 layers of PAH/PSS. The particles were prepared by the LbL-CT approach shown in Fig. 12.1. The 21-layer coating resulted in an increase in particle diameter from 640 nm to approximately 720 nm. The polyelectrolyte coating cannot be seen by TEM due to the similar electron contrast of the core and coating [6].

The internal structure of polyelectrolyte multilayers is known to consist of an overlapping network of polycations and polyanions. That is, polyelectrolytes in multilayer films do not form strictly stratified layers but show an overlap (or interpenetration) over about 4 neighboring layers [27, 45]. This is supported by experiments involving PS particles coated with PAH/PSS multilayers of varying thickness (1 to 34 nm or 1 to 21 layers) and loaded with the multivalent fluorescent dye, pyrenetetrasulfonic acid, tetrasodium salt (4-PSA) [41]. After exposure to PSS solution, the PSS displaces the dye from layers within the film, suggesting that the top polyelectrolyte layer extends at least 4 layers downwards into the film, whilst the seventh layer contacts the fourth layer from the top.

Polymer–inorganic particles

By substituting one of the charged polyelectrolyte components with *nanoparticles*, nanoparticle-based multilayer assemblies can be constructed on colloid particles by the LbL-CT technique. The step-wise and regular formation of a wide range of nanoparticle-based coatings, from metals to metal oxides and semiconductors, have been prepared on submicrometer-sized particles via this approach. These include silica [37, 46–48], zeolite [49], iron oxide [50, 51] titania [48, 52], clays [48], gold [53], silica-coated gold (Au/SiO_2) [54], and luminescent semiconductors (CdTe) [55, 56]. The thickness of the multilayer coatings could be controlled with nanometer precision. Growth of the individual layers and morphology of the resulting coated particles were followed by electrophoresis, light scattering and electron microscopy. The representative TEM images in Fig. 12.6 show the highly uniform coatings obtained and the nanoscale control over the coating layer thickness (and hence the composite particle diameter) through simple variation of the number of deposition cycles for Au/SiO_2 nanoparticles ($\sim$20 nm diameter) [54]. (The nanoparticles were deposited in alternation with PDADMAC on 640 nm diameter

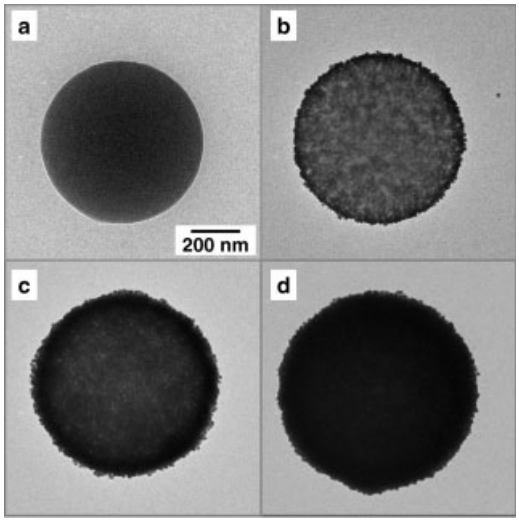

Fig. 12.6 TEM micrographs of PS spheres coated with (a) PDADMAC/PSS/PDADMAC and an additional (b) one, (c) three, and (d) five Au/SiO_2 nanoparticle/PDADMAC multilayers. A high uniformity of the Au/SiO_2 nanoparticle coating on the PS spheres can be seen, as well as a systematic increase in diameter of the particles with increasing layer number [54].

PS spheres.) By using processing conditions that screen the silica surface charge on the nanoparticles sufficiently (e.g., salt-based solutions), thereby allowing them to pack closely on the particle surface, approximately one monolayer of nanoparticles was adsorbed at each deposition step. The coated particles remain as individual, unaggregated colloidal entities in solution. If the Au/SiO_2 nanoparticles were deposited directly from pure water solutions, only sparse nanoparticle coverage on the spheres was obtained, and particle clumping occurred. The above study, as well as others [37, 46–53, 55, 56], underscores the importance of controlling the solution conditions to achieve uniform nanoparticle coatings on larger colloids when using the LbL technique. Microelectrophoresis experiments also show a reversal of surface charge when oppositely charged nanoparticles and polyelectrolytes are deposited onto larger colloid spheres, while SPLS and scanning electron microscopy (SEM) data verify that the coatings can be tuned with a thickness precision equal to the diameter of the nanoparticles for each nanoparticle deposition step [37, 46–53]. Additionally, atomic force microscopy (AFM) can be used to reveal a uniform nanoparticle coating and a systematic increase in the diameter of the coated colloids [47].

In contrast to the pure polyelectrolyte coatings, the incorporation of nanoparticles can introduce further structural stability to the layers. This is especially important in the creation of hollow spheres (see Section 12.3.1.2 and Chapter 13).

Polymer–proteins

The LbL-CT approach has also been shown to be suitable for the construction of protein multilayer architectures on colloid particles [57–61]. By the alternate deposition of protein and oppositely charged polymer on PS spheres, multilayer films of various proteins have been formed, including bovine serum albumin (BSA) [57], immunoglobulin G (IgG) [57], glucose oxidase (GOD) [58, 59], horse-

radish peroxidase (POD) [59], β-glucosidase (β-GLS) [60], and urease [61]. The thicknesses of the protein coatings varied from several to tens and even hundreds of nanometers [57], depending on the protein, the number of protein layers deposited, and the conditions of assembly. For example, by using the appropriate refractive indices for the protein ($n = 1.43$)/polyelectrolyte (1.47) coatings, the average thickness of the coatings could be determined from the SPLS data. For the fluorescein isothiocyanate-labeled BSA (FITC-BSA) multilayers, the coating thickness increases linearly with the number of protein layers deposited [57]. (The thickness of the polyelectrolyte interlayers, separating FITC-BSA layers, is approximately 0.5 nm.) The calculated average layer thickness increment for the FITC-BSA layers was 3.3 ± 1.1 nm when adsorbed from pure water (pH $\sim$ 5.6), and 5.8 ± 2.5 nm when deposited from a phosphate-buffered saline solution, pH 7. This difference in thickness was largely attributed to the higher percentage of charged groups on BSA at pH 7, and hence the greater degree of electrostatic interaction with the PDADMAC surface onto which it adsorbed. For IgG coatings, individual

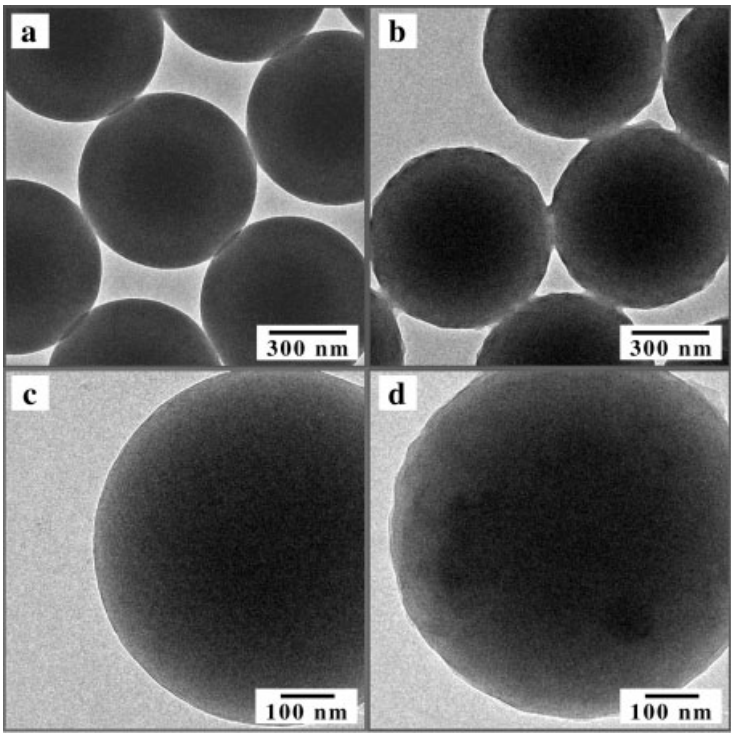

Fig. 12.7 TEM micrographs of PDADMAC/PSS/PDADMAC-coated PS spheres (a and c) and the same spheres additionally coated with [(FITC-BSA/PDADMAC)$_2$/FITC-BSA] (b and d). FITC-BSA was adsorbed from pure water. The presence of FITC-BSA on the surface can be seen (images b and d). The "bridging" seen at the surface where the particles are in contact is due to sample drying effects. (Reproduced by permission of the American Chemical Society [57].)

layer thicknesses of up to ~37 nm were observed, corresponding to the equivalent of several monomolecular protein layers [57].

TEM micrographs of PS particles (a and c) and those coated with three BSA multilayers (b and d) are shown in Fig. 12.7 [57]. The "control" PS particles display a smooth surface, whereas the PS particles coated with BSA multilayers show both an increase in surface roughness and an increase in diameter (compared with the "control" PS spheres). From the TEM images, the diameter increase of the particles coated with the three BSA layers is approximately 20 nm, corresponding to a coating/layer thickness increase of ~10 nm, a value which is in accord with the SPLS data. Although there can be a tendency for protein-coated particles to aggregate during or immediately after the protein deposition step, careful selection of the processing conditions for the coatings can alleviate this. Additionally, enhanced colloidal stability can be imparted to the systems by the presence of one or more outermost polyelectrolyte layers; subsequent deposition of outer polyelectrolyte layers is typically performed prior to storage and use of the particles. The LbL-CT approach permits the preparation of biofunctional coatings on colloids with a high density of biomolecules, making them of interest in applications where the signal, as a result of biological interaction, needs to be amplified for the successful detection of various species, or where a higher efficiency of product from enzyme–substrate reactions is required [58–61]. (Examples of this will be given in Section 12.3.2.)

Polymer–low molecular weight compounds

The alternating adsorption of multivalent ions and oppositely charged polyelectrolytes on colloid particles has been investigated recently [62]. Multilayer films composed of Tb^{3+}/PSS and 4-PSA/PAH were assembled on PS and melamine formaldehyde (MF) particles. The amount of assembled material was estimated by fluorescence spectroscopy. Linear growth of the "coating amount" versus the number of layers deposited was demonstrated. These multilayers are not stable and can be decomposed by the addition of salt and by varying the temperature, providing a means of altering the stability of the layers. Extraction of the low-molecular weight compounds from the coating can also lead to the break up of the layers.

Polymer–lipids

Lipids were shown to be involved in the LbL assembly on colloid particles when alternately adsorbed with polyelectrolytes. Lipid assembly can be performed by adsorbing the lipids on the particles from methanol solution or by adsorption of lipid vesicles from aqueous solution, following spreading of the lipids on the colloid particle surface [62–65]. The conformation of the assembled lipids is presumably in the form of bilayers, as was indicated by energy transfer measurements [63], but can depend on the type of lipids used. In the particular case investigated, the charged lipids formed bilayers and the non-charged lipids formed multilamellar structures. The attractive forces between the lipids and polyelectrolytes appear to determine the final conformation of the lipids on the particles.

In the case of lipid-coated hollow polyelectrolyte shells (obtained after core removal; see Chapter 13), the lipid coating was shown to affect the permeability properties of the polyelectrolyte shells. The shell wall becomes impermeable to water-soluble dyes [64] and less permeable to ions [65]. The presence of lipid layers on a supporting skeleton of polyelectrolyte, as for the polyelectrolyte shells, makes such systems attractive models for basic biophysical studies. They have a high stability and can be prepared with a defined size and shape (see Chapter 13).

12.2.1.2 Coating of Specific Cores

Influence of core size

Colloids of different sizes, shapes and composition can be employed as template particles in the LbL-CT method. Concerning organic colloid spheres, typically latex particles, both PS and MF, in the approximate range of 500 nm to 5 μm diameter are utilized [35–41]. Reducing the size of the latex particles represents a challenge with respect to establishing the appropriate experimental methods and conditions to generate uniform coatings and stable dispersions of the coated colloids. The importance of the experimental protocol mainly resides in the effectiveness of the separation procedures; that is, separating excess polyelectrolyte from coated particles that are less than 100 nm in diameter. It was shown that conventional centrifugation, using commercial, bench-top systems, could be applied to separate latex particles down to about 70 nm in diameter [42], although the centrifugal force needed (40 000 *g*) was considerably higher than that required for colloids larger than 500 nm in diameter ($\sim$10 000 *g*). If latex particles of even smaller size are employed, centrifugation becomes less attractive for routine separation of polymer and particles, particularly with respect to the time required, as typically several centrifugation/water wash cycles are employed. However, inorganic colloids, especially metals, can be readily separated by centrifugation, due to their inherently high density (compared with latex particles, for example). Gold nanoparticles are especially attractive for this purpose because the optical properties of the colloids can also be used to investigate the deposition of coatings on their surface [66, 67]. Despite the fact that the separation science is quite clear for the use of metal nanoparticles, as the template particles reduce in size, issues with regard to particle curvature become important. As already mentioned in Section 12.2.1, some of the important general experimental parameters that affect the coating of particles with polyelectrolytes are the nature of the polymer, polymer length, polymer concentration, and total salt concentration in the adsorbing solution. By taking into account the polymer length, polymer stiffness and added salt (leading to finite screening lengths), suitable conditions can be established that lead to polyelectrolyte-coated *nanoparticles* [66, 67]. In agreement with theoretical predictions [68], experimental conditions of 1 mM salt and polymers in the range of about 15–20 kDa were used to LbL deposit polyelectrolyte multilayers on gold nanoparticles of 30 nm in diameter. Red shifts in the spectral position of the surface plasmon absorption band peak (with little broadening) of the gold nanoparticles were observed, confirming the uniform deposition of polyelectrolyte multilayers [66, 67].

Preliminary studies show that sub-10 nm diameter particles can also be LbL coated; the importance here lies in modulating the unique size-dependent optical properties afforded by colloids in this size range, as well as their surface characteristics.

Enzyme particles

The LbL-CT protocol has been extended to coat, or more specifically to encapsulate, biologically significant materials in the form of biocolloids. Enzyme crystals (e.g., catalase) were encapsulated via the sequential deposition of oppositely charged polyelectrolytes onto their surface [69]. The catalase crystals, approximately 10 μm in diameter, exhibit a positive surface charge in water at pH 5 (ζ-potential = +20 mV, catalase isoelectric point = 5.8). This positive charge on the surface of the crystals facilitated the adsorption of FITC-PAH/PSS multilayers. As is the case for other colloidal systems, alternating ζ-potentials were obtained depending on the outermost layer (FITC-PAH, +20 mV; PSS, 30 mV), which is characteristic of polyelectrolyte multilayer growth on colloid templates (see earlier). Since the crystals are soluble in water above pH 6 and below pH 4, the coating steps were performed at pH 5 and 4 °C, and from polyelectrolyte solutions containing 1 M potassium acetate, to minimize enzyme dissolution. Fig. 12.8 shows a fluorescence micrograph of coated catalase crystals: the fluorescence originates from the surface of the polymer multilayer-coated enzyme crystals. No change in morphology of the crystals was observed as a result of coating. These particles contain an extremely high enzyme loading in each polyelectrolyte multilayer coating, and the activity of the encapsulated catalase is preserved after coating. The polymer multilayers assembled on the enzyme crystals underwent a morphology change from essentially rectangular to almost spherical upon solubilization (at pH 2) of the enzyme crystals [69]. This was attributed to the osmotic pressure build up inside the capsules as a result of solubilization of the enzyme (the coatings are permeable to small ions and water), since the enzyme was entrapped inside the polyelectrolyte

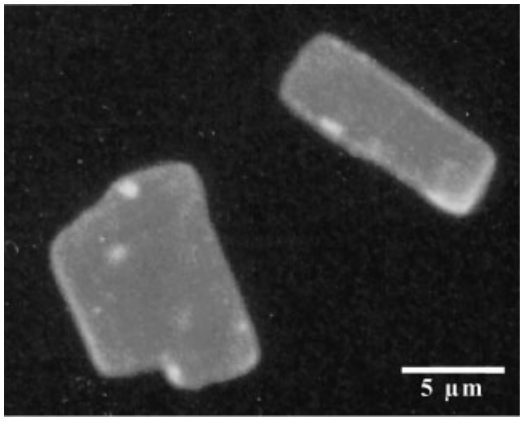

Fig. 12.8 Fluorescence optical micrograph of micrometer-sized catalase crystals coated with eight $[(PSS/FITC\text{-}PAH)_4]$ polyelectrolyte layers, highlighting the applicability of the LbL-CT method for encapsulation. The multilayer coating does not alter the enzyme crystal morphology, or the activity of the enzyme. (Adapted from [69].)

coating. The thin coatings also act as protective layers for the catalase, shielding them from enzyme degrading substances, such as proteases [69].

Polyelectrolyte multilayer assembly can also be performed on *amorphous* particles consisting of aggregates of proteins, which are formed prior to multilayer build-up. The use of micron-sized amorphous protein aggregates as templates for polyelectrolyte multilayer assembly was demonstrated for lactate dehydrogenase [70] and chymotrypsin [71]. As for the enzyme crystals, the polyelectrolyte multilayer coating of these aggregates encapsulates them and also provides a selective barrier for the diffusion of different species (substrates, inhibitors) from the exterior. A general scheme of protein aggregate encapsulation by polyelectrolyte multilayers is presented in Fig. 12.9. The concept of polyelectrolyte multilayer formation on protein aggregates is similar to that of multilayer deposition on colloid particles. It was shown that chymotrypsin, chosen as a model protein because its activity can be easily monitored [71], could be salted out to form chymotrypsin aggregates (Fig. 12.9 a, b). The precipitation of protein started immediately after mixing of the enzyme and saline solutions and was followed by an increase in turbidity of the solution. After a certain time the turbidity remained constant. Variations in the α-chymotrypsin and sodium chloride concentrations used permitted optimization of the enzyme precipitation reaction. Due to the positive charge of chymotrypsin at pH 2.3, the negatively charged polyelectrolyte PSS was deposited as a first layer to begin the multilayer assembly process (Fig. 12.9 c). PAH was assembled next (Fig. 12.9 d). Finally, these aggregates could be covered with a defined number of polyelectrolyte layers (Fig. 12.9 e). A typical SEM image of chymotrypsin aggregates coated with PSS/PAH/PSS layers is shown in Fig. 12.10. Rather amorphous aggregates of micron size were found. Each aggregate consisted of numerous, smaller protein particles, so called primary aggregates, in the shape of small spheres with a diameter of the order of 100–300 nm. This indi-

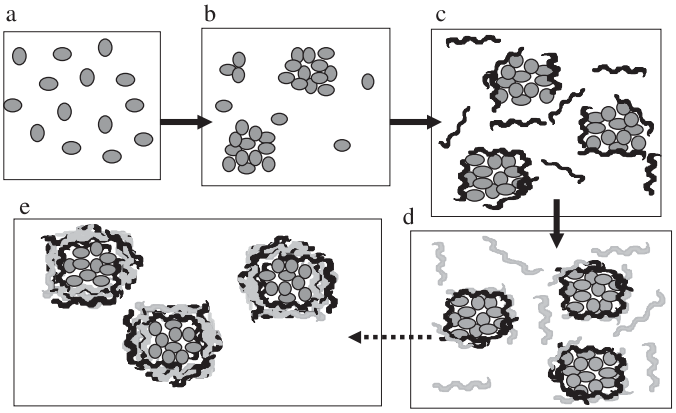

Fig. 12.9 Schematic of the LbL adsorption of polyelectrolytes onto protein aggregates preformed in salt solutions. See text for details. (Reproduced by permission of John Wiley and Sons [71].)

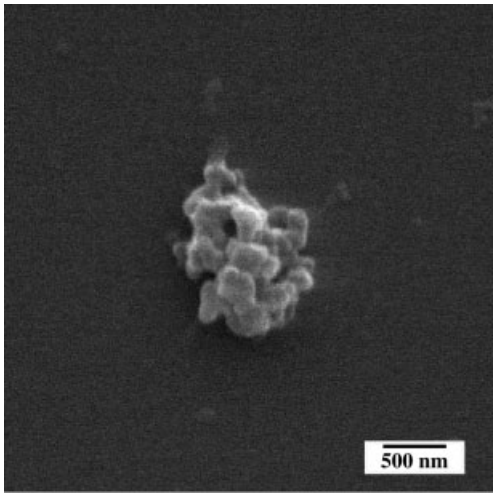

Fig. 12.10 SEM image of protein aggregates coated with PSS/PAH/PSS. (Reproduced by permission of John Wiley and Sons [71].)

cates a hierarchy in the formation of the protein aggregates. A characteristic feature of the aggregates is their large surface area, where pores within the aggregates can be observed. Such structures can be formed as a result of secondary aggregation of the primary aggregates, which is enhanced upon polyelectrolyte deposition. Further sequential polyelectrolyte layer assembling then preserves the structure of the secondary aggregates. Generally, the morphology of aggregates should depend on the preparation conditions, such as the time of aggregate growth, the nature of the polyelectrolyte used, and the number of layers deposited, which might influence the composition of aggregates. Enzymatic studies revealed that about 70% of the activity of the encapsulated chymotrypsin remained. As was the case for the enzyme crystals [69], the encapsulated enzyme is protected from high molecular weight inhibitors, which cannot penetrate the polyelectrolyte coating and influence the enzyme functionality [70]. In a related study, the assembly of three polyelectrolyte layers was performed on condensed DNA particles, with sizes of about 50–100 nm. Certain polymer compositions used for coating the DNA particles yield stable suspensions [72, 73], and facilitate the uptake of these particles by biological cells with sequential gene expression [73, 74].

Crystals of low molecular weight species

Similar to the crystals comprised of enzymes, crystallized, largely water-insoluble low molecular weight substances can also be encapsulated by LbL coating [75, 76]. However, unlike latex and biocrystal particle templates, the crystals used, either pyrene or fluorescein diacetate (FDA) [75, 76], were uncharged and required a precharging step prior to polyelectrolyte multilayer coating. Following exposure to a solution containing amphiphilic molecules (e.g., surfactants or phospholipids), the crystals could be redispersed in aqueous solution and were then found to be amenable to coating with polyelectrolyte multilayers. The pyrene and FDA tem-

plates could then be removed by exposure of the encapsulated particles to ethanol solution, which resulted in their solubilization. The LbL-CT coating of uncharged templates represents a significant step forward in encapsulation technologies, as the process can be applied to a variety of other low molecular weight, crystallized (or amorphous) materials, such as drugs. Studies have also shown that the release rate of the encapsulated low molecular weight materials is a function of the polymer coating thickness and the nature of the precharging layer [76].

Biological cells

Biological cells can also be utilized as cores for encapsulation. Gluteraldehyde-fixed echinocytes have been coated with polymer [77, 78] and polymer/nanoparticle [39] multilayers. The biocolloids have a jagged and highly structured surface, however the coating tends to follow the contour with nanoscale precision. Following removal of the core by treatment with a highly oxidizing solution, it was shown that the structure of the coating left behind mimics the original shape, including the secondary structure (spikes) of the biocolloid [39, 77, 78]. This is shown in Fig. 12.11 for the polymer/nanoparticle coatings [39]. Coating of biological cells in

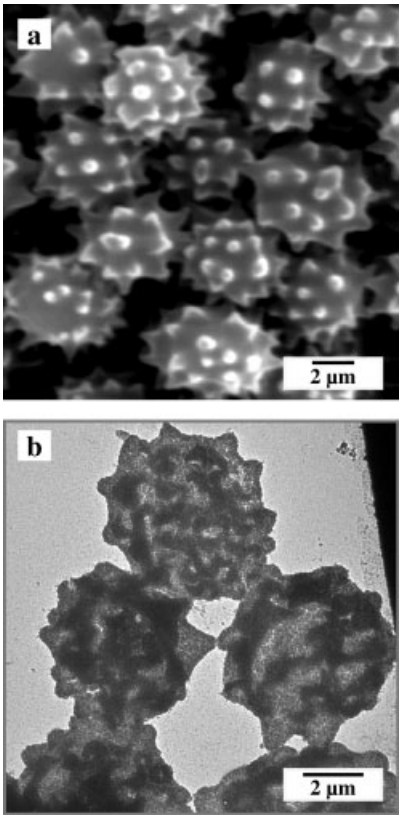

Fig. 12.11 (a) SEM image of echinocytes and (b) TEM image of hollow composite nanoparticle/polymer structures, derived by depositing three SiO_2 nanoparticle/PDADMAC layer pairs on polyelectrolyte-modified echinocytes and then removing the core by using an oxidizing solution [39].

this manner can provide an attractive means to encase them in ultrathin coatings, thus protecting them from external, undesirable species. Additionally, the surface properties of the cells can be modified by simple solution self-assembly of components onto their surface.

Overall, the above examples highlight the versatility and effectiveness of the LbL-CT method for preparing core–shell colloids with unique properties (see Section 12.3) and as a novel means for the facile encapsulation of a variety of compounds.

12.2.2 Colloid Precipitation

In contrast to the LbL method, the controlled surface precipitation (CP) approach consists of forming coatings of only one component. Additionally, this method can use charged and non-charged polymers and nanoparticles as coating constituents. The idea lies in controlling the heterocoagulation process when the quality of polymer or nanoparticle solution worsens (with respect to solubility), and precipitation begins. Since a particle suspension contains a large number of colloid particles, the precipitating materials collect on the surface of the particles. It was demonstrated that the slow heterocoagulation of polymer within a suspension of colloids leads to the controlled coating of particles by polymeric films [79]. Precipitation could be caused either by non-soluble complex formation between the polyelectrolyte and multivalent ions or by mixing the polymer solution with non-solvent. The proper choice of concentration ratio between the polymers, particles, and the speed of coagulation provides a coating coverage with a defined amount of precipitated polymer on each particle. The particles harvest the coagulated polymers and their complexes with multivalent ions on the particle surface. A theoretical consideration of this heterocoagulation of polymers in the presence of collector particles has been presented [79]. Experimental observations of the formation of a smooth film on the colloid particles have also been reported [80, 81], where it was shown that coatings composed of only one component (DNA), utilizing non-charged polymers (dextran), or complexes between ions and polyelectrolytes (Me^{3+}/PSS) [80], and coatings composed of PAH/PSS complexes formed in the solution prior to precipitation could be formed on colloid particles. The PAH/PSS complex was formed by slightly changing the solution pH from alkaline (pH $\sim$ 12), where there is no complex between these polymers, to pH around 8, resulting in polyelectrolyte complex formation. DNA and dextran were precipitated on the particle surface by the dropwise addition of ethanol in aqueous solution. As revealed by confocal microscopy images, the resulting coating is homogeneous for the investigated systems. The thickness of the polymeric film on colloids can be tuned down to the level of a few monomolecular layers. The CP method has an advantage in that it can be applied to compounds that cannot be deposited by means of LbL assembly. Conditions for precipitation, such as changing the solvent conditions or adding complexing ions, might be found for a wide class of polymers and nanoparticles as well. As shown by TEM, a homogeneous coating

on submicron sized latex particles can be formed from 4 nm semiconductor CdTe nanocrystals by their precipitation in ethanol (Fig. 12.12) [82]. These coatings can be formed with tunable thicknesses. Homogeneous and complete coverage of the colloid cores with a shell of luminescent nanocrystals with a thickness in the range 15–40 nm was achieved [82]. Controlling the precipitation of the solution components on the colloids implies that an adequate window is found with regard to the range of concentration of polymers, particles, and coagulation speed for each species to be deposited. Theoretical estimations of the concentration parameters in the system on the basis of a simple coagulation model give good agreement with experimentally observed optimal values [79]. Another advantage of the CP method of coating colloid particles, compared with the LbL technique, is that it is significantly less time-consuming, especially if thicker coatings (e.g. tens of monomolecular layers) are desired. By CP, the assembly is complete within minutes. The drawback of the CP approach is the crucial dependence of aggregation of the components on the diameter of the collector particles. Successful coatings by CP were obtained on particles with diameters of more than 400 nm, while the LbL-CT method has been explored for particles of diameter below 30 nm. Both the CP and LbL-CT methods complement each other. Additionally, the ordering of the monomolecular layers in the *z*-direction to the particle surface appears to be higher for coatings prepared by the LbL-CT method than those obtained by CP. While the LbL technique usually results in the formation of stable films, the CP assembled films can be easily decomposed by solubilizing the polymer again or by extracting the complexed ions. Added benefits should be brought by a combination of both of these methods, allowing the assembly of multicomposite films. LbL- and CP-processed colloid building blocks may provide solutions to diverse tasks related to the manufacture of micro- and nanostructured materials.

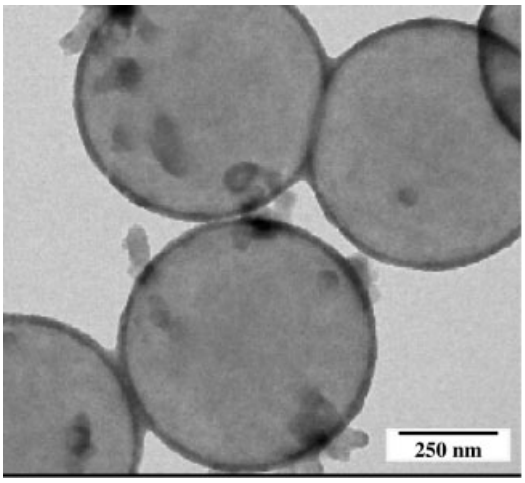

Fig. 12.12 TEM image of PS spheres covered by CdTe nanocrystals. The coating was formed by precipitation of the nanocrystals onto the spheres by drop-wise addition of ethanol into the aqueous nanocrystal solution. The coating can be seen as a ring around the spheres. Some excess (i.e., non-adsorbed) material can also be seen [82].

12.3
Assembly and Utilization of Coated Colloids

12.3.1
Mesoscopic Arrangement

12.3.1.1 Colloidal Crystals

Monodisperse colloid spheres (e.g., silica or polystyrene) can spontaneously self-organize into crystal structures at optical wavelength scales with long-range periodicity [83–88]. These ordered colloidal assemblies, otherwise known as colloidal crystals, can possess an optical stop band in the visible and near-IR spectral ranges when the spheres are in the micron- and submicron-size regime. Although numerous studies exist on the formation of photonic materials from colloids, few have exploited the use of *coated colloids* as building blocks [89, 90]. The employment of LbL coated colloids in the formation of these crystals, with independent control over the size of the core, as well as thickness and composition of the coating, opens up a versatile and attractive route to tailoring their optical properties. Recently, via LbL control of the coating thickness and coating composition, colloidal crystals with tunable optical properties have been constructed [56, 91, 92]. Coatings comprised of pure polyelectrolyte multilayer [91, 92], semiconductor nanoparticle/polyelectrolyte [56], and gold nanoparticle/polyelectrolyte [92] coatings have been formed on submicron-sized PS spheres, and the resulting coated colloids have been assembled into ordered arrays by either sedimentation of the colloids or by using a specially designed filtration-flow cell. Fig. 12.13 shows a representative example of the utilization of CdTe(S)/polyelectrolyte-coated PS particles to form colloidal crystals. Such LbL-CT processed colloids can be crystallized [56], although optimized coating conditions should be employed to prepare uniformly coated, isolated particles in solution since the presence of even a small number of aggregates can significantly influence or prevent their crystallization. The position of the optical stop band of colloidal crystals prepared from LbL coated colloids can be tuned with nanoscale precision, through variation of the coating thickness and/or by the composition of the coating [91, 92]. The above investigations into the formation of colloidal crystals from LbL-CT prepared colloids are very recent. It is anticipated that following further elaborate studies into the crystallization behavior of multilayer-coated particles, considerable progress will be made with the formation of novel colloidal crystals with unique optical properties.

12.3.1.2 Macro- and Mesoporous Materials

Colloid particles have also found wide use in the formation of a broad range of three-dimensional macroporous materials. These materials are generally comprised of highly ordered air spheres interconnected by small channels [93, 94]. They can be produced by using colloidal crystals as a three-dimensional ordered scaffold, around which other materials can be infiltrated or synthesized using wet chemistry techniques, such as sol–gel processes. The templates are then removed

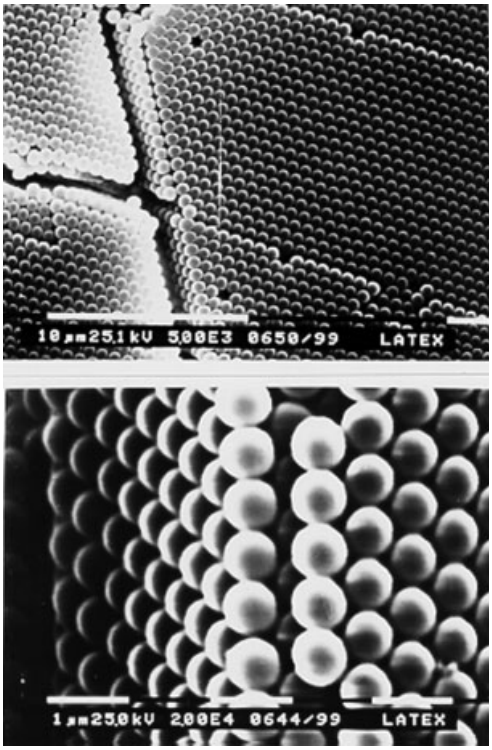

Fig. 12.13 SEM images of 3D colloidal crystals of 640 nm diameter PS spheres coated with polyelectrolyte/CdTe(S) nanocrystals. The coating thickness is 5–8 nm [56].

by calcination or decomposition with a solvent, leaving a periodic and open pore structure in the dielectric matrix, also known as "inverse opals". Inverse opals of metals [95, 96], metal oxides [97, 98], semiconductors [99], carbon and silicon [100, 101], and polymers [102–105], have been fabricated by using a variety of colloidal crystal templates. LbL-CT constructed colloids have also been used to prepare macroporous inorganic and inorganic-composite materials [49, 106]. It was shown that an ordered silicalite (zeolite) macroporous monolith was formed by gravity sedimenting prefabricated PS sphere–silicalite nanoparticle/polyelectrolyte core–shell particles into close-packed assemblies, followed by calcination (Fig. 12.14) [49]. The wall thickness and pore diameters of the hierarchically ordered monolith were controlled by the coating thickness and template diameter, respectively. In a related study, macroporous TiO_2 and inorganic-composite structures were produced by infiltrating a titanium dioxide precursor into templates of sedimented, close-packed coated colloid spheres, followed by removal of the organic material by calcination [106]. The pore morphology of the resulting macroporous structures was controlled by the nature of the multilayers deposited on the colloid particles: open and closed pore structures were observed for spheres coated with polyelectrolyte multilayers and silica nanoparticle/polyelectrolyte multilayers, respectively. The wall thickness of the pores was tuned on the nanometer scale by

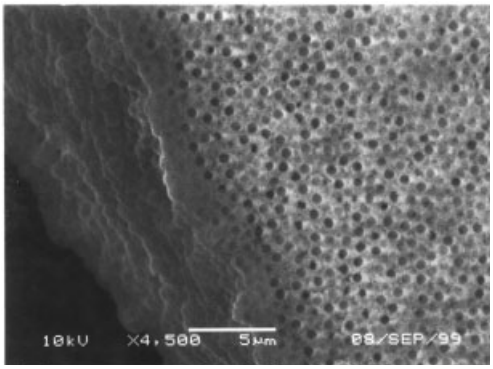

Fig. 12.14. SEM image of an ordered macroporous monolith, formed by assembling PS spheres coated with five silicalite nanoparticle/polyelectrolyte layer pairs into a close-packed arrangement, and subsequently calcining. (Reproduced by permission of the American Chemical Society [49].)

varying the number of deposited multilayers (e.g., from about 10 to 40 nm for PS spheres coated with 5 and 21 polyelectrolyte multilayers, respectively). In a further study, regularly spaced, linear chains of up to 600 μm of core–shell particles comprising latex cores and iron oxide nanoparticle shells have been formed under the influence of an external magnetic field [107]. The separation and the length of the individual chains can be tuned by the magnetic field strength and the concentration of the particle solution. This opens new avenues for the creation of organized structures from magnetic core–shell building blocks.

Coated colloids can also be used as precursors to the formation of hollow colloids (or hollow capsules), which are of immense interest in a range of areas, including drug delivery, catalysis, waste removal, piezoelectric transducers, and functional materials processing [39]. The hollow colloids can be derived from the coated colloids upon removal of the core by either chemical or thermal means (see Chapter 13). Since the coatings are semi-permeable, the core can be removed, leaving behind a "shell", that is, the coating. Hollow polymer [34, 38, 42, 66, 108, 109], inorganic [37, 48, 49, 51, 52, 54], and organic–inorganic composite [37, 39] colloids have been prepared. The hollow polyelectrolyte colloids are usually generated by using a solvent-decomposable colloid, which acts as the template for coating. When hollow inorganic colloids are formed, the nanoparticles in the coating are sintered through the high temperature treatment used to generate them, providing structural integrity for the hollow colloids. The hollow capsules can be LbL engineered to be robust, biocompatible, decomposable, and with tuned permeability. Additionally, they can exhibit macropores, mesopores and/or micropores in their walls. Chapter 13 deals specifically with the formation of hollow capsules and their application.

12.3.2 Enzymatic Catalysis

12.3.2.1 Dispersions

Enzyme multilayer-coated colloids are attractive enzyme reactors. This is mainly due to the inherently high surface area of colloids, which provides the potential to yield higher enzymatic reaction efficiencies than their planar film counterparts. It was shown that by using the LbL-CT approach, control could be exerted over both the total amount of enzyme deposited on colloid particles and the architecture of the enzyme film [58–61]. Glucose oxidase (GOD), horseradish peroxidase (POD), or preformed enzyme–polyelectrolyte complexes were assembled in alternation with oppositely charged polyelectrolytes onto PS particles [58, 59]. It was found that deposition of polyelectrolyte onto particles with GOD or POD forming the outermost layers resulted in partial removal of the adsorbed enzyme layer, whereas no such enzyme removal was observed with subsequent polyelectrolyte deposition onto coated particles when the enzyme was pre-complexed with polyelectrolyte prior to adsorption. The latex carrier particles coated with the enzyme multilayers such as GOD and/or POD were exploited as specific enzyme reactors [58, 59]. Use of the colloidal biocatalysts for enzymatic catalysis showed that the enzymatic activity (per particle) increased with the number of enzyme layers immobilized, irrespective of whether or not the enzyme was pre-complexed. Particles coated with preformed enzyme–polyelectrolyte complexes, however, displayed a significantly lower enzymatic activity (about 10 times less) than those prepared by the direct adsorption of free enzyme. Fig. 12.15 shows the rate of change of absorbance at 500 nm (i.e., a direct measure of the enzymatic activity) for PS particles coated with one to four PEI/GOD layers, and with one to five PSS/POD layers [59]. (Here, the enzyme and polyelectrolytes were not pre-complexed before deposition.) The differences in the relative increase in activity with layer number for the two systems was attributed to differences in the enzyme/polymer layer structure. These studies demonstrate that enzyme multilayer-coated particles with tailored enzymatic yields could be prepared. Multi-component enzyme multilayer films on colloids were also prepared and exploited in sequential enzymatic catalysis. In addition, particles pre-modified with an electrostatically deposited layer of magnetic nanoparticles and subsequently coated with enzyme multilayers were repeatedly used as catalysts [59, 61]. These particles were fabricated by using the LbL approach, beginning with the magnetic nanoparticles, followed by the enzyme multilayers. They were rapidly and easily separated with a magnet after the enzymatic reactions were performed. These colloidal systems are of major significance because of their inherently high surface area for reaction, their ability to increase the catalytic output in relation to the number of immobilized enzyme layers, their complex and multiple catalytic functions, and because the particles can be easily separated and reused multiple times.

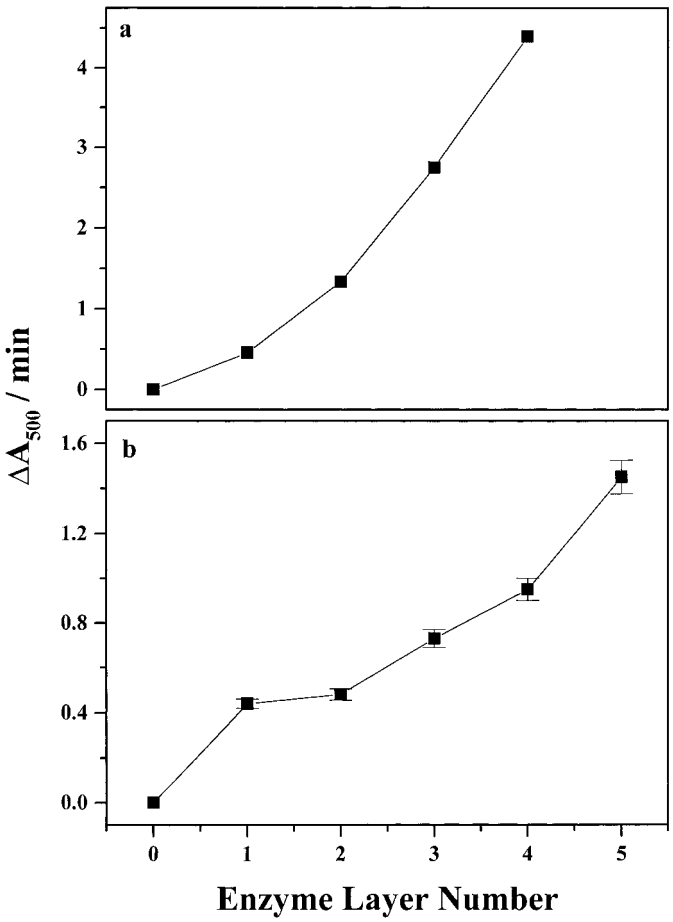

Fig. 12.15 Activity (ΔA_{500}/min) of colloidal catalysts–PS particles coated with enzyme multilayers: (a) PEI/GOD bilayers and (b) PSS/POD bilayers. The data is normalized for particle number. (Adapted from [59].)

12.3.2.2 **Thin Films**

As outlined in Section 12.2.1.2 enzyme particles, the LbL-CT encapsulation of crystallized enzymes yields a high loading of encapsulated biomaterial within a very thin coating of polyelectrolytes [69]. Such encapsulated enzyme microcrystals are attractive for use as immobilized catalysts. This was achieved by employing them as building blocks in the preparation of novel enzyme multilayer films. They were LbL assembled on planar supports with an oppositely charged polymer to create stable, relatively thin (few micrometers), high enzyme content multilayer films for biocatalysis applications [110]. Through the number of layers deposited, thin films of controllable thickness and biocomponent content were prepared. The formation of the films was monitored by using a quartz crystal microbalance,

which showed that each enzyme layer formed from polyelectrolyte-encapsulated catalase crystals had a mass of about 3870 ng (equivalent to 120 mg m^{-2}), compared with 378 ng for uncoated catalase crystals and about 100 ng for solubilized catalase. This highlights the fact that the polyelectrolyte coating facilitated film growth with regard to higher enzyme loadings. The thin films were found to be highly bioactive, exhibiting biocatalytic activities of up to 50 times higher than those prepared by conventional LbL deposition of solubilized enzyme. Even films formed by the deposition of the encapsulated catalase crystals for only 10–30 s (adsorption equilibrium was reached after 60 min) showed enzymatic activities 20–30 times higher than corresponding films formed from solubilized enzyme. These films can also be used as biosensors: since they are very thin, they can provide fast response times [111]. Additionally, multicomponent films can be prepared simply by depositing polyelectrolyte-encapsulated colloids of different enzymes. These films form attractive candidates for use in various biotechnological applications.

12.3.3 Tailored Optical Properties

Coating colloids with optically functional materials such as dye-labeled polymers and metal nanoparticles permits the creation of colloids with unique optical properties [53, 54, 112]. Fluorescent microspheres were prepared by the LbL assembly of dye-labeled PAH and PSS onto PS particles [112]. By selecting different fluorescent dyes (FITC, RhBITC, Cy5) to conjugate with PAH, 640 nm diameter particles with three different emission maxima were prepared. As shown in Fig. 12.16, the emission maxima of FITC–PAH, RhBITC–PAH and Cy5–PAH coated PS particles were 526 nm, 586 nm, and 665 nm, respectively, showing that particles with predetermined emission wavelengths can be readily prepared. Equally important is that the fluorescence intensity of LbL-CT prepared particles can be tuned, depending on the number of dye-labeled polyelectrolyte deposition cycles. Fluorescence microscopy image (FMI) analysis of individual particles showed that the fluorescence intensity of the coated particles increases linearly with increasing number of FITC–PAH layers [112]. The LbL-CT approach represents a promising method to fabricate powerful fluorescent particles, which may be utilized in immunoassays (see Section 12.3.4).

The deposition of metal nanoparticles on larger spheres provides a new class of micron-scale colloidal entities with optical properties that can be tailored by changing the hierarchical assembly of the nanoparticles [53, 54]. It was shown that the optical properties of PS–Au/SiO_2/PDADMAC core–shell particles, prepared by LbL-CT (e.g., see Fig. 12.6), can be modulated via altering the thickness of the nanoparticle-based multilayer shell [54]: the spectral position of the surface plasmon absorption band maximum, λ_{max}, due to the core of Au/SiO_2 nanoparticles, red-shifted with increasing shell thickness. λ_{max} for the particles coated with one, three, and five Au/SiO_2 nanoparticle/PDADMAC multilayers shifted from 588 ± 2 to 618 ± 2 to 642 ± 2 nm, respectively. This red shift in λ_{max} is due to the coupling of the surface

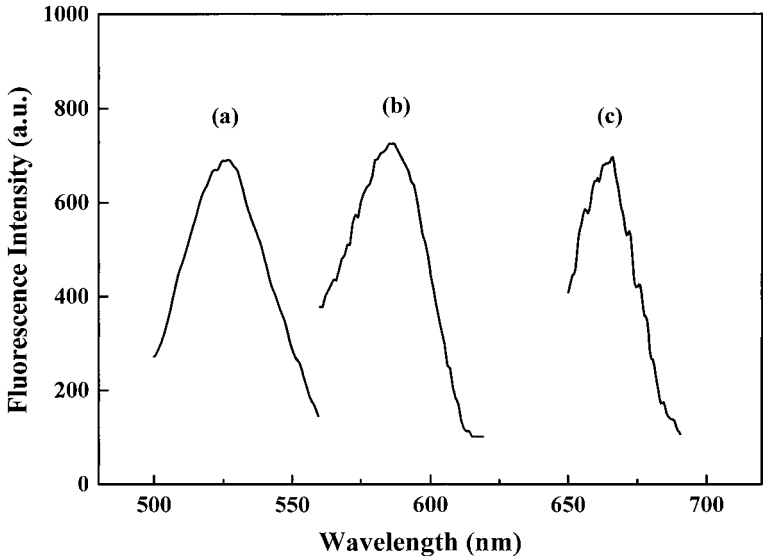

Fig. 12.16 Normalized fluorescence spectra of ~640 nm diameter PS particles LbL coated with dye-labeled PAH. The unlabeled polyelectrolyte PSS was used as the interlayer. (a) PS/(FITC-PAH/PSS); (b) PS/(RhBITC-PAH/PSS); (c) PS/(Cy5-PAH/PSS). The morphology of the coated particles is similar to that of the particles shown in Fig. 12.5. (Reproduced by permission of Academic Press [112].)

plasmons in neighboring particles. (λ_{max} of the Au/SiO_2 nanoparticles in aqueous solution is at 520 ± 1 nm.) However, the gold nanoparticles behave as discrete but coupled particles and not as a thin, continuous metal shell.

Colloids coated with CdTe nanoparticle/polyelectrolyte multilayers were also prepared and used to form colloidal crystals (as mentioned in Section 12.3.1.1; see Fig. 12.13) [56]. These particles display luminescence properties due to the nanoparticles embedded in the polymer coatings. The luminescence maximum red-shifted from 590 nm for CdTe(S) nanoparticles in aqueous solution to 595 nm for the nanoparticles in the colloidal crystal. This difference was attributed to the close packing of the CdTe(S) nanoparticles in the polyelectrolyte layers and the change in the environment for the semiconductor nanoparticles from water to polymer. Designing colloidal crystal systems where the emission spectrum of, say the nanocrystals in the coating, overlaps with the photonic stop band of the colloidal crystal provides the opportunity to control the spontaneous emission using both the electronic (semiconductor nanoparticles) and photonic (artificial opals) states.

12.3.4 Other Applications

Biologically-modified particles are widely used in immunodiagnostics. Such particles are commonly fluorescent with specific immunoreagents adsorbed onto their

surfaces. Biofunctional fluorescent microparticles for application in immunoassays were prepared by the LbL-CT method: multiple layers of fluorescently labeled polyelectrolytes were deposited onto colloid particles, followed by deposition of the protein [112]. The suitability of the mouse immunoglobulin G (IgG)-coated fluorescent PS particles for immunodetection was investigated by a solid-phase immunotest. Goat anti-mouse IgG adsorbed on the polystyrene culture dish surface acted as the capture antibody to recognize mouse IgG. Strong binding between anti-mouse IgG and mouse IgG immobilized on the fluorescent PS microparticles was observed, leading to fluorescence from the dish. Control experiments verified the specific interaction between passively adsorbed immunospecies on the particles and the immobilized antibodies or antigens on the dish. Similar studies were conducted with smaller particles (< 100 nm) as templates in order to compare the sensitivity of the biofunctional particles with conventional immunoprobes. The preliminary data of the sandwich microplate assay showed this to be a promising approach to increase the sensitivity of fluorescent immunoassays.

When low molecular weight uncharged model drugs in crystalline form are encapsulated in polyelectrolyte multilayers (see Section 12.2.1.2 Crystals of low molecular weight species), the drug release rate, after solubilization of the drugs, can be tuned by varying the number of layers deposited and the nature of the precharging species [76]. This, and similar systems [113], are highly attractive for the sustained release of drugs (also see Chapter 13). They are also appealing for immunoassay applications when the low molecular weight compounds are fluorescent and when receptor molecules are attached to the surface of these coated particles. Biomodified, polyelectrolyte-encapsulated crystals of low molecular weight, fluorescent compounds have recently been utilized in immunoassays [114]. After interaction of these particles with the immobilized biomolecules in the immunotests and exposure to ethanol to solubilize the uncharged core molecules, extremely high fluorescent signals are obtained, providing a novel means to conduct highly sensitive immunoassays.

Core–shell microspheres containing catalytically active complexes [115] or metal nanoparticles [116] have also been prepared for catalysis investigations. These studies make use of the LbL-CT protocol to prepare multilayer-coated colloids.

12.4 Summary and Outlook

The examples presented in this chapter demonstrate the wide range of coated colloids that can be nanoengineered through application of the LbL technique to colloids. The inherent flexibility and unparalleled simplicity of the LbL method, demonstrated for over a decade on planar supports, can be equally well adapted to colloids, provided that parameters such as the concentration, and the nature and size of the core particles are considered along with the appropriate conditions to deposit the coating layers; for example, polymer type, length, and concentration for polyelectrolyte coatings, and nanoparticle type and size for nanoparticle coatings.

As documented in studies involving the formation of planar thin films, the role of salt in the adsorption solutions is important in determining the final structure and thickness of the layers; however, the influence of salt on the interaction between the template particles and the coating species needs also to be considered when LbL coating colloids, as it can lead to aggregation of the particles. Use of "suitable" salt concentrations can make the polyelectrolyte more flexible so that it coats more effectively, and can screen the charges between the nanoparticles being deposited to make them pack closer to each other and give more uniform nanoparticle coatings. These conditions need to be determined and optimized for specific systems and become more important as the size of particles to be coated is decreased into the nanometer regime. The control that has been available for processing thin films on planar supports has also been shown to apply to coatings on particles: the coating thickness can be modulated with nanometer precision, and the coating composition is defined by the step-by-step deposition of each species. The LbL-CT approach not only allows the creation of novel core-shell colloids with various functions (e.g. catalytic, optical, chemical magnetic etc.) but it provides a facile means to encapsulate a variety of significant compounds. Examples given of the utilization of LbL processed coated/encapsulated colloids emphasize the enormous technological relevance of such colloids. When used as building blocks, complex, hierarchical structures with predefined functions can be constructed. This opens new, exciting opportunities for the application of these colloids in various applications in the physical and life sciences, including photonics, catalysis, sensing, diagnostics, and drug delivery.

Acknowledgements

We thank our many outstanding colleagues from around the world, whose names are listed in the bibliography, for their excellent contributions to the research and for their fruitful collaboration. We also thank H. Möhwald for support of this work. We acknowledge funding from the BMBF under the BioFuture, Functional Supramolecular Systems, and Sofia Kovalevskaja programs, the Volkswagen Foundation, the DFG, the DAAD, the Alexander von Humboldt Foundation, and the companies Bayer, BASF, and Henkel.

12.5 References

1 J. N. Israelachvili, *Intermolecular and Surface Forces*, Academic Press, New York, 2nd edn., 1991.

2 P. M. Claesson, T. Ederth, V. Bergeron, M. W. Rutland, *Adv. Colloid Interface Sci.* **1996**, *67*, 119.

3 D. C. Blackley, *Polymer Latices: Science and Technology*, Chapman and Hall, London, 2nd edn., 1997, vol. 2.

4 Colloidal Gold: Principles, Methods and Applications, Ed. M. A. Hayat, Academic Press, New York, 1989, vol. 1.

5 E. Matijevic, *Chem. Mater.* **1993**, *5*, 412.

6 For a review, see: F. Caruso, *Adv. Mater.* **2001**, *13*, 11, and references therein.
7 C.H.M. Hofman-Caris, *New J. Chem.* **1994**, *18*, 1087, and references therein.
8 S.M. Marinakos, J.P. Novak, L.C. Brousseau, A.B. House, E.M. Edeki, J. C. Feldhaus, D.L. Feldheim, *J. Am. Chem. Soc.* **1999**, *121*, 8518.
9 C.L. Huang, E. Matijevic, *J. Mater. Res.* **1995**, *10*, 1327.
10 R.H. Ottewill, A.B. Schofield, J.A. Waters, N.St.J. Williams, *Colloid Polym. Sci.* **1997**, *275*, 274.
11 L. Quaroni, G. Chumanov, *J. Am. Chem. Soc.* **1999**, *121*, 10642.
12 R.K. Iler, *U.S. Pat.*, 2,885,366, 1959.
13 N. Kawahashi, E. Matijevic, *J. Colloid Interface Sci.* **1991**, *143*, 103.
14 L.M. Liz-Marzan, M. Giersig, P. Mulvaney, *Langmuir* **1996**, *12*, 4329.
15 S. Ramesh, Y. Cohen, R. Prosorov, K.V P.M. Shafi, D. Aurbach, A. Gedanken, *J. Phys. Chem. B* **1998**, *102*, 10234.
16 N. Arul Dhas, A. Zaban, A. Gedanken, *Chem. Mater.* **1999**, *11*, 806.
17 F. Lim, A.M. Sun, *Science* **1980**, *210*, 908.
18 *Hollow and Solid Spheres and Microspheres: Science and Technology Associated With Their Fabrication and Application*, Eds. D.L. Wilcox, M. Berg, T. Bernat, D. Kellerman, J.K. Cochran, Materials Research Society, Pittsburgh, **1995**.
19 E. Matijevic, in *Fine Particle Science and Technology*, Ed. E. Pelizetti, Kluwer, Dordrecht, 1996, pp. 1–16.
20 S.J. Shuttleworth, S.M. Allin, P.K. Sharma, *Synthesis* **1997**, *11*, 1217.
21 R. Partch, in *Materials Synthesis and Characterization*, Ed. D. Perry, Plenum Press, New York, **1997**, pp. 1–17.
22 R. Davies, G.A. Schurr, P. Meenan, R.D. Nelson, H.E. Bergna, C.A.S. Brevett, R.H. Goldbaum, *Adv. Mater.* **1998**, *10*, 1264.
23 R. Langer, *Acc. Chem. Res.* **2000**, 33, 94.
24 R.K. Iler. *J. Colloid Interface Sci.* 1966, *21*, 569.
25 G. Decher, J.-D. Hong, *Ber. Bunsen-Ges. Phys. Chem.* **1991**, *95*, 1430.
26 Decher, G., Hong, J.-D. *Makromol. Chem., Macromol. Symp.* **1991**, *46*, 321.
27 For reviews, see: (a) G. Decher, *Science* **1997**, 277, 123, and references therein; (b) G. Decher, in *Templating, Self Assembly and Self-Organisation*, Eds. J.-P. Sauvage, M.W. Hosseini.,Pergamon Press, Oxford, 1996, vol. 9, pp. 507–528.
28 S.W. Keller, S.A. Johnson, E.S. Brigham, E.H. Yonemoto, T.E. Mallouk, *J. Am. Chem. Soc.* **1995**, *117*, 12879.
29 T. Chen, P. Somasundaran, *J. Am. Ceram. Soc.* **1998**, *81*, 140.
30 R. Pommersheim, J. Schrezenmeir, W. Vogt, *Macromol. Chem. Phys.* **1994**, *195*, 1557.
31 P. Rilling, T. Walter, R. Pommersheim, W. Vogt, *J. Membr. Sci.* **1997**, *129*, 283.
32 O. Gaserod, A. Sannes, G. Skjak-Braek, *Biomaterials*, **1999**, *20*, 773.
33 A. Bartkowiak, D. Hunkeler, *Chem. Mater.* **2000**, *12*, 206.
34 E. Donath, G.B. Sukhorukov, F. Caruso, S.A. Davis, H. Möhwald, *Angew. Chem. Int. Ed. Engl.* **1998**, *37*, 2201.
35 F. Caruso, E. Donath, H. Möhwald, *J. Phys. Chem. B* **1998**,*102*, 2011.
36 G.B. Sukhorukov, E. Donath, H. Lichtenfeld, E. Knippel, M. Knippel, H. Möhwald, *Colloids Surf A* **1998**, *137*, 253.
37 F. Caruso, R.A. Caruso, H. Möhwald, *Science* **1998**, *282*, 1111.
38 G.B. Sukhorukov, E. Donath, S. Davis, H. Lichtenfeld, F. Caruso, V.I. Popov, H. Möhwald, *Polym. Adv. Technol.*, **1998**, *9*, 759.
39 For a review see: (a) F. Caruso, *Chem. Eur. J.* **2000**, *6*, 413, and references therein.
40 A. Voigt, H. Lichtenfeld, G.B. Sukhorukov, H. Zastrow, E. Donath, H. Baümler, H. Möhwald, *Ind. Eng. Chem. Res.* **1999**, *38*, 4037.
41 F. Caruso, H. Lichtenfeld, E. Donath, H. Möhwald, *Macromolecules* **1999**, *32*, 2317.
42 F. Caruso, C. Schüler, D.G. Kurth, *Chem. Mater.* **1999**, *11*, 3394.
43 D.G. Kurth, F. Caruso, C. Schüler, *Chem. Commun.* **1999**, 1579.
44 G.B., Sukhorukov, J. Schmitt, G. Decher, *Ber. Bunsen-Ges. Phys. Chem.* **1996**, *100*, 948.

45 Hsieh, M.C. Farris, R.J., McCarthy, T.J. *Macromolecules* **1997**, *30*, 8453.

46 F. Caruso, H. Lichtenfeld, H. Möhwald, M. Giersig, *J. Am. Chem. Soc.* **1998**, *120*, 8523.

47 F. Caruso, H. Möhwald, *Langmuir* **1999**, *15*, 8276.

48 R.A. Caruso, A. Susha, F. Caruso, *Chem. Mater.* **2001**, *13*, 400.

49 K. Rhodes, S.A. Davis, F. Caruso, B. Zhang, S. Mann, *Chem. Mater.* **2000**, *12*, 2832.

50 F. Caruso, A.S. Susha, M. Giersig, H. Möhwald, *Adv. Mater.* **1999**, *11*, 950.

51 F. Caruso, M. Spasova, A. Susha, M. Giersig, R.A. Caruso, *Chem. Mater.* **2001**, *13*, 109.

52 F. Caruso, X. Shi, R.A. Caruso, A. Susha, *Adv. Mater.* **2001**, *13*, 740.

53 D.I. Gittins, A.S. Susha, B. Schöler, F. Caruso, *Adv. Mater.* **2002**, *14*, 508.

54 F. Caruso, M. Spasova, V. Salgueirio-Maceira, L.M. Liz-Marzán, *Adv. Mater.* **2001**, *13*, 1090.

55 A. Susha, F. Caruso, A. L. Rogach, G.B. Sukhorukov, A. Kornowski, H. Möhwald, M. Giersig, A. Eychmüller, H. Weller, *Colloids Surf. A* **2000**, *163*, 39.

56 A. Rogach, A. Susha, F. Caruso, G. Sukhorukov, A. Kornowski, S. Kershaw, H. Möhwald, A. Eychmüller, H. Weller, *Adv. Mater.* **2000**, *12*, 333.

57 F. Caruso, H. Möhwald, *J. Am. Chem. Soc.* **1999**, *121*, 6039.

58 C. Schüler, F. Caruso, *Macromol. Rapid Commun.* **2000**, *21*, 750.

59 F. Caruso, C. Schüler, *Langmuir* **2000**, *16*, 9595.

60 F. Caruso, H. Fiedler, K. Haage, *Colloids Surf A* **2000**, *169*, 287.

61 Y. Lvov, F. Caruso, *Anal. Chem.* **2001**, *73*, 4212.

62 I.L. Radtchenko, G.B. Sukhorukov, S. Leporatti, G.B. Khomutov. E. Donath, H. Möhwald, *J. Colloid Interface Sci.* **2000**, *230*, 272.

63 S. Moya, E. Donath, G.B. Sukhorukov, M. Auch, H. Bäumler, H. Lichtenfeld, H. Möhwald, *Macromolecules* **2000**, *33*, 4538.

64 G.B. Sukhorukov, E. Donath, S. Moya, A.S. Susha, A. Voigt, J. Hartmann, H. Möhwald, *J. Microencapsulation* **2000**, *17*, 177.

65 R. Georgieva, S. Moya, S. Leporatti, B. Neu, H. Bäumler, C. Reichle, E. Donath, H. Möhwald, *Langmuir* **2000**, *16*, 7075.

66 D.I. Gittins, F. Caruso, *Adv. Mater.* **2000**, *12*, 1947.

67 D.I. Gittins, F. Caruso, *J. Phys. Chem. B* **2001**, *105*, 6846.

68 K.-K. Kunze, R.R. Netz, *Phys. Rev. Lett.* **2000**, *85*, 4389.

69 F. Caruso, D. Trau, H. Möhwald, R. Renneberg, *Langmuir* **2000**, *16*, 1485.

70 M.E. Bobreshova, G.B. Sukhorukov, E.A. Saburova, L.I. Elfimova, B.I. Sukhorukov, L.I. Sharabchina, *Biophysics* **1999**, *44*, 813.

71 NG. Balabushevitch, G.B. Sukhorukov, N.A. Moroz, D.V. Volodkin, N.I. Larionova, E. Donath, H. Möhwald, *Biotechnol. Bioeng.* **2001**, *76*, 207.

72 V.S. Trubetskoy, A. Loomis, J. E. Hagstrom, V.G. Budker, J.A. Wolff, *Nucleic Acids Res.* **1999**, *27*, 3090.

73 D. Finsinger, J.S. Remy, P. Erbacher, C. Koch, C. Plank, *Gene Therapy* **2000**, *7*, 1183.

74 R. Dallüge, A. Haberland, S. Zaitsev, M. Schneider, H. Zastrow, G.B. Sukhorukov, M. Böttger, *Gene Str. Expres. BRA*, **2002**, *1576*, 45.

75 F. Caruso, W. Yang, D. Trau, R. Renneberg, *Langmuir* **2000**, *16*, 8932.

76 X. Shi, F. Caruso, *Langmuir* **2001**, *17*, 2036.

77 E. Donath, G.B. Sukhorukov, H. Möhwald, *Nach. Chem. Tech. Labor.* **1999**, *47*, 400.

78 B. Neu, A. Voigt, R. Mitlöhner, S. Leporatti, E. Donath, C. Y. Gao, H. Kiesewetter, H. Möhwald, H. J. Meiselman, H. Bäumler, *J. Microencapsulation* **2001**, *18*, 385.

79 V. Dudnik, G.B. Sukhorukov, I.L. Radtchenko, H. Möhwald, *Macromolecules* **2001**, *34*, 2329.

80 I.L. Radtchenko, G.B. Sukhorukov, H. Möhwald, *Colloids Surf A* **2002**, *202*, 127.

81 A. Voigt, E. Donath, H. Möhwald, *Macromol. Mater. Eng.* **2000**, *282*, 13.

82 I. L. Radtchenko, G. B. Sukhorukov, A. L. Rogach, A. Kornowski, H. Möhwald, *Adv. Mater.* **2001**, *13*, 1684.

83 S. H. Park, Y. Xia, *Langmuir* **1999**, *15*, 266.

84 P. Jiang, J. F. Bertone, K. S. Hwang, V. L. Colvin, *Chem. Mater.* **1999**, *11*, 2132.

85 S. A. Asher, J. Holtz, J. Weissman, G. Pan, *MRS Bull.* **1998**, *October*, 44.

86 W. L. Vos, M. Megens, C. M. van Kats, P. Boeseche, *Langmuir* **1997**, *13*, 6004.

87 A. van Blaaderen, R. Ruel, P. Wiltzius, *Nature* **1997**, *385*, 321.

88 O. D. Velev, A. M. Lenhoff, E. W. Kaler, *Science* **2000**, *287*, 2240.

89 M. L. Breen, A. D. Dinsmore, R. H. Pink, S. B. Qadri, B. R. Ratna, *Langmuir* **2001**, *17*, 903.

90 K. P. Velikov, A. van Blaaderen, *Langmuir* **2001**, *17*, 4779.

91 G. Kumaraswamy, A. M. Dibaj, F. Caruso, *Langmuir* **2002**, *18*, 4150.

92 Z. Liang, A. S. Susha, F. Caruso, *Adv. Mater.* **2002**, in press.

93 O. D. Velev and E. W. Kaler, *Adv. Mater.* **2000**, *12*, 531.

94 Y, Xia, B. Gates, Y, Yin, Y. Liu, *Adv. Mater.* **2000**, *12*, 693.

95 O. D. Velev, P. M. Tessier. A. M. Lenhoff, E. W. Kaler, *Nature* **1999**, *401*, 548.

96 K. M. Kulinowski, P. Jiang, H. Vaswani and V. L. Colvin, *Adv. Mater.* **2000**, *12*, 833.

97 J. E. G. J. Wijnhoven, W. L. Vos, *Science* **1998**, *281*, 802.

98 B. T. Holland, C. F. Blanford, A. Stein, *Science* **1998**, *281*, 538.

99 Y. A. Vlasov, N. Yao, D. J. Norris, *Adv. Mater.* **1999**, *11*, 165.

100 A. A. Zakhidov, R. H. Baughman, Z. Iqbal, C. X. Cui, I. Khayrullin, S. O. Dantas, I. Marti, V. G. Ralchenko, *Science* **1998**, *282*, 897.

101 A. Blanco, E. Chomski, S. Grabtchak, M. Ibisate, S. John, S. W. Leonard, C. Lopez, F. Meseguer, H. Miguez, J. P. Mondia, G. A. Ozin, O. Toader, H. M. van Driel, *Nature* **2000**, *405*, 437.

102 B. Gates, Y. Yin, Y. Xia, *Chem. Mater.* **1999**, *11*, 2827.

103 S. A. Johnson, P. J. Olivier, T. E. Mallouk, *Science* **1999**, *283*, 963.

104 P. Jiang, J. Cizeron, J. F. Bertone, V. L. Colvin, *J. Am. Chem. Soc.* **1999**, *121*, 11630.

105 Wang, D., Caruso, F. *Adv. Mater.* **2001**, *13*, 350.

106 D. Wang, R. A. Caruso, F. Caruso, *Chem. Mater.* **2001**, *13*, 364.

107 E. L. Bizdoaca, M. Spasova, M. Farle, M. Hilgendorff, F. Caruso, *J. Magn. Magn. Mater.* **2002**, *240*, 44.

108 I. Pastoriza-Santos, I., B. Schöler, F. Caruso, *Adv. Functional Mater.* **2001**, *11*, 122.

109 C. Schüler, F. Caruso, *Biomacromolecules* **2001**, *2*, 921.

110 W. Jin, X. Shi, F. Caruso, *J. Am. Chem. Soc.* **2001**, *123*, 8121.

111 D. Trau, R. Renneberg, F. Caruso, in preparation.

112 W. Yang, D. Trau, R. Renneberg, N. T. Yu, F. Caruso, *J. Colloid Interface Sci.* **2001**, *234*, 356.

113 A. A. Antipov, G. B. Sukhorukov, E. Donath, H. Möhwald, *J. Phys. Chem. B* **2001**, *105*, 2281.

114 W. Yang, D. Trau, M. Lehmann, F. Caruso, N. T. Yu, R. Renneberg, *Anal. Chem.* **2002**, in press.

115 S. Mecking, R. Thomann, *Adv. Mater.* **2000**, *12*, 953.

116 A. Dokoutchaev, J. T. James, S. C. Koene, S. Pathak, G. K. S. Prakash, M. E. Thompson, *Chem. Mater.* **1999**, *11*, 2389.

Multilayer Thin Films. Edited by Gero Decher, Joseph B. Schlenoff

Copyright © 2002 Wiley-VCH Verlag GmbH & Co. KGaA
ISBNs: 3-527-30440-1 (Hardback); 3-527-60057-4 (Electronic)

13
Smart Capsules

Helmuth Möhwald, Edwin Donath and Gleb Sukhorukov

Abstract

A procedure to produce hollow capsules with equally defined walls from a defined polyelectrolyte multilayer is described. Decomposable colloid particles are coated by the layer by layer technique, the core is then dissolved and low molecular weight residuals permeate through the wall. The core may consist of inorganic, organic or biological materials, polymers, or cells, consequently the removal chemistry is highly varied. The walls can consist of the whole diversity of materials that have been used for planar multilayers. Because of the great diversity and modularity permeation can be controlled by pH, ionic strength or temperature, and there are also prospects for control via light. The stability and mechanical properties can be optimized via material selection but also via additional chemical treatment, e.g. crosslinking. One may make use of specific physical and chemical processes inside the wall, in particular

- precipitation and crystallization
- polymerization and polymer functionalization
- enzymatic and heterogeneous catalysis
- photocatalysis and crosslinking

Use is made of the specific wall features, selective permeability, and controlled composition of inner and outer surface. The rapid progress in the field has been achieved by building on the knowledge of the preparation and characterization of planar multilayers with the addition of newly developed techniques of colloid characterization such as scanning force microscopy, confocal microscopy and single particle light scattering, in combination with traditional methods. Thus a system is described with many application perspectives in materials and life sciences but also with new features for additional film characterization by techniques requiring much surface.

13.1 Preparation and Structure

13.1.1 General Aspects

13.1.1.1 Core materials

In Chapter 12 the coating of different core materials by polyelectrolyte multilayers was discussed. This will not be reiterated here. Instead the special issues that concern removal of the core to obtain a hollow capsule or a capsule with a specific function inside will be addressed.

The first hollow capsules were made from a polymeric core, in this case weakly crosslinked melamine formaldehyde [1, 2]. For this core, methods of preparation were established to obtain very uniform core diameters between 100 nm and 10 μm, spherical shapes and low surface roughness and it was also known that the core could be destroyed by going to a pH < 1.6 or by treatment with dimethylformamide. In addition, techniques to fabricate latices are very well developed and hence are presumably economical. One may also envisage other ways to destroy the polymer e.g. by light, heat or enzymes. However, there may also arise polymer-specific problems like unspecific side reactions or residual oligomers sticking to or inside the walls. These aspects will be considered in detail in Section 13.1.2.

The problem of product removal after core destruction is less severe if the core is an inorganic colloid. Also one does not need to worry about toxic side effects if the core is e.g. $CaCO_3$, which in addition is very cheap. The kinetic hindrance of a reaction induced by a pH change or by a complexing agent like EDTA is also a less severe problem than with polyelectrolytes. However, techniques to obtain inorganic particles of uniform sizes in the μm range are not yet well developed for most candidate materials. Depending on the demands for a certain application, inorganic cores are a promising alternative. A special case of an inorganic, rather low-cost, sufficiently monodisperse core is silica. It can be easily coated and the silica can be removed afterwards by treatment with hydrofluoric acid. The disadvantage of silica is that the core removal procedure involves a dangerous step when the hydrofluoric acid is applied. The polyelectrolyte coat was found to be rather stable in hydrofluoric acid.

Other alternatives are organic particles of low molecular weight compounds [3, 4]. They often have the problem of being soluble in solvents different from those for polyelectrolytes. This may be overcome by using surfactants or polymeric amphiphiles covering the particle surface, thus rendering them water soluble and/or charged. However, one thus obtains a multicomponent system and some of these surfactants remaining in solution may undergo unwanted reactions, or complexation, during further coating processes. Also the techniques to prepare organic particles of uniform size and shape in the μm range do not exist, and one typically has to use organic solvents which are undesirable from many other, e.g. environmental aspects.

Special types of core are precipitates of enzymes [5] or of DNA [6]. They are not meant to be destroyed but to function while being protected by the shell that may

later be destroyed, e.g. after attaching to a cell nucleus. To this class also belong cores of inorganic/organic composites where later the organic component is removed and the inorganic one remains inside as a particulate catalyst, fluorophore or magnetic tag.

Compared to the solid core, liquid cores are more difficult to handle due to their higher flexibility and mobility. However, it has been possible to freeze this flexibility by coating oil droplets with polyelectrolytes. For this the oil did not have to be coated and charged by an ionic surfactant since even charged polyelectrolytes like PSS are somewhat enriched at the oil/water interface and are then amenable to further coating by oppositely charged polyelectrolyte. It is desirable to use polymeric amphiphiles with higher interfacial activity because polymers not residing at the interface may complex with oppositely charged ones on further coating and the resulting unwanted structures may have to be removed. In any case, coating of oils is technically very promising since it yields a new type of emulsion with low dynamics and stabilized by Coulombic forces, for use e.g. in cosmetics, the food industry or pharmacy.

Early in the development of the subject, erythrocytes or yeast cells were successfully coated [7]. Here the coat may be useful as a protective surface or as a way to target the cell to a specific location. On the other hand many cells have very peculiar shapes and one may obtain hollow capsules with anisometric shapes. Red blood cells have been fixed in shape by glutardialdehyde crosslinking (thus losing their function). Although the charge pattern on a cell surface is very nonuniform it was possible to obtain alternating overall surface charge patterns after four coating cycles. Methods to destroy cell material have also been developed, e.g. treatment with NaOCl, called a deproteinizer. It has been possible thus to obtain hollow capsules with templated shapes (see Fig. 13.1). However, the treatment is very harsh and in Section 13.1.2 various side reactions will be discussed.

13.1.1.2 **Wall materials**

First we set technical limits to the selection of wall materials:

- The coating process includes the bending of a polymer on a curved surface. This is not a problem for micron-sized colloids but becomes an issue for dimensions below 100 nm when the particle size approaches the length of the polymer. As an important example DNA wrapping a histon protein has also been studied theoretically, where the competition between electrostatic interaction and bending yields an ionic strength window where coating is possible.
- For smaller particles at reasonable concentration (100 nm, (1% *v*/*v*)) stability against flocculation becomes a problem because the time between particle collisions due to thermal motion and that of charge reversal becomes comparable. Acceleration of charge reversal is possible using smaller polymers or oligomers.
- Another problem associated with the smaller size is that at particle concentrations as low as 1–3% it becomes increasingly difficult to adjust the polyelectrolyte concentration in such a way that polymer is present in sufficient excess in

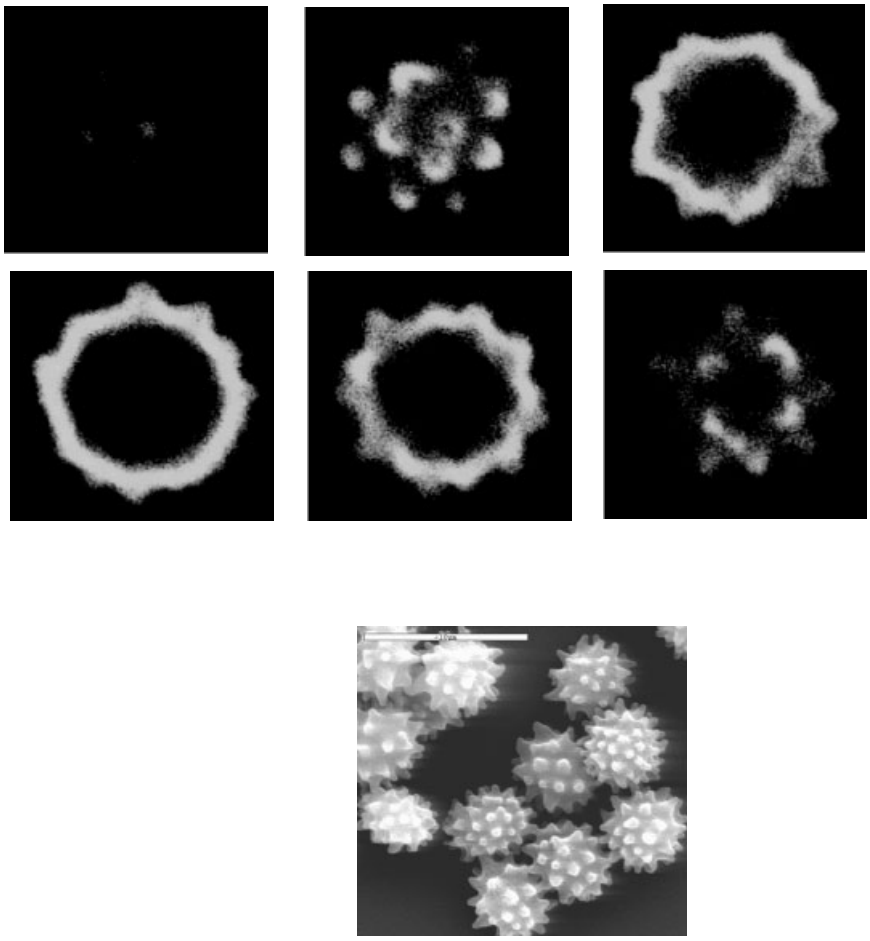

Fig. 13.1 Confocal microscopy scans of a polyelectrolyte shell consisting of 11 layers of PSS/PAH templated on an echinocyte. The outer layer is FITC labelled PAH. The width of the images is 7 μm. The scans (left-right, top-bottom) were made in two planes separated by a distance of 1 μm. Scan runs through the upper part of the shell. The SEM image on the bottom shows the initial echinocyte cells.

the aqueous solution. The total surface area of the particles at the same volume fraction increases with r^{-1} while the polyelectrolyte concentration has a practical limit due to solubility and the viscosity of the solution.

The first wall materials used were polyelectrolytes poly(styrene sulfonate) (PSS) and poly(allylamine hydrochloride) (PAH). Since then a variety of polymers have been used and there is virtually no restriction if the polymer contains multiple charges. Depending on some specific requirement chitosane, chitosanesulfate and a variety of other modified polysaccharides have been used as biocompatible and

biodegradable polymers, DNA was used as a stiff polymer that later may offer some function like gene therapy. Co-polymers with another functionality, e.g. thermal responsiveness were used successfully where the second uncharged component could be in fractions close to 90%. Also other building principles than electrostatics like biospecific ligand binding, hydrogen bonding and metal coordination were applied successfully to the preparation of shells. In these latter cases special care had to be taken to ensure colloid stability, because Coulomb repulsion as a stabilizing mechanism is at least reduced.

Inorganic particles could be used as a wall material in combination with an oppositely charged polyelectrolyte to render the wall magnetic [8], luminescent or simply to change the elastic properties of the wall. As an extreme into the latter direction SiO_2 particles could be calcined, leading to sintering and thus building of solid bridges between the particles [9]. This leads to porous inorganic hollow capsules. Another promising route may be metal particle incorporation to give a conducting wall and/or to have an efficient microwave absorber.

It is also possible to build up the walls from a combination of multiply charged low molecular weight molecules or metal ions [10]. This is attractive if the wall is supposed to absorb or to emit light and if the chromophore is arranged at a specific location along the surface normal. This may be required, e.g. to build an electron transfer chain through the wall, to study the accessibility to quenchers and thus their diffusion or to generate a charge separation by light at a specific location inside the wall. In many of these cases, however, it is simpler to incorporate a polyelectrolyte with a dye covalently coupled to it. A special advantage of using low molecular weight compounds may be that their coupling is not very stable. Thus the wall can be destroyed again, e.g. by adding high salt concentrations ($\sim$1 M).

In order to achieve specific functions it has also been possible to incorporate proteins as a structural material. Because the build-up defines a position along the normal it is thus possible to design enzyme cascades whilst still protecting the enzymes against proteases. Of course, in this case one has to be careful that the core removal chemistry does not destroy the enzymes. For the purposes of targeting one may envision attaching antibodies or other specific ligands at the outer surface. These attempts, however, are far from being optimized.

The more biomimetic approach would be to adsorb a lipid monolayer or bilayer at the outer surface. In this case the capsules become soluble in hydrophobic solvents or impermeable to hydrophilic components [11]. In these attempts binding occurred through Coulombic interactions, but these could be reduced by e.g. using mixtures of charged lipids. In the latter case the problem of having exclusively bilayers has not yet been solved, but the coupling was low enough to keep liquid crystalline and solid phases as observed for free bilayers. In Section 13.2.1 we will also discuss the problem of controlling defects in the bilayers which dramatically affect their ion permeability such that we are far from the insulating properties of a black lipid membrane. Still, at this stage, the bilayer coating is sufficiently homogeneous and perfect that studies with incorporated ion channels and receptors become meaningful.

13.1.1.3 Molecular Dynamics

Obviously the dynamics of molecules is of high relevance for the control of wall properties, e.g. permeability, but the shells also provide a unique possibility of studying this dynamics: because of their large specific surface area they enable the application of typical bulk techniques like NMR and flash spectroscopy. For typical diameters near 1 μm they may be considered as free standing film which can be made asymmetric at will, and for smaller dimensions curvature effects may come into play. These features are just beginning to be explored, and therefore this section does not contain many hard facts. Dynamics usually involves many motional modes, length and time scales. There are not yet any data available on time scales below 1 μs and the segment mobility also could not be elucidated. A way to get access to this could be ^{2}D NMR for highly swollen walls, but this is demanding as regards technique, deuterated material and preparation with the proper degree of swelling. The translational motion of polymer melts is generally described by the reptation model, where a polymer moves in a tube with diameter equivalent to its cross section. For polyelectrolyte multilayers one expects electrostatic coupling with neighboring molecules, and it is thus not surprising that one could not measure any lateral polyelectrolyte mobility in planar films, i.e. the diffusion coefficient is below 10^{-15} cm^2 s^{-1} as measured by fluorescence recovery after photobleaching (FRAP). One also expects similarly small values for capsules.

More interesting, and also quantitatively measurable, is the translational mobility of small molecules and ions. This process is generally described by a free volume model, i.e. in order for a species to move a free volume V_f has to be created thermally and the molecule can then jump into this vacancy. The free energy of this hole depends exponentially on the necessary free volume and the compressibility and one therefore expects a drastic dependence on these parameters. This has been verified for polymeric glasses, and also for polyelectrolyte multilayers by studying the fluorescence quenching by molecules of different sizes. In the latter cases diffusion coefficients between 10^{-15} and 10^{-12} cm^2 s^{-1} were determined, and modeling of the data also revealed that the mobility was up to two orders of magnitude larger in the top 10 nm of the multilayer adjacent to water. This has been ascribed to swelling of the film adjacent to water and one may expect even ten orders of magnitude faster diffusion if one has a completely swollen film. This has not yet been verified for planar films, and also the equivalent experiments have not yet been performed for capsules. One could principally learn about diffusion from the permeation experiments described in Section 13.2.1 if the latter were due to diffusion through the matrix, not through the pores. In this case values of $D \approx 10^{-11}$ cm^2 s^{-1} were derived. These might be attributed to a different preparation protocol of capsules (always in water) compared to planar films (dried after each adsorption step) but more probably it is due to the fact that diffusion is not the permeation mechanism.

Obtaining more quantitative information on diffusion has been inhibited by the fact that there are slow aging mechanisms (see Section 13.2.2). These may be related to the internal dynamics of the polyelectrolyte complex which is basically

due to the low stability of the Coulomb interaction in an aqueous environment. As a simple estimate the attractive energy E of two opposite charges a distance $R = 2.5$ Å apart in matter ($\varepsilon = 80$) amounts to $E = \frac{e_0^2}{4\pi\varepsilon\varepsilon_0 r} = 2.8\ kT$, where k is Boltzmann's constant and T the absolute temperature.

The lifetime τ of the bond would thus be $\tau = \tau_0 \exp(nE/kT)$, where n is the number of bonds, and with $\tau_0 \sim 10^{-13}$ s, a typical inverse vibration frequency, one obtains $\tau = 2.5$ μs for six simultaneous bonds. Thus individual bonds would reform much faster than 1 μs if they were not stabilized by lower water content in the film and by neighboring bonds. These effects, however, depend strongly on the individual polymers and one should not be surprised to find drastic differences in the internal dynamics when comparing different systems.

Indirect information on the dynamics of water in the shells can be obtained from ^{1}H-NMR relaxation experiments. There one basically determines the fraction of water immobilized multiplied by its "immobilization strength". One thus finds that water is immobilized in the film, even in the inner layers, but the amount depends drastically on the charge of the outer layer, as if the latter either compresses or expands the total film to remove or create water pockets. Recently the swelling kinetics of films brought into contact with water or with air of different humidity were analyzed in terms of two processes, the faster one (100 s) ascribed to permeation of water into the films and the slower one to reorganization of the matrix. Such a slow water diffusion (100 s) would be very surprising since, judging from experiments with dye probes, one would expect diffusion of water, metal ions, protons, and other small solvent molecules to penetrate in less than 1 ms.

13.1.2 Physics and Chemistry of Core Removal

The above, mostly qualitative, remarks on dynamics were necessary to conceive that small molecules can permeate the walls and that the multilayers possess viscosity and possibly also elasticity. Hence to remove the core one first has to break it into small entities that can diffuse through the wall. Consequently, we will first discuss the process of core destruction and then removal of core material and concomitant changes of the wall.

13.1.2.1 Core Destruction

Depolymerization

The first core material used was melamine formaldehyde. It is prepared by polymerization from a precondensate solution. The particle formation involves kinetic control of droplet growth as well as crosslinking. This leads to uniform size distribution with polydispersities of less than 5%. The crosslinking reaction is acid catalyzed and proceeds more slowly than particle formation. It can be stopped at an early stage. In this way melamine resin particles are fabricated which can easily be dissolved afterwards in 0.1 M hydrochloric acid.

The decomposition process of the melamine formaldehyde cores has been studied in detail [12]. The melamine resin represents a network of melamine formaldehyde crosslinked either by ether linkages or methylene bridges. Primary hydroxy and amino groups not utilized for crosslinking are also present. Upon treatment with hydrochloric acid the ether linkages are hydrolyzed, while the methylene bridges remain intact; as a result the core is decomposed into oligo- as well as polymeric units. In parallel with the hydrolysis of the ether bridges, melamine is hydrolyzed to ammeline, as was evidenced by the appearance of a characteristic amide group.

It is remarkable that in parallel with hydrolysis a second acid catalyzed re-polymerization reaction occurs which results in the formation of C–N–C linkages. If this reaction is faster than the hydrolysis the core will be converted to an insoluble resin. It is hence a subtle balance which should be obeyed, otherwise hollow shells cannot be produced. This occurs frequently if the pH is either too large or too small. A mild acid pretreatment will typically produce insoluble cores. If the hydrochloric acid is too strong (> 0.1 M) the re-polymerization becomes increasingly faster than the hydrolysis.

The size of the degradation products was estimated from diffusion coefficient measurements which were conducted by means of fluorescence correlation spectroscopy. It was concluded that the products of hydrolysis were on average composed of melamine formaldehyde polymers consisting of about 60 monomers. If, however, the core was dissolved in dimethyl formamide, a good solvent for melamine formaldehyde, polymeric products composed of about 4000 monomers were obtained. The hydrodynamic radius of the melamine formaldehyde polymer obtained by means of hydrolysis is about 3–4 nm. This is too large for fast diffusion through the shell walls. The increase in osmotic pressure is currently thought to be responsible for widening the pre-existing pores or for the formation of new pores which then allow passage of the melamine resin degradation products. The physico-chemical aspects of this process will be discussed later. The osmotically induced stretching of the wall is clearly visible when the degradation is followed under the confocal microscope. In parallel with a remarkable diameter increase the core products are released. If the layer is too thick this pore widening is impossible. As a result of the increased osmotic pressure the shells will break. This occurs typically if, for example, more than 8 pairs of PAH and PSS are assembled onto a micron sized core. Other shell wall materials may be less suitable for shell formation due to their different mechanical and permeability properties.

The polymeric nature of the degradation products has another less favorable consequence. Some core material almost always remains inside the shells. As soon as the driving force for release disappears, which takes place toward the end of release, the pores will close and some core material is captured inside. Various fluorescence techniques such as confocal microscopy and Förster energy transfer have revealed that most of the remaining material is adsorbed on the wall. Since the melamine formaldehyde degradation products are positively charged they preferentially interact with the polyanion in the multilayer. This may lead to a modification of the layer properties and has to be taken into account if the shells are used afterwards.

Another alternative core could be protein precipitates or cells. For their destruction a treatment with NaOCl, called deproteinizer, is well established [7]. Hypochlorite is widely used as a strong disinfecting and cleaning agent. Its function is based on its reductive potential, +0.89 mV, as a result of electron release when the compound is hydrolyzed. It is interesting to recall that hypochlorite is an agent released in the human body by neutrophils during their immune reaction against bacteria. It destroys the proteins of the invading microorganism by oxidation in very much the same way that an erythrocyte core can be destroyed inside a polyelectrolyte multilayer adsorbed on top of it. The proteins are broken into smaller pieces which can leave the shell. However, a deeper analysis showed that, for example, PSS is also degraded. It was found that as much as 90% of the originally present PSS was lost during the deproteinizer treatment. PAH is also degraded. A large variety of oxidation reactions occur which convert the amino groups into nitrile, nitro and nitroso groups. Aldehydes and carboxylic acid groups are also produced. Secondary reactions may then cross-link these entities forming azo, azomethine and azoxy-bridges.

Hence it can be concluded that the deproteinizer treatment finally produces a loose polymer network which is completely different from the original multilayer structure. It does not have any cationic groups. The nature of the obviously present anionic groups is still uncertain, the negative charge may result from some remaining sulfonic acid groups.

It is worth mentioning that successful shell formation is closely connected with the presence of the PAH. With other polycations the process of shell fabrication does not yet work properly. For example pure polysaccharide multilayers were completely degraded during core decomposition.

Core dissolution

If the core is made of precipitates of low molecular weight compounds destruction requires merely change of the solubility product. This can be achieved by changing the pH, as exemplified for an organic molecule by adding a strongly complexing agent, e.g. EDTA in the case of $CaCO_3$ or $CdCO_3$ [13]. In these cases one does not expect any side reactions. There are problems related to the attraction of divalent ions or EDTA to the polyelectrolyte but these problems are not major. The limiting factor lies more in obtaining inorganic cores of the desired size and dispersity and free of stabilizing polymer.

Since techniques to prepare SiO_2 particles of defined dimensions have been well developed it is desirable to develop these techniques to induce core removal. It has been possible to dissolve these cores in HF, a standard method for dissolving glass and applicable here, too.

Other techniques of core destruction

In principle, it should also be possible to destroy cores with light, but this has not yet been attempted successfully. Another way is heat treatment and the extreme of this is calcination [9]. For this case protocols have been developed to destroy

thermally a polymeric core while leaving an inorganic shell largely intact, although porous. Such a treatment was elaborated for cores coated with a SiO_2/polyelectrolyte composite. In this case the organic components were destroyed, the SiO_2 particles at the walls were sintered, i.e. bridges were built between individual particles. This enabled the formation of porous hollow SiO_2 spheres. These shells are stable even after calcination from walls with one monolayer SiO_2, but of course they are much more stable if prepared from SiO_2 in many multilayers.

13.1.2.2 **Core Material Release**

As has become clear above, different core materials require different destruction processes, and this in turn will affect material removal and its optimization. The process has been investigated in detail for MF cores [12] and these will now be considered in detail here. In this way it will become clear that there are many features to be optimized for a successful preparation, and these may depend drastically on the system.

Fig. 13.2 shows a confocal microscopy sequence of the removal of fluorescently labeled MF. One clearly observes the removal of the material first from the outer parts and this process takes of the order of 1000 s. One also sees an increase in the capsule diameter followed later by a decrease. This indicates an increase in osmotic pressure that is later relaxed due to material permeation into the external medium. The shells are apparently elastic, the degree depending on the material.

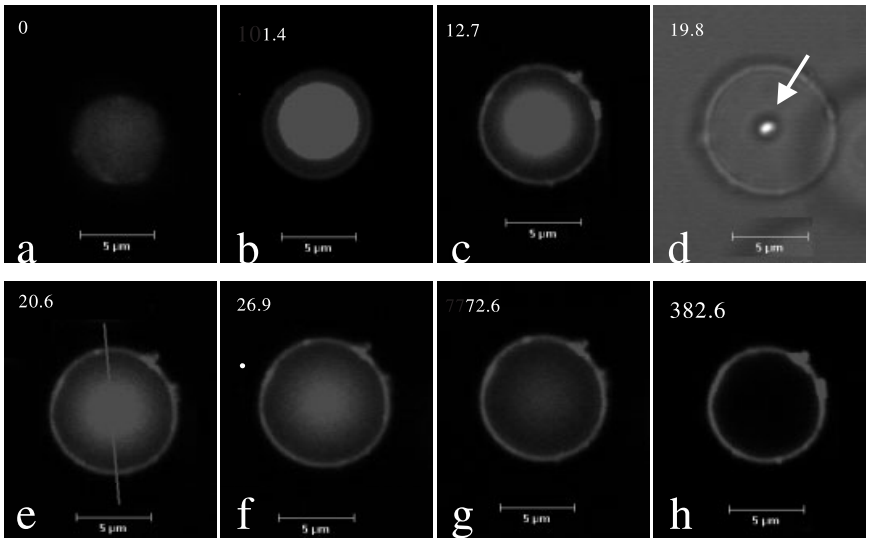

Fig. 13.2 CLSM images of the core decomposition process as a function of time. Rd-labeled MF colloids with a diameter of 6.4 µm deposited with $(PSS/PAH)_8$. The arrow in (d) indicates the residue of the core. 13.2d corresponds to transmission light microscopy. The numbers in the insets indicate the core decomposition time.

E.g. for PSS/PAH we observe full recovery of the initial diameter after a long time but for PSS/PDADMAC there is only partial recovery.

The osmotic pressure release may also lead to shell rupture, and this again depends sensitively on the preparation conditions. Thus Fig. 13.2 shows for the specific system MF coated with 8 layers PSS/PAH that there is a narrow optimum of pH at which the preparation is successful. Then one obtains more than 90% intact capsules. Next we present some estimate of important numbers to demonstrate which parameters are crucial and where one does expect limits.

Let us first estimate the maximum osmotic pressure that might be built up if the core material were not released. If we assume that it breaks up into small entities of molecular weight 200 g mol^{-1} this would correspond to a density of about $v = 5$ mol l^{-1} and according to van't Hoffs law $\mu_{max} = RTv$ to 10 MPa. This very high value may be reduced by up to an order of magnitude due to volume increase, it may also be reduced if the fragments are larger. However, if the fragments are ionic the counter ions will dominate the osmotic pressure. Hence values of 10 MPa are realistic upper limits. The case of inorganic particle dissolution is less relevant for the estimate since the resulting ions may quickly diffuse through the wall.

The next question to be asked is: Is this pressure π_{max} ever reached? For this we consider a capsule of volume $\frac{4\pi}{3}r^3$, surface $4\pi r^2$, permeability P and solute concentration $c_i (c_i \ll c_{external})$.

From $\frac{-dc_i}{dt} \cdot \frac{4\pi}{3} r^3 = P \cdot 4\pi r^2 \cdot c_i$ we obtain

$$c_1 = c_i^0 \exp\left(\frac{-3P}{r}\right) t \tag{1}$$

From permeability studies (Section 13.2.1) we derive for typical organic dyes $P = 2\text{–}7 \times 10^{-9}$ m s^{-1}, hence for a typical radius $r = 1$ µm we obtain $\left(\frac{3P}{r}\right) = (6 - 21) \times 10^{-3} s^{-1}$ with the lower values for the thicker walls. In the experiment of Fig. 13.2 we saw that core removal takes some 10^2 s. Consequently the maximum osmotic pressure may be reached.

Inspecting Eq. (1) one also realizes that release slows down with r, i.e. because of the lower surface to volume ratio a larger osmotic pressure may build up. We should also remark that with diffusion coefficients measured for planar films a three orders of magnitude lower permeability would be obtained, hence the maximum osmotic pressure would be reached. This indicates that during core removal the osmotic pressure of 10 MPa leads to a tension of 10 N m^{-1} in the wall of a particle of 1 µm in radius. This tension is rather large given the very small thickness of the layer. It exceeds, for example, the known limit of stability of a lipid bilayer by a factor of 100. Pores are created in the shell through which material may escape. Consequently we expect that pores are formed by templating from polymeric cores and there remains an open question whether these pores may anneal with time.

Altogether we conclude that to template a capsule from a polymeric core the shell has to sustain osmotic pressures of the order of 10 MPa, templating is easier for smaller cores, since the tension responsible for rupture is proportional to the particle radius. As regards the dependence on wall thickness d, the permeability decreases with d leading to an increase in π, but the rupture strength is also expected to increase with d. Since both features are nonlinear and opposite one cannot yet make a prediction as to the dominating effect. Experimentally, however, it was observed that there is an optimum thickness corresponding to a minimum of broken shell fraction. For the example of PSS/PAH this is close to 10 layers.

Another question on core removal concerns sticking of core material to the wall. The fluorescence micrographs in Fig. 13.2 show enhanced intensity from the walls. Obviously there were also fluorescent oligomers produced which were sticking to the walls. In order to quantify this amount single particle light scattering may contribute. Fig. 13.3 shows the distribution of scattering intensities before and after core removal. Also shown is the distribution expected theoretically if all core material is removed. From the comparison one may deduce that about 1% of the core material remains in the wall. This may not only be problematic for medical and pharmaceutical applications but it may also affect the physico-chemical properties of the wall. E.g. for a typical wall thickness of 10 nm and a core radius of 2 μm the volume ratios of wall and core are:

$$\frac{V_{\text{wall}}}{V_{\text{core}}} = \frac{r^2 \times 10\ \text{nm}}{3r^2} = 1.5\% \tag{2}$$

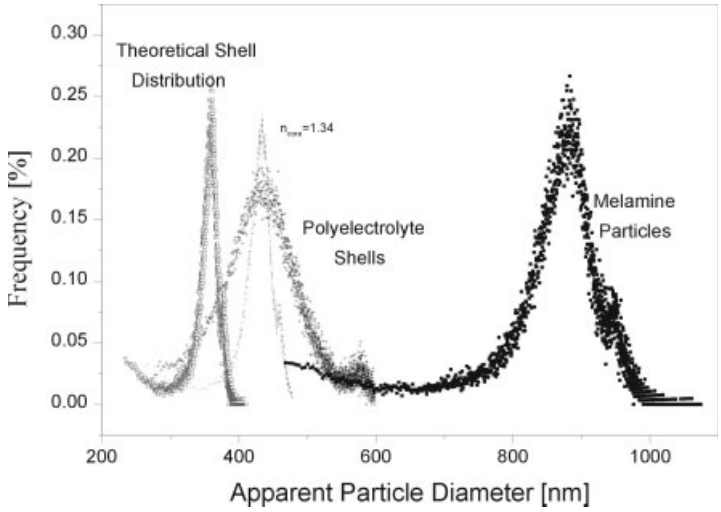

Fig. 13.3 Experimental and theoretical single particle light scattering distribution as a function of capsule radius.

Hence in the example above almost half of the wall material consists of oligomers from the unremoved core.

Finally some remarks on inorganic templates. One expects diffusion through the walls to be fast, hence there is no osmotic pressure build-up and no mechanical stress. This is certainly the case if the water permeability is of the order of the ion permeability. While current experience supports this assumption it may not generally be the case. Sticking to the wall may also be less of a problem. The remaining task then is to have cores with the desired dimensions.

13.1.3 Modification of walls

The last section on core removal already hinted at a process that may become useful if performed in a dedicated way: The covalent cross-linking of polyanion and polycation, for the special case of amino and sulfonate groups.

For steric reasons one does not expect it to proceed quantitatively, but even so the cross-linking may lead to an elastic network. This should not necessarily give a higher elastic modulus but a lower loss modulus and a shape memory, which have not yet been tested. Also, having in mind the network of an elastomer, controlling the mesh size should yield selective permeability for nanometer-sized entities.

Another method of wall modification results if homopolymers are grafted from the walls. This was achieved by incorporating polymers with benzophenone side groups into the shell. These side groups then serve as photoinitiator for the light-induced polymerization of styrene sulfonic acid. Thus an additional (anionic) PSS shell could be built up with thickness and density depending on the polymerization parameters. This should lead to ion selective permeability and it was indeed shown that the wall was impermeable to low molecular weight anions [14].

Another way to control the wall permeability might be through a photoreaction in the wall. It was shown that the photoisomerization of azobenzenes as main chains and as side chains is possible, presumably due to a sufficiently large free volume inside the wall, however a change of properties has not yet been established.

In recent years much progress has been achieved in enriching polymer matrices by inorganic ions that later were reacted to form inorganic particles [15]. This should also be possible in a polyelectrolyte multilayer since there are many polar groups available for metal coordination. Moreover one may use the fact that metal organic precursors are more soluble in the wall than in the water surroundings. Thus Ti·org was dissolved in the wall, then reacted to give TiO_2 particles causing the wall to have a higher refractive index [16]. This may become useful if the shells are to be arranged periodically to become a photonic crystal. As another example Ag^+ ions were used to construct shells. These could then be reduced by light to form metallic silver particles. Because they absorb light they can be visualized by confocal microscopy, and hence the process may be used to label individual shells (Fig. 13.4) [17]. On the other hand the process may be used to form con-